



Spring 1989

Petrology and Structure of the Cascade River Schist, in the Sibley Creek Area, Northern Cascades, Washington

Joe D. Dragovich

Western Washington University

Follow this and additional works at: <https://cedar.wwu.edu/wwuet>



Part of the [Geology Commons](#)

Recommended Citation

Dragovich, Joe D., "Petrology and Structure of the Cascade River Schist, in the Sibley Creek Area, Northern Cascades, Washington" (1989). *WWU Graduate School Collection*. 776.

<https://cedar.wwu.edu/wwuet/776>

This Masters Thesis is brought to you for free and open access by the WWU Graduate and Undergraduate Scholarship at Western CEDAR. It has been accepted for inclusion in WWU Graduate School Collection by an authorized administrator of Western CEDAR. For more information, please contact westerncedar@wwu.edu.

PETROLOGY AND STRUCTURE
OF THE CASCADE RIVER SCHIST,
IN THE SIBLEY CREEK AREA,
NORTHERN CASCADES, WASHINGTON

By

Joe D. Dragovich

Accepted in Partial Completion
of the Requirements for the Degree
Master of Science

[Handwritten signature]

Dean of Graduate School

May 15, 1989


ADISORY COMMITTEE

[Handwritten signature]

CHAIRMAN
[Handwritten signature]

MASTER'S THESIS

In presenting this thesis in partial fulfillment of the requirements for a master's degree at Western Washington University, I agree that the library shall make its copies freely available for inspection. I further agree that extensive copying of this thesis is allowable only for scholarly purposes. It is understood, however, that any copying or publication of this thesis for commercial purposes, or for financial gain, shall not be allowed without my written permission.

Signature 

Date 6-7-89

MASTER'S THESIS

In presenting this thesis in partial fulfillment of the requirements for a master's degree at Western Washington University, I grant to Western Washington University the non-exclusive royalty-free right to archive, reproduce, distribute, and display the thesis in any and all forms, including electronic format, via any digital library mechanisms maintained by WWU.

I represent and warrant this is my original work and does not infringe or violate any rights of others. I warrant that I have obtained written permissions from the owner of any third party copyrighted material included in these files.

I acknowledge that I retain ownership rights to the copyright of this work, including but not limited to the right to use all or part of this work in future works, such as articles or books.

Library users are granted permission for individual, research and non-commercial reproduction of this work for educational purposes only. Any further digital posting of this document requires specific permission from the author.

Any copying or publication of this thesis for commercial purposes, or for financial gain, is not allowed without my written permission.

Name: Joe Dragovich

Signature: _____

Date: 5/20/18

Please distribute
thesis at will—
U . . .
U . . .

PETROLOGY AND STRUCTURE
OF THE CASCADE RIVER SCHIST
IN THE SIBLEY CREEK AREA,
NORTHERN CASCADES, WASHINGTON

A Thesis
Presented To
The Faculty of
WESTERN WASHINGTON UNIVERSITY

In Partial Fullfillment
of the Requirements for the Degree
Master of Science

by
Joe D. Dragovich

May, 1989

ABSTRACT

The focus of this study is on the protolith types, metamorphism and structure of the Cascade River Schist in the Sibley Creek area of the North Cascades, Washington. The two general lithologic packages are an arc and ocean floor unit termed the Cascade River and Napeequa units, respectively, by Tabor and others (in press). The Cascade River unit has a recognizable stratigraphy which is inverted and repeated across strike from the southwestern to northeastern sides of the field area, apparently as a result of macroscopic synclinal folding. The Napeequa unit lies on top of the Cascade River unit, in the center of the syncline, probably as a result of thrust faulting.

Metamorphic zones and facies in the field area increase from the biotite zone of the greenschist facies, west of the Le Conte fault, to the garnet and staurolite-kyanite zones of the epidote amphibolite facies east of the fault. The greenschist facies is estimated to be metamorphosed at pressures of 3-5 Kb, and temperatures of 450-500 C and the amphibolite facies at 8-10 kb and 600-700 C. Structural control of the greenschist-amphibolite facies transition by the Le Conte fault is suggested by the first appearance of the garnet and oligoclase with the fault, as well as a P-T differential across the fault, which suggests considerable dip-slip displacement across the fault.

The metamorphic structures in the field area consist of: 1) a syn-metamorphic first deformation characterized by steeply dipping S-tectonites containing weakly defined down-dip mineral lineations and flattened conglomerate clasts, and 2) a late-metamorphic and commonly retrogressive second deformation characterized by steeply dipping L-S tectonites containing a sub-horizontal stretching lineation, prolate spheroidal conglomerate clasts, and dextral kinematic indicators. Later

post-metamorphic structures are folds and faults related to forceful emplacement of the 73 Ma Hidden Lake pluton and Eocene strike-slip offset along the Le Conte fault.

ACKNOWLEDGEMENTS

This project would have been impossible without the love and support of my wife, Natasha. It is to her that this document is dedicated. A huge thanks is also extended to my parents Jerry and Rosalie Dragovich for enduring those turbulent teenage years and for giving me the gift of endurance, love of science, and a sense of stability.

Special thanks to Ned Brown for guiding me through the cracks, veins, fractures, porphyroblasts and dead-ends of meta-structural studies both in the field and the lab. Thanks to my fellow Cascade River Schistian Jeff Cary for the endless hours of stimulating rock discussion, to Jim Talbot for editing the manuscript and guiding me through the complexities of structures and computer programs, to Russ Burmester for carefully editing the manuscript at the last minute, and to Scott Babcock for helpful insights. Several field assistants waged war with me against the infamous Devils club, mosquitoes, weather, brutal morning coffee, never-ending slopes and horse-flies. These hearty hobbit-like people include Mike Gallagher, Bernie Dougan, Scott Wallace, Andy Buddington and Scott Spees.

Like any scientific endeavor, this study is built upon the sweat and hard-work of previous workers, several of which are cited in the text. Noteworthy in their contributions are Rowland Tabor and the late Peter Misch. I consider this document an extension of the pioneering work of Rowland Tabor in the Mount Johannesburg area.

If all there is to life is science then I would have been better off being born as a computer with legs. My stay in W.W.U. was incredibly enriched by several new-found friends and acquaintances. For all the belly-laughs, Hawk games, get-togethers and gigs with the "Anomalies" I thank-you. Patty Combs, Vicki Critchlow and George Mustoe were always there to help with those little details.

TABLE OF CONTENTS

	<u>Page</u> <u>Number</u>
Abstract.....	i
Acknowledgements.....	iii
List of Figures.....	ix
List of Tables.....	xii
I. INTRODUCTION.....	1
A. Regional Setting.....	1
B. The Sibley Creek Area.....	11
1. Marblemount Metaquartz Diorite.....	11
2. Cascade River Schist.....	11
3. Syn and Post-Tectonic Plutons.....	13
4. Faults in the Study Area.....	13
C. Statement of the Problems.....	14
II. PETROGRAPHY, FIELD RELATIONS, AND ROCK UNITS OF THE CASCADE RIVER SCHIST.....	15
A. Introduction.....	15
B. Rock Units West of the Le Conte Fault.....	15
1. Greenschist Unit.....	15
2. Brown Phyllite Unit.....	18
3. Metaconglomerate Unit.....	22
4. Metatuff Bed.....	27
5. Metamarl-semipelite-pelite Unit.....	27
C. Rock Units in the Central Part of the Field Area....	30
1. Quartz Biotite Schists.....	30
2. Amphibolites.....	32
3. Ultramafic Rocks.....	33
4. Metagabbro.....	33

D. Rock Units in the Northeastern Part of the Field Area	38
1. Quartzo-Feldspathic Schists.....	39
2. Mica Schists.....	42
3. Amphibolites.....	44
4. Quartz Mica Schists.....	44
5. Calcareous Amphibolites, Calcic Mica Schists and Marble.....	48
6. Graphitic Mica Schists.....	49
E. Discussion.....	51
1. Possible Depositional Environment for the Cascade River Schist West of the Le Conte Fault.....	51
2. Relationship Between the Western Cascade River Unit and the Marblemount Metaquartz Diorite.....	54
3. Correlation of the Rock Units in the Western Cascade River Unit.....	55
4. Correlation of the Rock Units in the Northeastern Cascade River Unit.....	58
5. Correlation of the Central Napeequa Unit.....	58
6. Comparison of the Western and Northeastern Cascade River Units.....	61
III. METAMORPHIC SECTION.....	63
A. Introduction.....	63
B. Mineral Assemblages.....	63
1. Introduction.....	63
2. Greenschist Facies Mineral Assemblages.....	63
3. Lower Amphibolite Facies Mineral Assemblages.....	67
4. Middle Amphibolite Facies Mineral Assemblages....	68

C. Petrogenetic Grid.....	68
1. Introduction.....	68
2. Upper Greenschist Facies Equilibria.....	68
a. Garnet Stability.....	68
3. Greenschist-Amphibolite Facies Transitional Equilibria.....	71
a. Actinolite-Hornblende Transition.....	71
b. Albite-Oligoclase Transition.....	73
4. Middle Amphibolite Facies Equilibria.....	73
a. Staurolite + Quartz Stability.....	73
b. Talc + Forsterite Stability.....	73
c. Kyanite and Staurolite + Hornblende Stability.	74
D. Geothermobarometry.....	74
1. Geothermometry.....	75
a. Garnet-Biotite Temperatures.....	75
2. Geobarometry.....	76
a. GRIPS.....	76
b. Aluminum in Hornblende.....	79
E. Summary of the P-T Estimates.....	79
1. Greenschist Facies.....	79
2. Lower Amphibolite Facies.....	80
3. Middle Amphibolite Facies.....	81
a. Comparison with the Amphibolite Facies in the Skagit Gneiss.....	81
F. Age of Metamorphism.....	84
IV. STRUCTURE SECTION.....	86
A. Introduction.....	86
1. Domain Analysis.....	86

B. The Description of the Penetrative Deformational Events (D1 and D2).....	86
1. The First Deformation.....	88
a. First Foliation (S1).....	88
b. First Folds (F1).....	88
c. First Lineation (L1).....	88
d. Timing of D1 with Respect to Metamorphism.....	100
2. The Second Deformation.....	101
a. Second Foliation (S2).....	101
b. Second Lineation (L2).....	102
c. Second Deformational Strain Analysis.....	103
d. Second Deformational Kinematics.....	103
e. Timing of D2 with Respect to Metamorphism.....	108
C. Later Isolated Structures.....	123
1. Structural Features Related to the Hidden Lake Pluton.....	123
a. Pre-tectonic Versus Post-tectonic Emplacement of the Hidden Lake Pluton with Respect to D2..	124
2. Late Folds.....	128
3. Lamprophyre Dikes.....	134
D. Discussion.....	135
1. Hypothetical Macroscopic Fold to the Southeast of the Field Area.....	135
2. Estimates of the Amount of Right-lateral Ductile Shear Offset.....	136
3. Tectonics and Orogeny.....	138
a. Northward Translation and Ductile Shear.....	138

b. Relationship Between Velocity Vectors and Structures.....	138
V. Summary.....	141
VI. References.....	144
VII. Appendix 1. Sample petrography and mineral assemblages	152
VIII. Appendix 2. Whole rock chemical analyses.....	159
IX. Appendix 3. Mineral compositions.....	163

LIST OF FIGURESPage Number

INTRODUCTION SECTION

Figure 1.	Regional setting of the Crystalline Core.....	3
Figure 2.	Location of the possible tectonostratigraphic terranes in the Crystalline Core.....	5
Figure 3.	Major rock types in the Crystalline Core.....	7
Figure 4.	Distribution of the Cascade River and Napeequa Units in the vicinity of the study area.....	9
Figure 5.	Major rock units in the study area.....	10

PETROGRAPHY, FIELD RELATIONS, AND ROCK UNITS SECTION

Figure 6.	Geologic map of the study area.....	17
Figure 7.	Geochemical discrimination diagrams.....	20
Figure 8.	Metaconglomerate handsample photos.....	24
Figure 9.	Photomicrograph of metaconglomerate.....	25
Figure 10.	Photomicrograph of a dacite clast in metaconglomerate.....	26
Figure 11.	Field sketch of bedded features in the metamarl- semipelite-pelite unit.....	28
Figure 12.	Semipelite handsample photo.....	29
Figure 13a,b	Handsample photo and photomicrograph of a quartz biotite schist.....	31
Figure 14a,b.	Photomicrographs of two serpentinites.....	34
Figure 15a,b.	Handsample photos and photomicrograph of forsterite-talc bearing ultramafite.....	35
Figure 16a,b.	Handsample photos of two metagabbros.....	37
Figure 17a,b.	Handsample photos of a quartzo-feldspathic schist containing a granitic clast.....	40

Figure 18. Field sketch of graded bedding in the quartzo-
feldspathic unit..... 41

Figure 19a,b. Photomicrographs of a mica schist..... 43

Figure 20a,b. Handsample photos of amphibolites and
garbenschiefer..... 45

Figure 21. Handsample photo of a quartz mica schist..... 46

Figure 22. Handsample photo of a calcareous amphibolite
layer in a kyanite bearing mica schist..... 47

Figure 23. Handsample photo and sketch of a graphitic mica
schist..... 50

Figure 24. Schematic sketch showing the possible deposition-
al environment for the Western Cascade River unit 52

Figure 25. Schematic sketch showing the principal facies
variation around a volcanic arc..... 53

Figure 26. Combined geologic maps of the Lookout Mountain
(Cary, M.S. thesis)-Sibley Creek areas (this
study)..... 57

Figure 27. Regional geologic map showing the distribution
of the Cascade River and Napeequa units and the
distribution of the correlated rock units..... 60

Figure 28. Generalized stratigraphic columns for the west-
ern and Northeastern Cascade River units..... 62

METAMORPHIC SECTION

Figure 29. Field map showing the locations of critical
assemblages and metamorphic facies..... 66

Figure 30. Petrogenetic grid..... 70

Figure 31. Ca-amphibole composition plot..... 72

Figure 32.	P-T grid showing the GRIPS and garnet-biotite results.....	77
Figure 33.	Map showing the location of samples used in geothermobarometry.....	78
Figure 34.	Graph showing the stability limits of index minerals across the Cascade River Schist-Skagit Gneiss belt.....	83
STRUCTURE SECTION		
Figure 35.	Equal area projections of the poles to foliations for domains A, B, C1 and C2.....	90
Figure 36.	Equal area projections of the lineations for domains A, B, C1 and C2.....	92
Figure 37.	Equal area projections of S1 + S2 and L1 + L2 and miscellaneous projections.....	94
Figure 38.	Cross-sections.....	96
Figure 39.	Field sketch of a F1 mesoscopic fold.....	97
Figure 40a,b.	Microfiche photo of L1 hornblende and an internal fabric in a garnet in a D1 tectonite.....	99
Figure 41.	Flinn plot of the axial ratios of clasts in D1 and D2 metaconglomerate tectonites.....	105
Figure 42.	Kinematic indicator map.....	107
Figure 43a,b.	Photomicrograph and sketch of boudinaged idiomorphic epidote.....	109
Figure 44.	Photomicrograph and sketch of a S-C mylonite showing dextral shear.....	111
Figure 45a,b.	Photomicrographs of quartz fibers adjacent to a magnetite grain and boudinaged hornblende.....	113
Figure 46a,b.	Photomicrograph of a sheared garnet.....	114

Figure 47.	Photomicrograph of a chloritized biotite adjacent to a C surface.....	115
Figure 48a-k.	Microfiche photographs of various deformational features.....	117-122
Figure 49.	Diagram showing overturning of the dextral kinematic indicators by folding.....	126
Figure 50.	Map showing structural features along the north-western margin of the Hidden Lake pluton.....	127
Figure 51.	Handsample sketch of a mesoscopic open later fold.....	130
Figure 52.	Handsample sketch of a graphitic mica schist showing a rare semi-penetrative axial planar cleavage related to later foling.....	131
Figure 53.	Microfiche photo of a garnet containing an internal planar fabric.....	133
Figure 54.	Diagram showing simple shear model and possible amounts of D2 shear across domains A and B.....	137
Figure 55	Velocity vector diagrams for the Kula and Farallon plates at the field area.....	140

LIST OF TABLES

	<u>Page Number</u>
Table 1. Geochemical descrimination diagram results.....	21
Table 2. Key mineral assemblages for the greenschist, lower, and middle amphibolite facies.....	64
Table 3. Upgrade grain size variation.....	68
Table 4. Garnet-biotite temperatures (ideal solution model)..	75

Table 5. Garnet-biotite temperatures (non-ideal solution models).....	76
Table 6. Pressure of solidification for the Marble Creek pluton using the Al-content of hornblende.....	79
Table 7. General domain characteristics.....	87
Table 8. Summary of the kinematic analysis.....	104
Table 9. Petrographic evidence for late-metamorphic D2 shear.	108
Table 10. Orientation of the velocity vectors at selected sites along Western North American.....	139

INTRODUCTION

Regional Setting

The Sibley Creek area is part of the Crystalline Core of the Northern Cascades of Washington (Misch, 1966). This geologic province is a fault bounded wedge, approximately 150 X 90 kilometers, consisting dominantly of schists, gneisses, migmatitic zones, and abundant plutons. Ages range from Precambrian to Late Cenozoic, but the most significant orogenic activity appears to be from Late Cretaceous to the Early Tertiary (90-60 Ma; Mattinson, 1972). Prior to dextral Tertiary offset (80-180 km) on the Straight Creek fault, the Crystalline Core resided next to, and is probably an extension of, the Coast Plutonic Complex of British Columbia (Fig. 1).

Tabor et al. (1987) divided the Crystalline Core into 5 tectonostratigraphic terranes (Fig. 2). The present study area is situated within the Chelan Mountains terrane, which is composed of two northwest trending belts. The more southwesterly belt consists of metaplutonic rocks, including the Dumbell-Marblemount plutons of Triassic age and the Entiat pluton of Late Cretaceous age (Fig. 3). The more northeasterly belt is composed of schists which are variable in lithology along the belt. The Cascade River Schist lies at the northwest end of the belt; the younger gneissic rocks of the Holden Area are in the center; and the southeast end are the migmatites of the Chelan Complex. Bordering the Chelan Mountains terrane to the northeast is the Skagit Gneiss, whereas to the southwest lies the Mad River terrane. The protoliths of the Chelan Mountains terrane are similar to the adjacent Mad River terrane, although the terranes are separated everywhere by faults (Tabor, et al., 1987; Fig. 3). Recently, Tabor et al. (in press) have expanded the Chelan Mountains terrane (Fig. 2) to include the Neepequa Schists and plutons of the Mad

Figure 1. Regional setting of the Crystalline Core (CC). Surrounding terranes and regional rock groups include the Northwest Cascade System (NWCS), which is separated from the CC by the Straight Creek fault (SCF), and the Methow (MT) by the Ross Lake fault (RLF). Other groups include the Hozomeen (HZ), Quesnellia (QN), Bridge River (BR), Coast Plutonic Complex (CPC), Nanaimo Group (N), Wrangellia (WR), Omineca Crystalline Belt (OCB) and Cenozoic lithologies (CZ). Location of the field area is shown by the small box. Note that the removal of the 80-180 km of right-lateral offset of the Tertiary Straight Creek fault places the Crystalline Core next to the Coast Plutonic Complex.

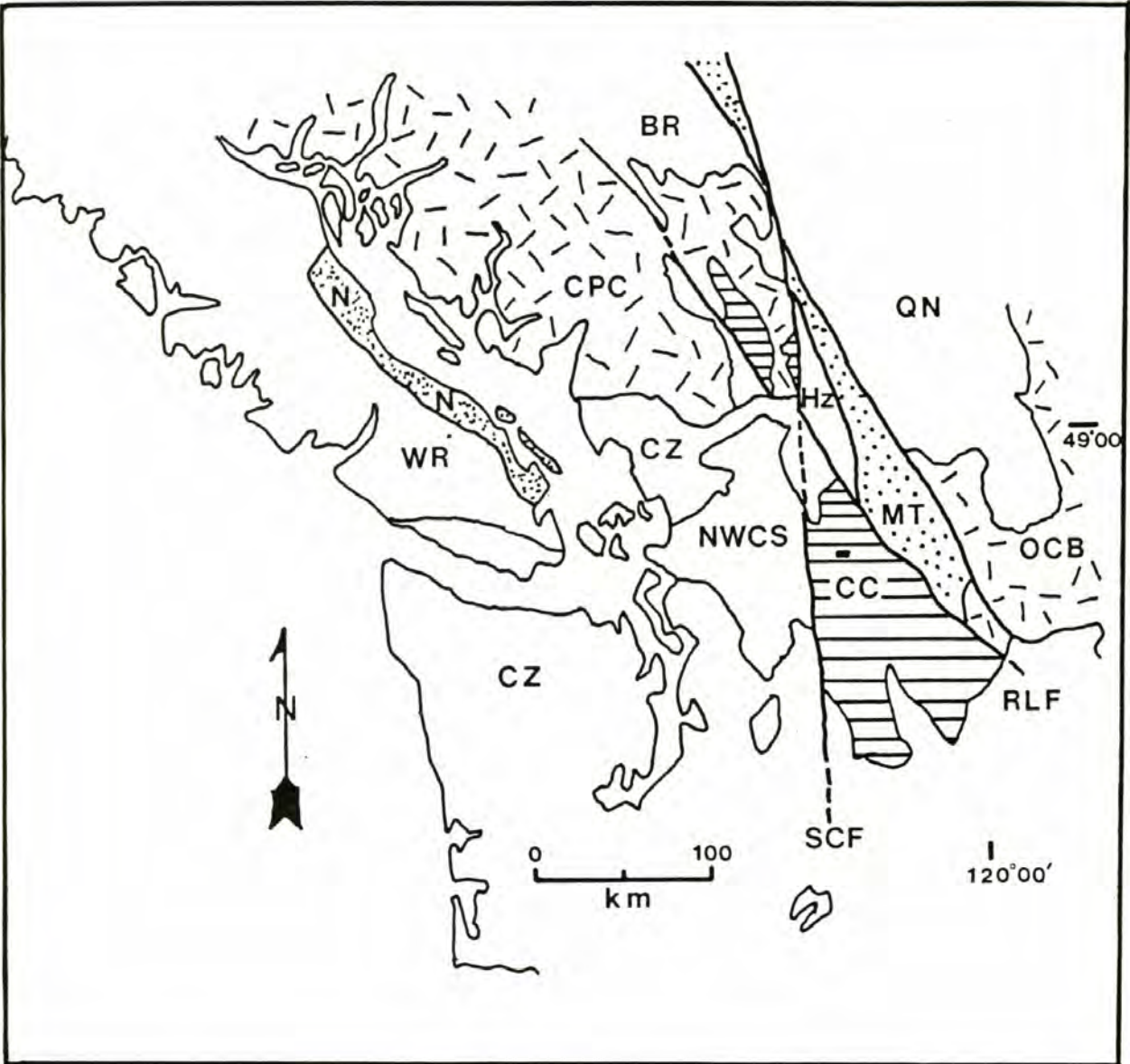


Figure 2. Location of possible major tectonostratigraphic terranes in the [Skagit] Crystalline Core adapted from Tabor et al. (1987). Recently Tabor (in press) has included the Mad River terrane in the Chelan Mountains terrane due to the compositional similarities of the schists in both terranes. Field area is shown by the box. ST = Swakane terrane, C.R.B. = Columbia River Basalts.

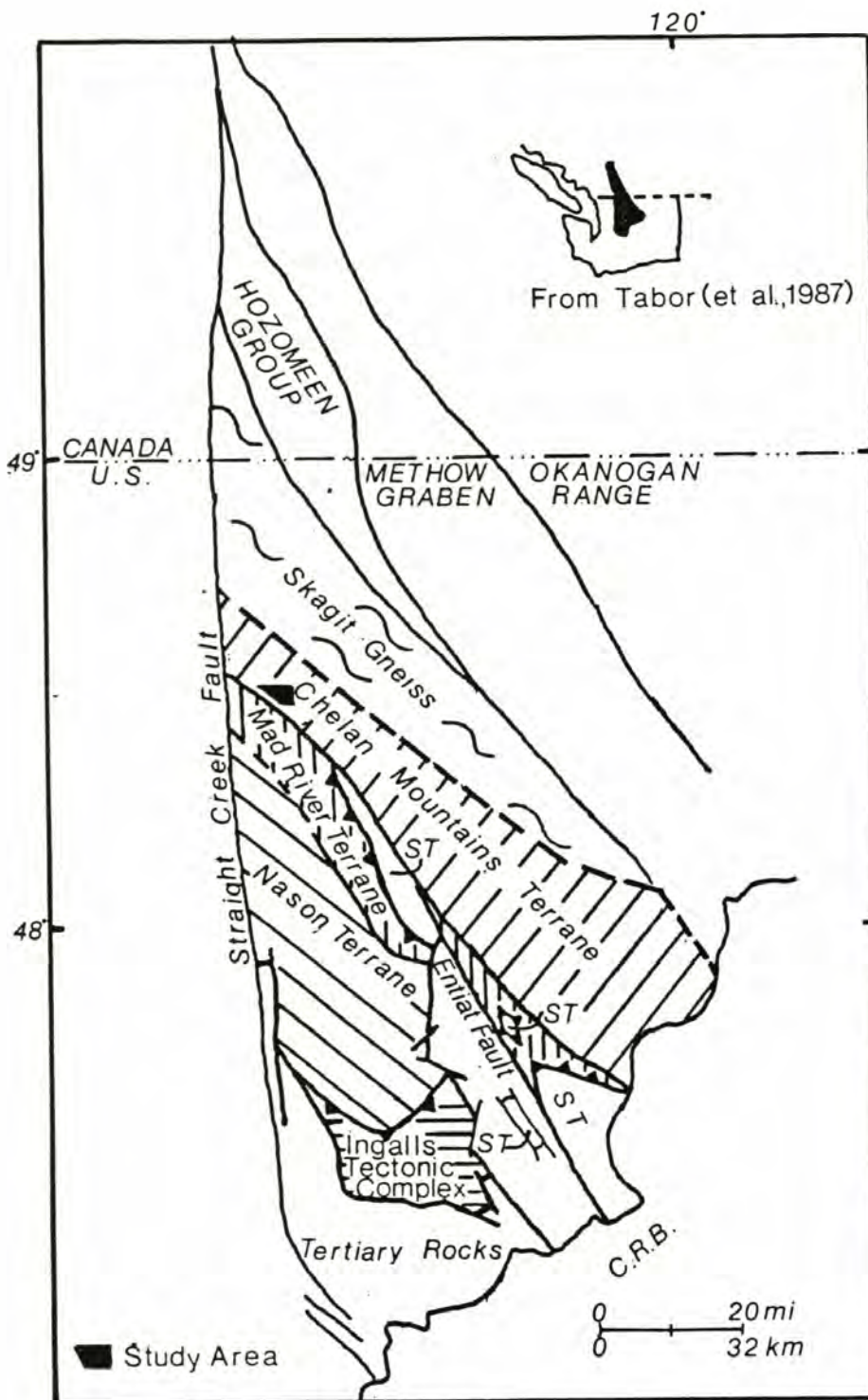


Figure 3. Major rock types of the Crystalline Core. From south to the north these rock types include the Mount Stuart pluton (MS), Tertiary granites (Tg), Entiat pluton (EN), Chelan pluton (CHL), Ten Peak pluton (TP), Sloan Creek plutons (SC), Sulfur Mountain pluton (SM), Downey Creek pluton (DC), Bench Lake pluton (BL), Chaval pluton (CH), Cyclone Lake pluton (CL), Jordan Lake pluton (JL), Cascade River Schist (CRS), Marblemount Meta-Quartz Diorite (MMQD), Eldorado Orthogneiss (EL), Hidden Lake pluton (HLP), Marble Creek pluton (MCP), Alma Creek pluton (A), Haystack Creek pluton (H). Field area is shown by the box. Adapted from E.H. Brown.

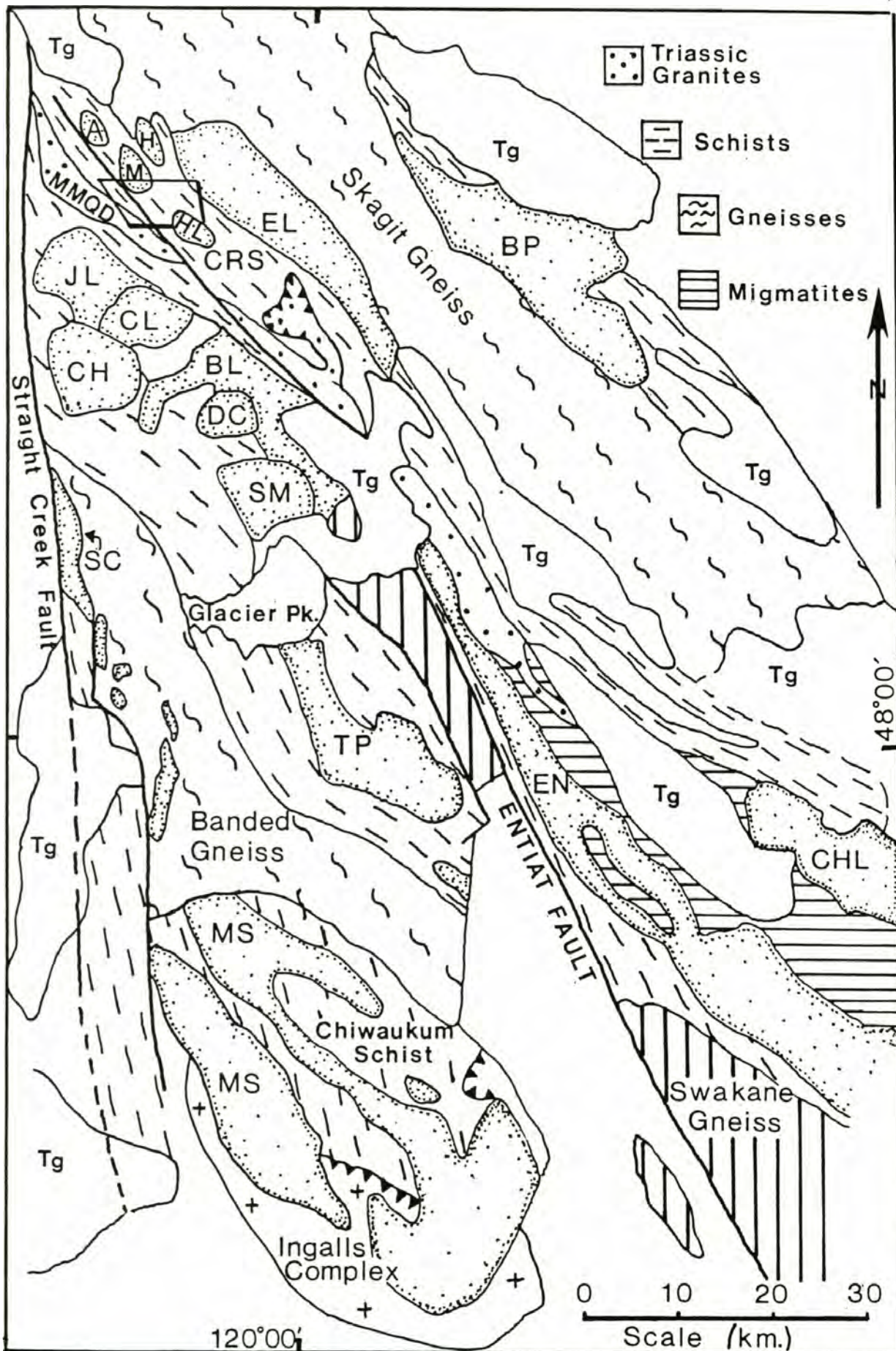
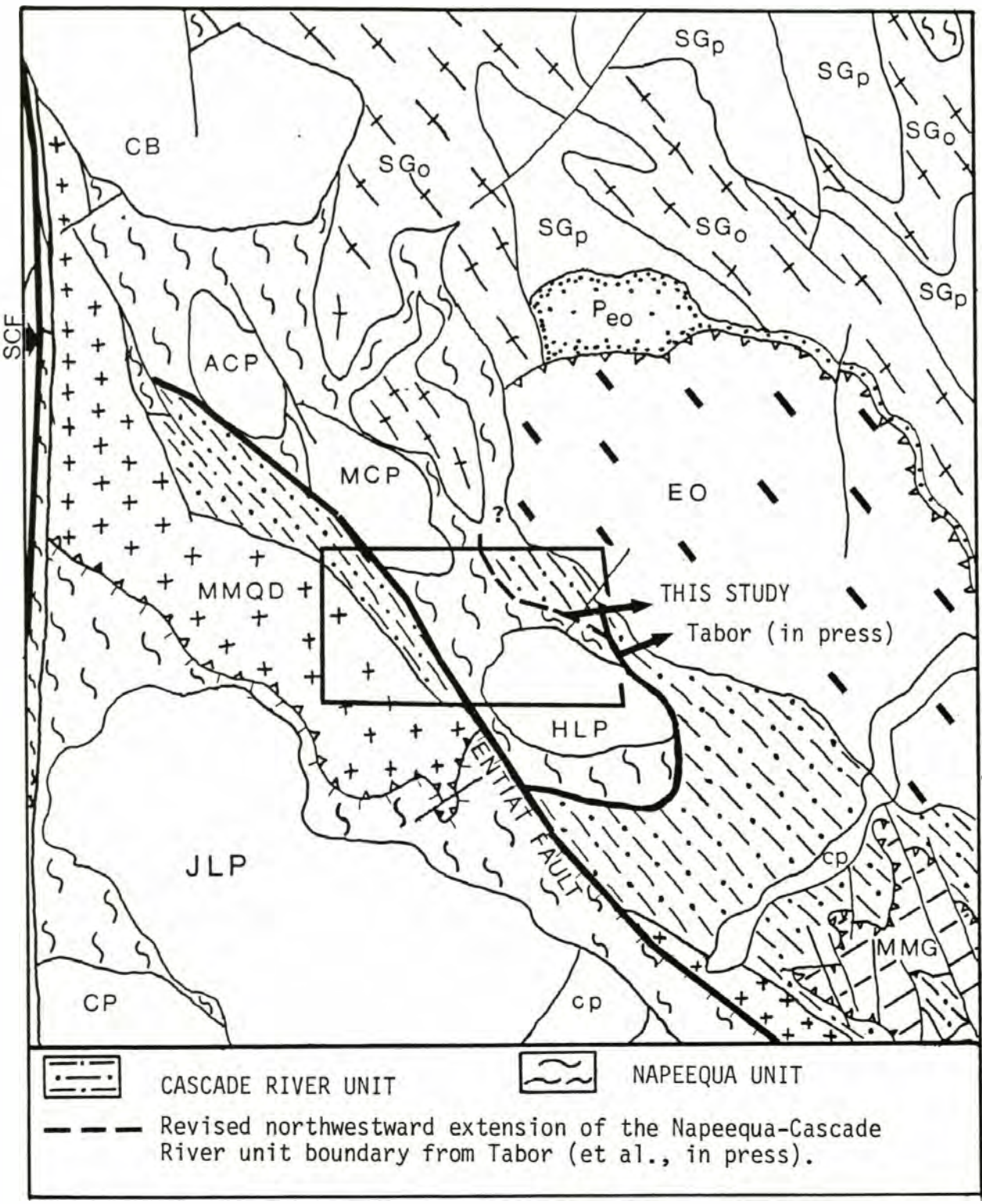


Figure 4. Distribution of the Cascade River and Napeequa units of the Chelan Mountains terrane (revised from Tabor et al., in press). Hatched line along the southern part of the Entiat fault and along the contact between the MMQD and the schists is the former Chelan Mountains-Napeequa terrane boundary. The boundary between the Cascade River and Napeequa units has been revised from Tabor (et al., in press; see dashed line in the study area box). Major rock units around the study area include the Magic Mountain Gneiss (MMG), Jordan Lake pluton (JLP), intrusives of the Cascade Pass family (Cp), Cheval pluton (CP), Hidden Lake pluton (HLP), Eldorado Orthogneiss (EO), pegmatite associated with the Eldorado Orthogneiss (Peo), Marblemount Meta-Quartz Diorite (MMQD), Marble Creek pluton (MCP), Alma Creek pluton (ACP), Chilliwack Batholith (CB), Skagit Orthogneiss and Paragneiss (SGo and SGp), and the Straight Creek fault (SCF). Study area is shown in the box.



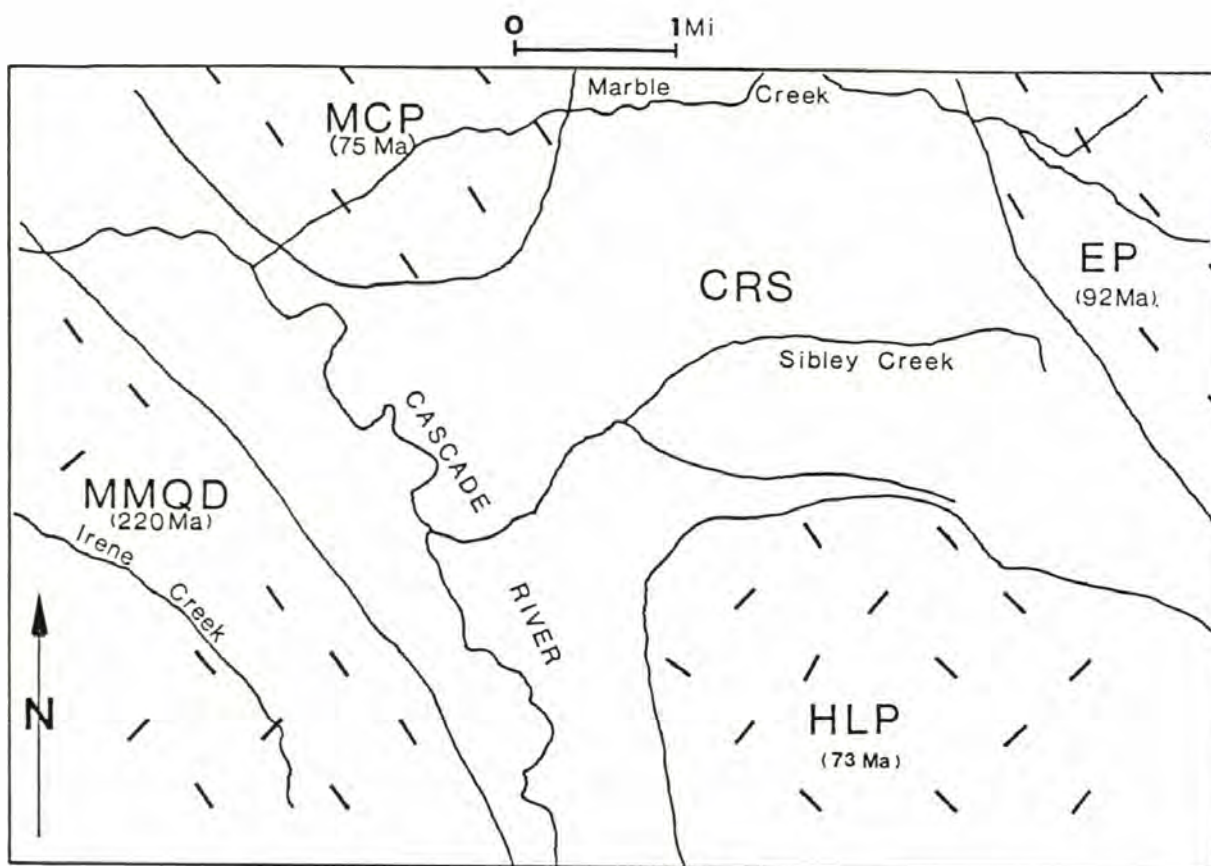


Figure 5. Major rock units in the field area. These include the Cascade River Schist (CRS) of Misch (1966), Triassic Marblemount Meta-Quartz Diorite (MMQD; 220 Ma, Mattinson, 1972), Eldorado pluton (EP; 92 Ma; Mattinson, 1972), Marble Creek pluton (MCP; 75 Ma; Haugerud et al., 1987), and the Hidden Lake pluton (HLP; 73 Ma; Haugerud et al., 1987).

River terrane (Fig. 3; Fig. 4). In this new scheme the Cascade River Schist of Misch (1966, 1968, 1979) includes oceanic rock types assigned to the Neepequa unit, as well as distinctive metaconglomerate and associated metagraywackes, rare pelites, and a variety of metavolcanic rocks, which are assigned to the Cascade River unit (Fig. 4).

The Sibley Creek Area

The study area is situated across the northwest trending Cascade River Schist belt (Fig. 5). Plutonic bodies associated with the Cascade River Schist in the study area are: the Eldorado Orthogneiss in the northeastern area, the Marblemount Meta-Quartz Diorite in western area, the Marble Creek pluton in the northwestern area, and the Hidden Lake pluton in the southeastern area (Fig. 5). The Eldorado, Marblemount Meta-Quartz Diorite and Marble Creek plutonic bodies are deformed, whereas the Hidden Lake pluton is generally not deformed.

Marblemount Meta-Quartz Diorite

The Marblemount Meta-Quartz Diorite is tonalitic to dioritic in composition, and is metamorphosed in the greenschist facies. Lead isotopic ratios from zircons of the Marblemount Meta-Quartz Diorite are concordant and give an age of 220 Ma (Mattinson, 1972). The Marblemount Meta-Quartz Diorite may be correlative with the Le Conte and Magic Mountain Gneisses, which are observed on strike 10 kilometers to the southeast (Tabor, 1961), as well as the Dumbell Mountain plutons in the Chelan area (Cater, 1982).

Cascade River Schist

The protoliths of the Cascade River Schist consist largely of arc-derived clastic deposits and minor volcanics. The clastics include metamorphosed graywackes and arkosic arenites, and siltstones of similar

composition which are now mica- and quartzofeldspathic schists (Misch, 1966). The geochemistry of meta-sediments suggests an immature provenance, probably a magmatic arc (Babcock and Misch, 1988). The protolith compositions of the volcanic rocks include tholeiitic basalts and andesites with an oceanic affinity, which are now amphibolites (Babcock and Misch, 1988). Some of the clastic rocks may have been tuffaceous, others show dolomitic admixtures, and some quartzites possibly represent cherty interbeds (Misch, 1966).

The similarity between the clasts in a conglomerate unit of the Cascade River Schist and the Marblemount Meta-Quartz Diorite led Misch (1966) to postulate that the Marblemount Meta-Quartz Diorite is basement to the adjacent Cascade River Schist. Cary (M.S. thesis in progress) reports a U/Pb zircon date of 220 Ma (by Stacey) on a metatuff unit located adjacent to the Marblemount Meta-Quartz Diorite, the same age as that determined for the Marblemount Meta-Quartz Diorite. Using this date, and field observations, Cary postulates that the Marblemount Meta-Quartz Diorite and the adjacent metabasites and tuffs of the Cascade River Schist represent cogenetic plutonic and volcanic members of a magmatic arc.

Metamorphism of the Crystalline Core, including the Cascade River Schist, has been interpreted from U/Pb dating of zircon and sphene to have occurred between 60 and 90 Ma (Mattinson, 1972). This metamorphism was generally of Barrovian type. Geothermometry and barometry on the Skagit Gneiss (Whitney, 1987), which borders the Cascade River Schist on the northeast, suggests that this part of the Crystalline Core reached temperatures of approximately 650–720 C and pressures of 8–10 Kb. In the Chiwaukum and Settler Schists, a Barrovian event was superimposed on a Buchan type metamorphism associated with the syntectonic intrusion of the Mount Stuart Batholith (Evans and Berti, 1986). In other areas of the

core the relationship between plutonism and metamorphism is less clear.

The Cascade River Schist is in the greenschist facies along a narrow zone along the southwestern side of the Cascade River. The grade rises abruptly to the amphibolite facies to the northeast towards the Skagit Gneiss, and slowly to the southeast along the Cascade River Schist belt towards the Chelan Complex (Misch, 1966). The northeasterly increase in grade, which is evident in the study area, reaches the kyanite zone along the boundary between the Cascade River Schist and the Skagit Gneiss (Misch, 1966). In the Skagit Gneiss, late growth of sillimanite is attributed to isothermal decompression following peak metamorphic conditions in the kyanite zone (Whitney, 1987).

Structural trends within the Cascade River Schist defined by fold axes, strike of the foliation, and post-orogenic faults are dominantly north to northwest, as they are throughout the Crystalline Core. Bedding, where preserved, is commonly parallel to foliation (Misch, 1966). A strike-parallel mineral lineation is commonly found on the foliation surface (Misch, 1966).

Syn and Post-Tectonic Plutons

Cretaceous syn-to post-metamorphic plutons are widespread, and appear to be important in the orogenic history of the Crystalline Core. Pre-to syn-tectonic plutons in the field area include the Marble Creek pluton and the Eldorado pluton, both of which are foliated and are concordant with the fabric in the Cascade River Schist. The U/Pb age of the deformed Marble Creek pluton is 75 Ma, and that of the deformed Eldorado pluton is 92 Ma (Mattinson, 1972; Haugerud, et al., 1987). The undeformed Hidden Lake pluton gives a U/Pb age of 73 Ma (Haugerud, et al., 1987).

Faults in the Study Area

The Le Conte fault, as mapped by Tabor (1961), has recently been correlated with the Entiat fault along strike to the southeast (Tabor, et al., in press; Fig. 3). This fault appears to be a significant tectonic boundary within the field area. Tabor (1961) reports that the fault is marked by contrasting lithologies and metamorphic grades on opposite sides in the South Cascade River area some 8 kilometers south of the study area. This indicates that movement has taken place after regional metamorphism to bring rocks of contrasting facies together (Tabor, 1961). The partial displacement of the Cloudy Pass quartz diorite and the apparent truncation of the South Cascade Glacier stock indicate that some Tertiary movement has occurred along the fault.

Statement of the Problems

Many questions concerning the tectonic evolution of the Crystalline Core remain unanswered. This study is focused upon the Cascade River Schist and contributes information concerning the protoliths of the metamorphic rocks, metamorphic conditions, deformational events and kinematics during and after metamorphism.

Problems investigated in this study are:

- (1) The distribution, composition, and tectonic setting of the protoliths of the Cascade River Schist.
- (2) The pressure-temperature conditions of metamorphism.
- (3) The number, sequence and kinematics of the deformational events affecting the Cascade River Schist, as well as their relationship to metamorphism.

These aspects will contribute to the understanding of the depositional environment of the Cascade River Schist and the mechanics of orogeny.

PETROGRAPHY, FIELD RELATIONS, AND ROCK UNITS OF THE CASCADE RIVER SCHIST

Introduction

The focus of this study is on the Cascade River Schist, which occupies the central part of the study area. The geologic and sample site maps are included in Plates 1 and 2 (pertinent sample numbers are given in the text). Mineral assemblages and whole rock geochemical data are given in Appendix 1 and 2. The Cascade River Schist in the study area is derived from a diverse assemblage of protolith rock types, it exhibits a metamorphic grade ranging from the greenschist to the amphibolite facies, and it contains several generations of structures. In the following, the rock units are described from west to east across the study area (Fig. 6). The grain size classification employed is: very fine-grained (less than .25 mm), fine-grained (.25-1.0 mm), medium-grained (1-5 mm), and coarse-grained (greater than 5 mm).

Rock Units West of the Le Conte Fault

The five rock layers west of the Le Conte fault include a greenschist, brown phyllite, metaconglomerate, metatuff, and metamarl-semipelite-pelite units (Fig. 7). These traceable units generally strike to the northwest and dip steeply to the southwest (Fig. 6), and include metasedimentary and metavolcanic lithologies assigned to the arc-related Cascade River unit of Tabor et al. (in press; Fig. 4). These rock units are similar in composition to the northeastern Cascade River unit and differ from the oceanic Napeequa unit in the central part of the field area (Fig. 4).

Greenschist Unit

The greenschists are dark green, well-foliated mylonites which contain sub-angular saussuritized relict plagioclase phenocrysts (1-5 mm)(20-30%) in a strongly sheared matrix of quartz and albite (30-40%).

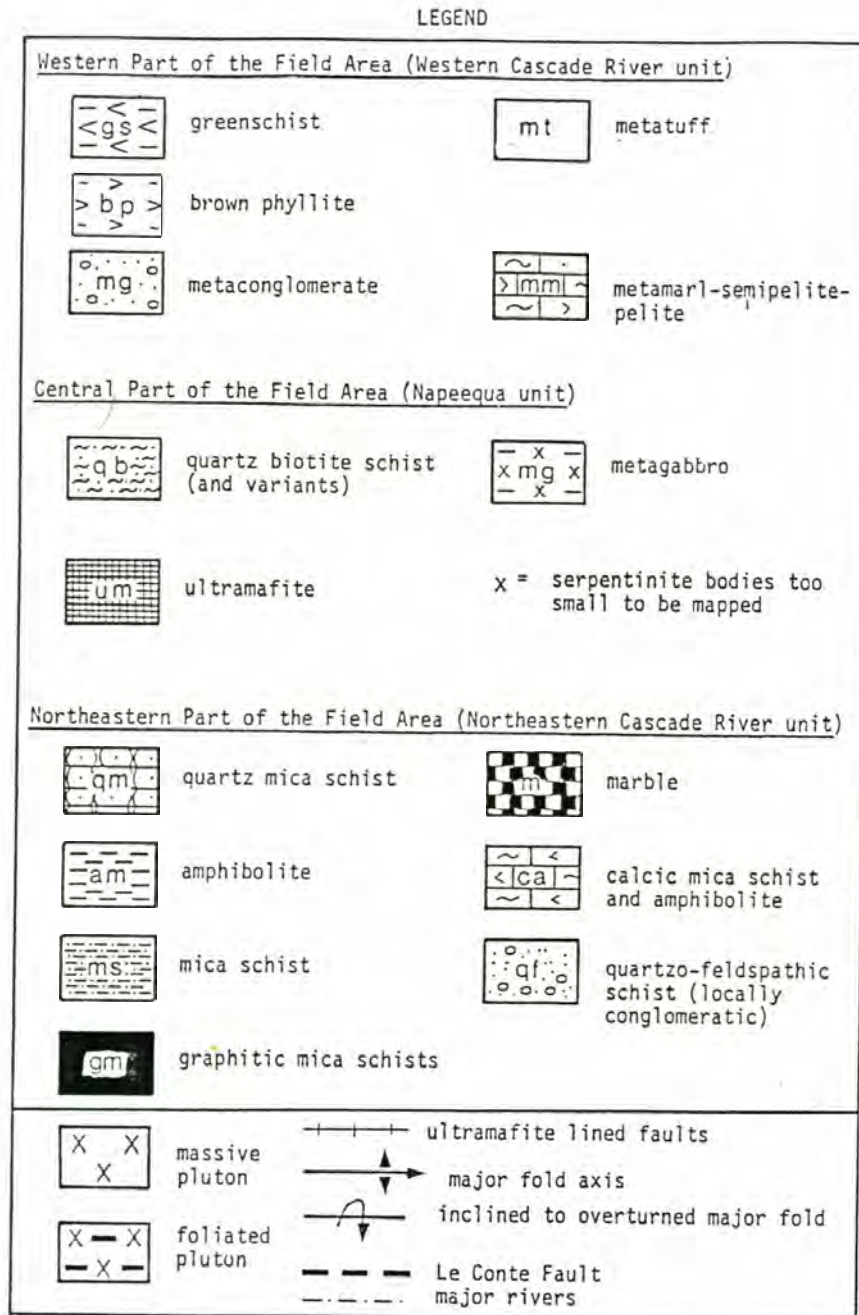
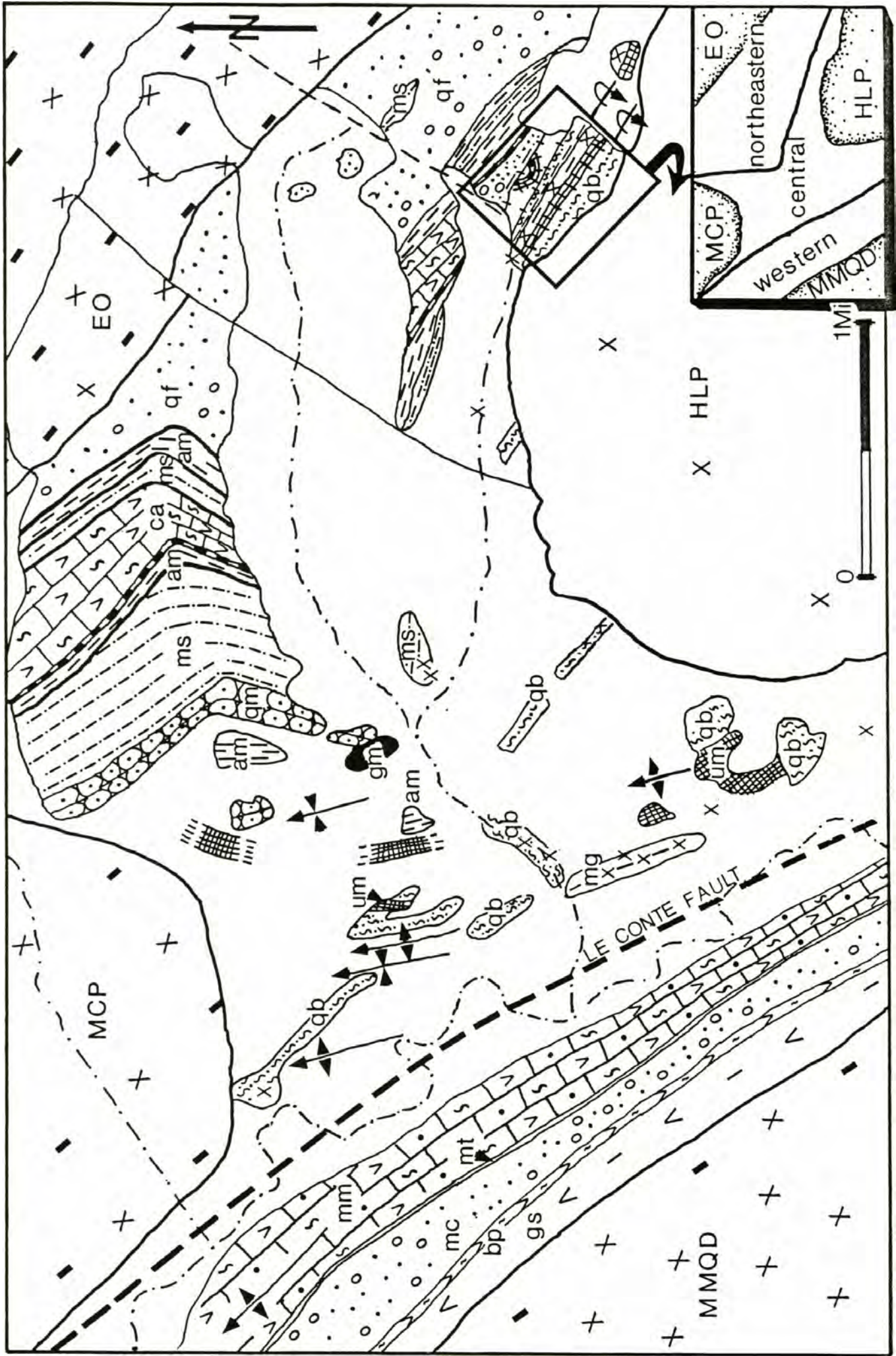


Figure 6. General geologic map of the study area. Inset shows regions referred to in the text. Details in the box are given in the more detailed field map (Plate 1). The portion of the map east of the Le Conte fault is an outcrop map, whereas the portion of the map west of the fault disregards the alluvium distribution, except for along the Cascade River.



The plagioclase phenocryst cores are more saussuritized than the rims indicating that the plagioclase was originally normally zoned with calcium rich cores. Other minerals include 1-2 mm in length aligned actinolite (7-10%), epidote, and chlorite (10%). Accessory minerals include pyrite, magnetite, and ilmenite. Biotite is present in all the units west of the Le Conte fault but is partially to wholly chloritized due to late shear (see Structure Section).

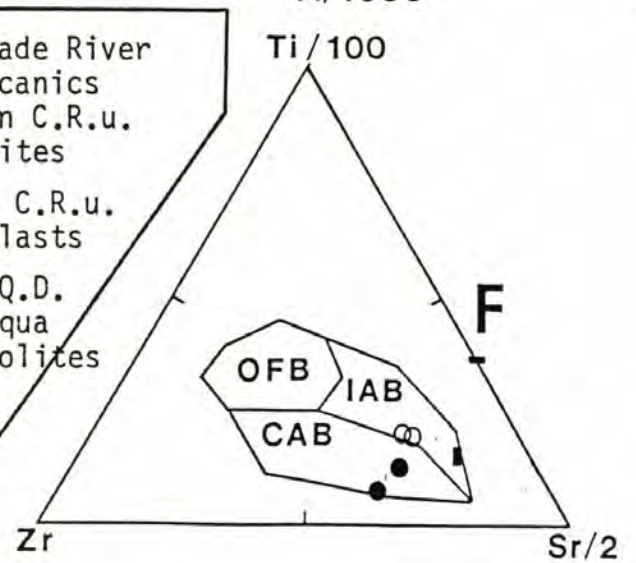
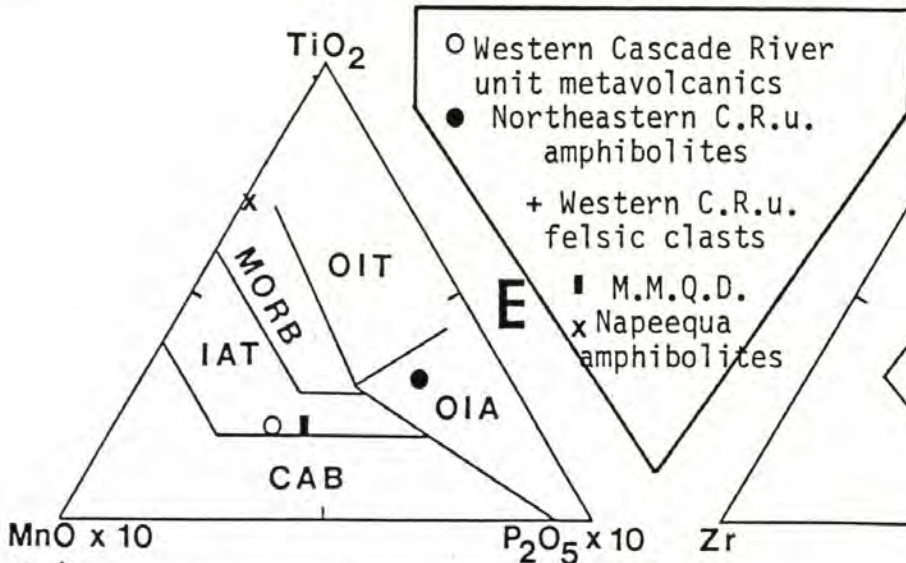
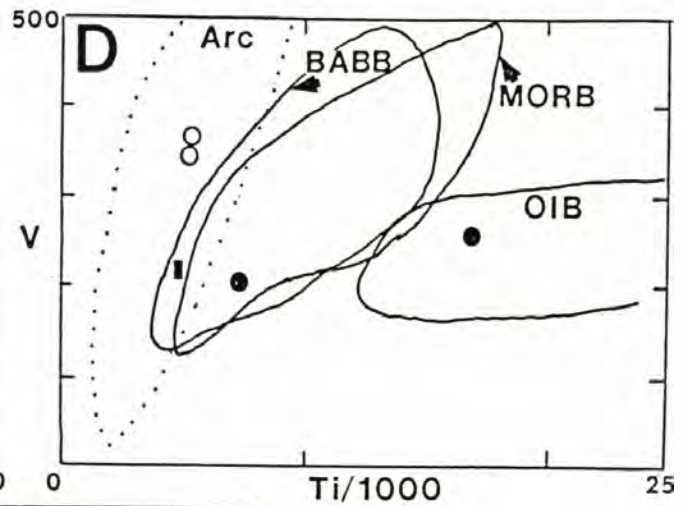
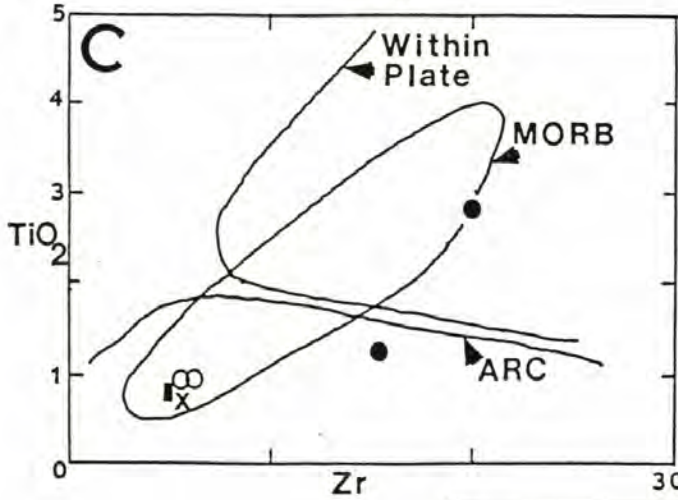
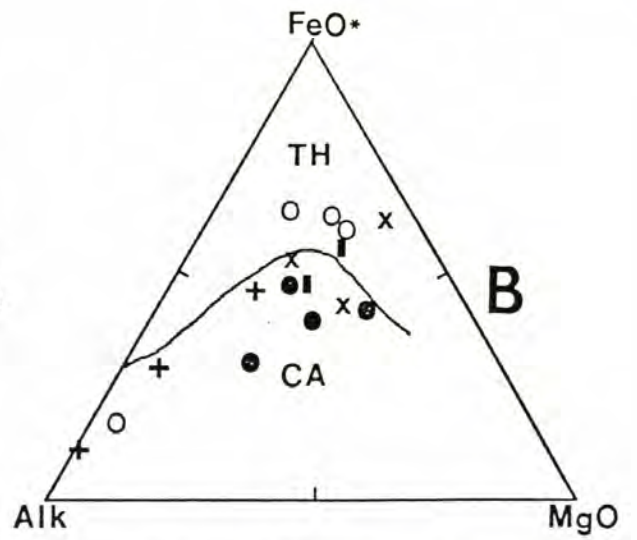
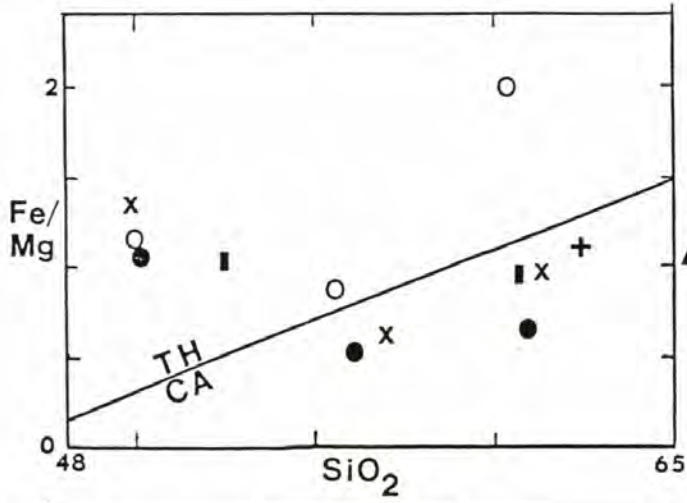
The contact between the Marblemount Meta-Quartz Diorite and the greenschists is defined by a gradational sheared border zone. The Marblemount Meta-Quartz Diorite is semi-massive and medium-grained west of the contact and becomes increasingly fine-grained towards the mylonitized greenschist unit. The possibility that these mylonitized greenschists are sheared Marblemount Meta-Quartz Diorite can not be excluded. However, the greenschist unit is continuous with less-sheared metavolcanics (Cary, pers. comm.) directly on strike to the northwest in the Lookout Mountain area, suggesting a similar protolith composition for the greenschists in this study area. The extensive sausseritization of the plagioclase phenocrysts indicates that the protolith contained calcic plagioclase, and thus was probably basalt or andesite. Whole rock geochemistry of similar rocks on Lookout Mountain suggests that the protoliths are tholeiitic basalt, andesite, and minor rhyolite of an arc-affinity (Fig. 7; Table 1).

Brown Phyllite Unit

The brown phyllitic unit is thin (10-20 meters thick), mylonitic, well-foliated, commonly fissile, and contains abundant white mica and plagioclase clasts. In comparison to the greenschist unit, epidote and actinolite are lacking, and white mica (30-40%) is abundant. The other minerals are chlorite, opaque and sphene. The rock is apparently derived

Figure 7. Geochemical discrimination diagrams (see Table 1 for synopsis). Diagrams based on; A) MgO/FeO vs. SiO_2 (Miyashiro, 1974); B) Alkalies- FeO - MgO (Irvine and Baragar, 1971); C) TiO_2 vs. Zr (Pearce and Cann, 1973); D) V vs. $Ti/1000$ (Shervais, 1982); E) $TiO_2-MnO \times 10-P_2O_5 \times 10$ (Mullen, 1983); F) $Ti/100-Zr-Sr/2$ (Pearce and Cann, 1973); G) Al_2O_3/TiO_2 vs. TiO_2 ; H) Plot of CRS amphibolites and other rock units in the Crystalline Core (Babcock and Misch, 1988).

Data from the western Cascade River unit (CRu) metavolcanics, MMQD and felsic clasts from Cary (pers. comm.). Metavolcanic affinities include CA (Calc-Alkaline), TH (Tholeiitic), Arc (basalt), MORB (Mid-Oceanic Ridge Basalt), within plate (basalt), BAB (Back-Arc Basin Basalt), OIA (Oceanic Island Arc basalt), IAT (Island Arc Tholeiite), CAB (Continental Arc basalt), IAB (Island Arc Basalt), and Oceanic (basalt).



○ Western Cascade River unit metavolcanics
 ● Northeastern C.R.u. amphibolites
 + Western C.R.u. felsic clasts
 ■ M.M.Q.D.
 x Napeequa amphibolites

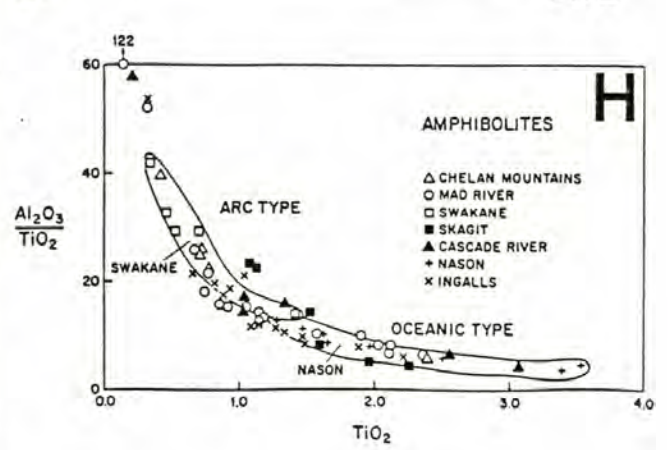
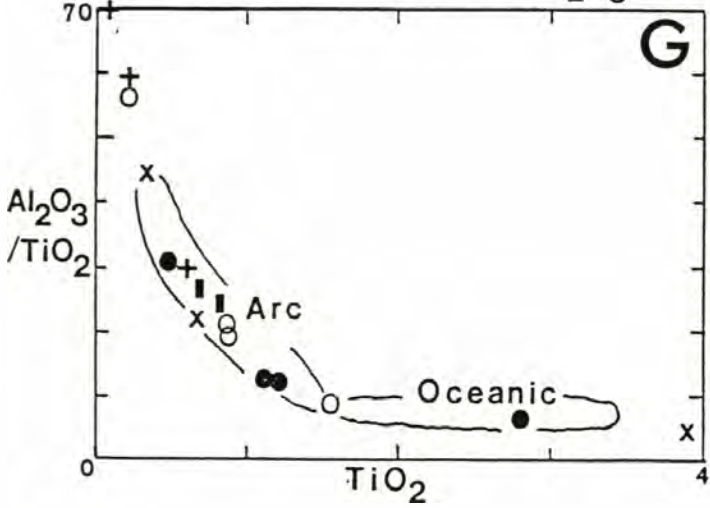


Table 1. Geochemical Discrimination Diagram Results

<u>Northeastern Cascade River Unit Metavolcanics</u>								
<u>#</u>	<u>A</u>	<u>B</u>	<u>C</u>	<u>D</u>	<u>E</u>	<u>F</u>	<u>G</u>	<u>% SiO₂</u>
6	CA	CA	-	-	-	-	-	66.9
117	CA	CA	Arc	BAB MORB	-	CAB	Arc	56.2
173	TH	CA	MORB Within Plate	OIB	OIA	CAB	Oceanic	50.1
188	CA	CA	-	-	-	-	-	60.9
<u>Western Cascade River Unit Metavolcanics (Cary, Lookout Mtn. Area)</u>								
156	CA	CA	-	-	-	-	-	79.7
14G	TH	TH	-	-	-	-	-	60.3
26I	TH	TH	MORB Arc	Arc	IAT	IAB	Arc	49.9
26H	TH	TH	MORB	Arc	-	IAB	Arc	55.5
<u>Marblemount Metaquartz Diorite (Cary, Lookout Mtn. Area)</u>								
26A	CA	CA	-	-	-	-	-	60.5
7B	TH	TH	MORB Arc	Arc BAB, MORB	IAT	IAB	Arc	52.5
<u>Felsic Clasts in the Metaconglomerate Unit (Cary, Lookout Mtn. Area)</u>								
33G	CA	CA	-	-	-	-	-	78.8
33H	CA	CA	-	-	-	-	-	62.2
31H	CA	CA	-	-	-	-	-	78.8
<u>Napeequa Metabasites</u>								
158	TH	TH	-	-	MORB	-	-	60.9
240	CA	CA	-	-	-	-	Oceanic	49.1
44*	CA	CA	-	-	-	-	Arc	54.6

Diagrams based on: A) MgO/FeO vs. SiO₂ (Miyashiro, 1974), B) Alkalies-FeO-MgO (Irvine and Baragar, 1971), C) TiO₂ vs. Zr (Pearce, 1973), D) V vs. Ti/1000 (Shervais, 1982), E) TiO₂ - MnOX₁₀ - P₂O₅X₁₀ (Mullen, 1983), F) Ti/100 - Zr - Sr/2 (Pearce and Cann, 1973), G) Al₂O₃/TiO₂ vs. TiO₂. Metavolcanic affinities include CA (Calc-Alkaline), TH (Tholeiitic), Arc (basalt), MORB (Mid-Oceanic Ridge Basalt), within plate (basalt), BAB (Back-Arc Basin Basalt), OIA (Oceanic Island Arc basalt), IAT (Island Arc Tholeiite), CAB (Continental Arc Basalt), IAB (Island Arc Basalt), Oceanic (basalt).

from a graywacke or tuff. The minor amounts of saussurite in the plagioclase clasts, characteristic of all the rock types in the Cascade River unit, except in the greenschist unit, indicate that the protoliths (or source environments) for these units contained less calcic plagioclase than the greenschist unit.

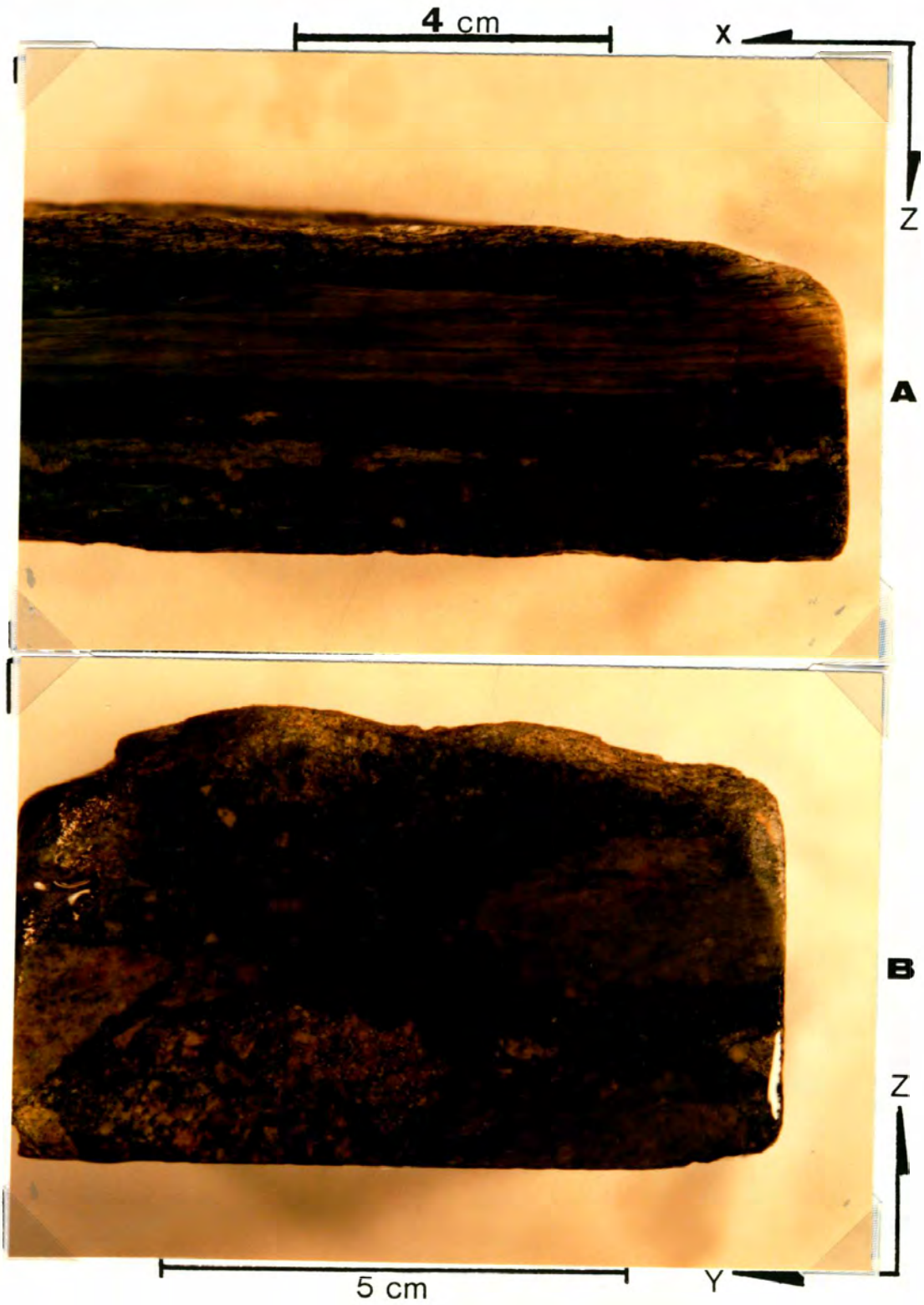
The contact between the brown phyllitic and metaconglomerate units is defined by a northwest trending linear swampish depression. This depression is the result of differential weathering, faulting, and/or shearing concentrated between these units. This zone also appears to be an area of hydrothermal alteration, as evidenced by abundant pyrite and iron oxide stain observed in the rocks adjacent to this depression.

Metaconglomerate Unit

The metaconglomerate unit contains rounded and stretched clasts of tonolitic to quartz diorite, dacite, minor fine-grained sedimentary rock, with plagioclase grains and a quartzo-feldspathic, micaceous matrix (Fig. 8, 9, 10). The clasts range in size from pebbles to rare boulders. The matrix and clasts are generally sub-equal in proportion, thus the rock is matrix supported. Chemical analysis of three felsic clasts from Lookout Mountain (Cary, pers. comm.) indicates that they are dacitic to rhyolitic in composition (Fig. 2).

The matrix contains sub-angular, medium-grained plagioclase clasts (20-40%) and a fine-grained, sheared matrix of quartz and albite in sub-equal proportions (20-30%), with 30% or less epidote, 30% or less chlorite, and white mica (Fig. 8, 9, 10). Biotite is minor due to pervasive late chloritization.

Figure 8. Metaconglomerate containing dacite and granitic clasts. Note the extreme stretching of the dacite clasts observed in the XZ plane (A) in contrast to the Y-Z section (B)(see Structure Section)(95- numbers in figure captions refer to sample numbers). Microphotograph of sample 95 is shown in Figure 9.



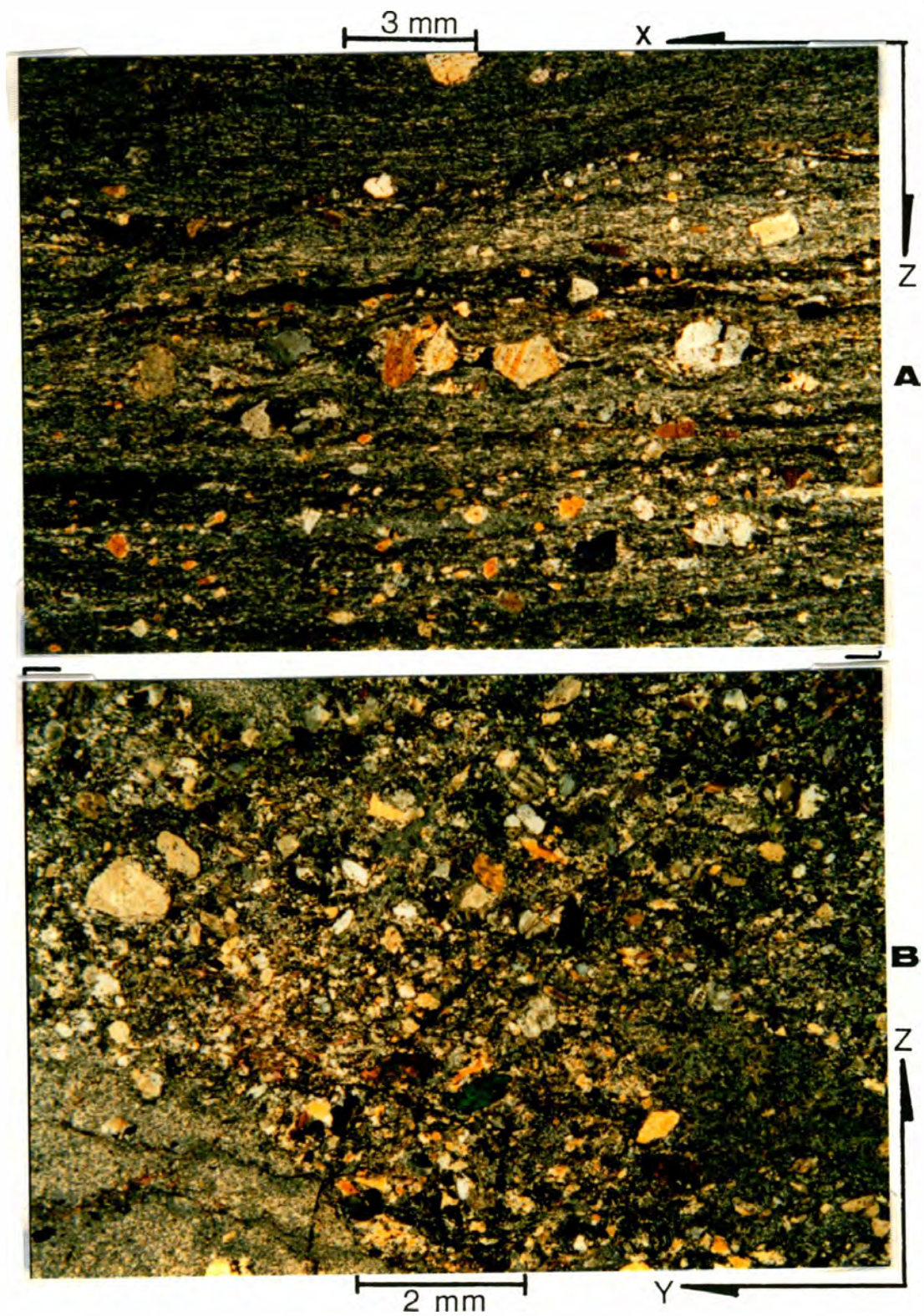


Figure 9. Photomicrograph of the matrix of a metaconglomerate (95) showing: (A) extreme granulation of the quartzo-feldspathic matrix and boudinage of the plagioclase clasts; (B) dacite clast in the lower left-hand corner.

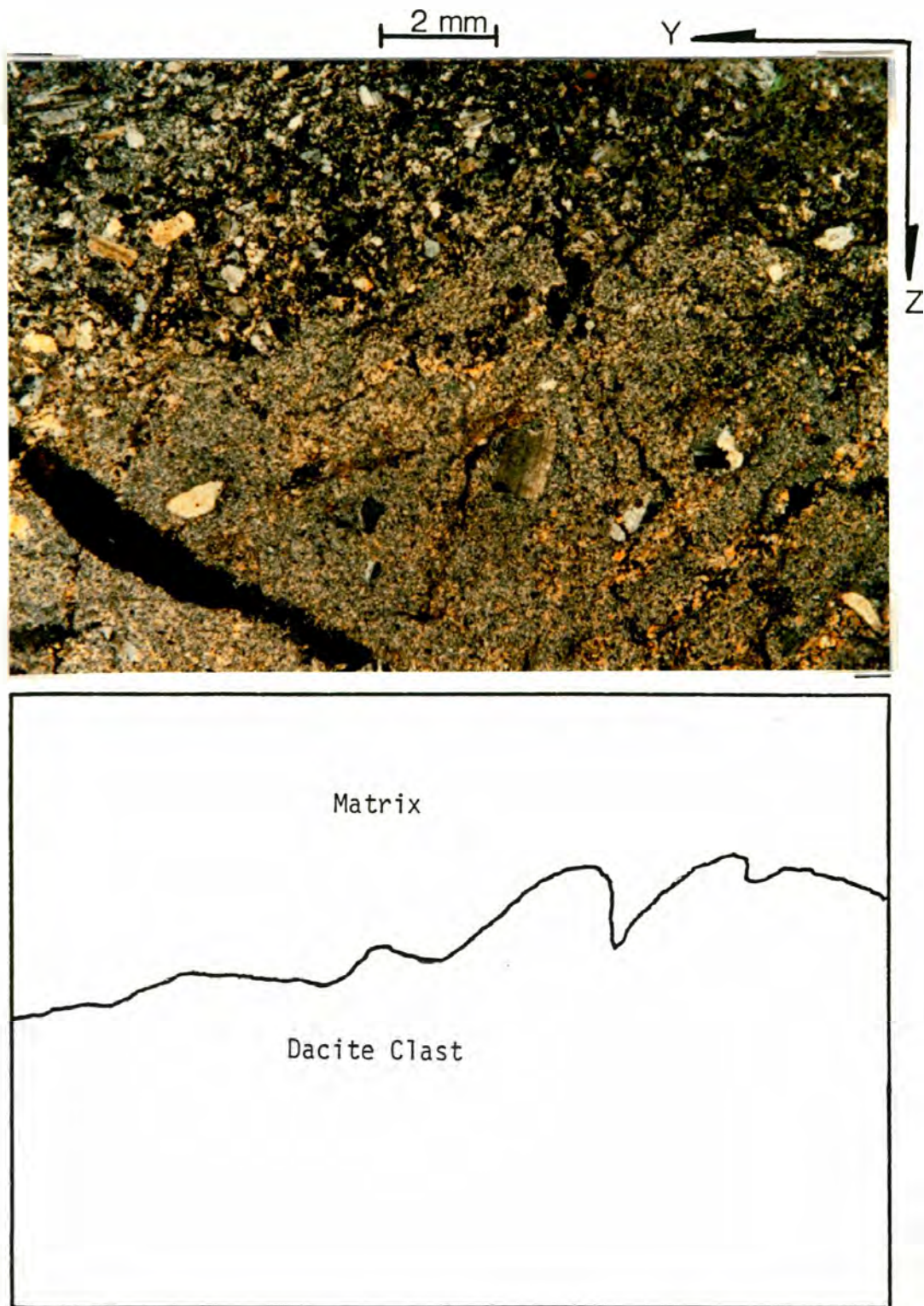


Figure 10. Photomicrograph of a dacite clast in a matrix containing plagioclase clasts, quartz and epidote. The abundant dacite clasts in the metaconglomerate unit are composed plagioclase phenocrysts in a matrix of sub-equal amounts of quartz and plagioclase.

Metatuff Bed

Directly northeast of the metaconglomeratic unit is a 5-10 meter thick metatuff bed. This foliated rock is a distinctive brownish white and forms a prominent rib in the hillside. It is separated from the adjacent units by sharp contacts. Probable lapilli occur locally (110). The unit is composed of approximately sub-equal amounts of fine-grained quartz and albite (55%), non-saussuritized plagioclase phenocrysts (20%), and minor white mica and chlorite. This bed is compositionally similar to some of the dacite clasts observed in the adjacent metaconglomeratic unit.

Metamarl-semipelite-pelite Unit

This unit commonly contains distinct bedding structures resulting from variations in the proportions of plagioclase clasts, carbonate, or mica. These variations are observable on a scale of centimeters or, more commonly, meters (Fig. 11). The rocks of this unit are moderately fissile, tan to black phyllites (Fig. 12), and phyllitic schists, with intercalated minor light-colored, carbonate-rich pods.

In general, the unit contains a matrix of fine-grained, mylonitized quartz and albite (20-40%), and larger .5 mm long clasts of albite (0-5%)(Fig. 43I). White mica is ubiquitous within this unit, and comprises up to 50% of the rock (Fig. 44). Chlorite is minor or absent (0-5%), and biotite is rare. The metamarl contains up to 70% carbonate, and up to 10% epidote (Fig 43). Nearly pure marble occurs, rarely, in pods. Minor fine-grained .25 mm long chloritoid (10b, 103, 140, 209) and medium-grained 3 mm in diameter almandine garnet (10b) occurs in the subordinate pelitic varieties of this unit. Accessory minerals include graphite, magnetite, ilmenite, sphene, hematite, rutile, and tourmaline.

The dominant protolith of this unit is a marl, with a tuffaceous, volcaniclastic, or clastic component. The abundance of white mica, quartz

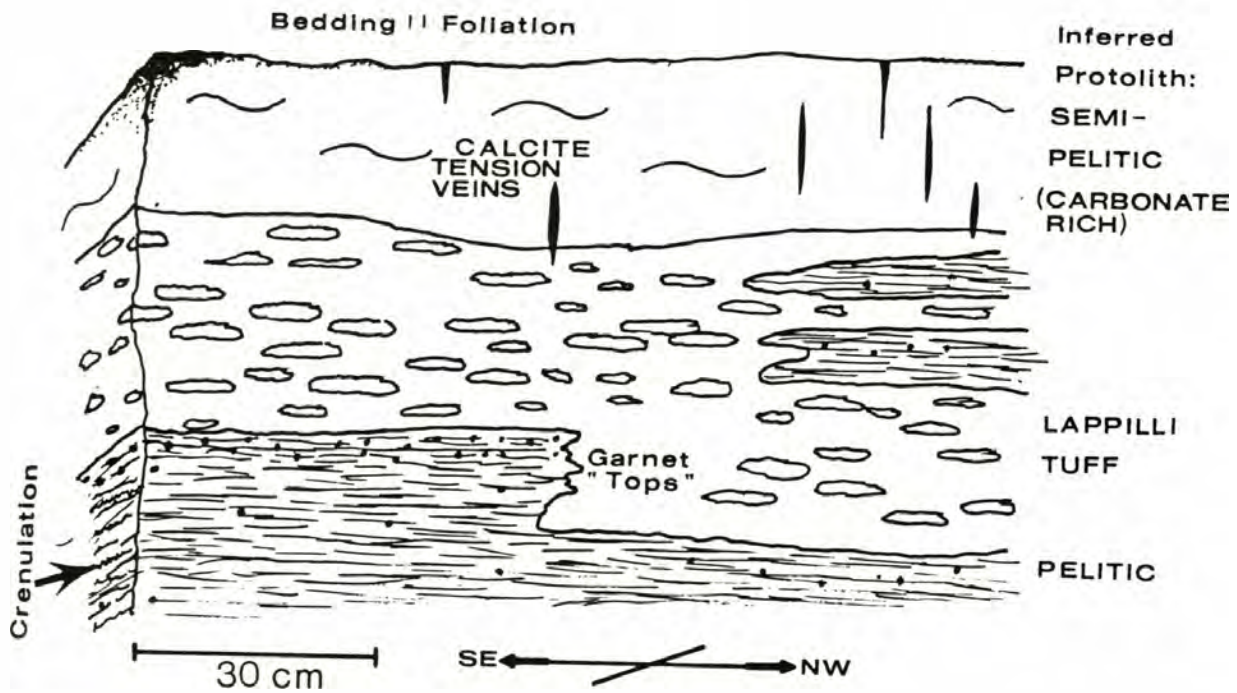


Figure 11. Bedding observed in the metamarl-semipelite-pelite unit west of the Le Conte fault (10). This picture demonstrates the parallel nature of bedding and foliation, and the composite protolith influence of this unit. This outcrop contains metamarl, semipelite (with minor pelitic "tops" containing chloritoid + garnet + white mica) and a lappilli tuff layer.

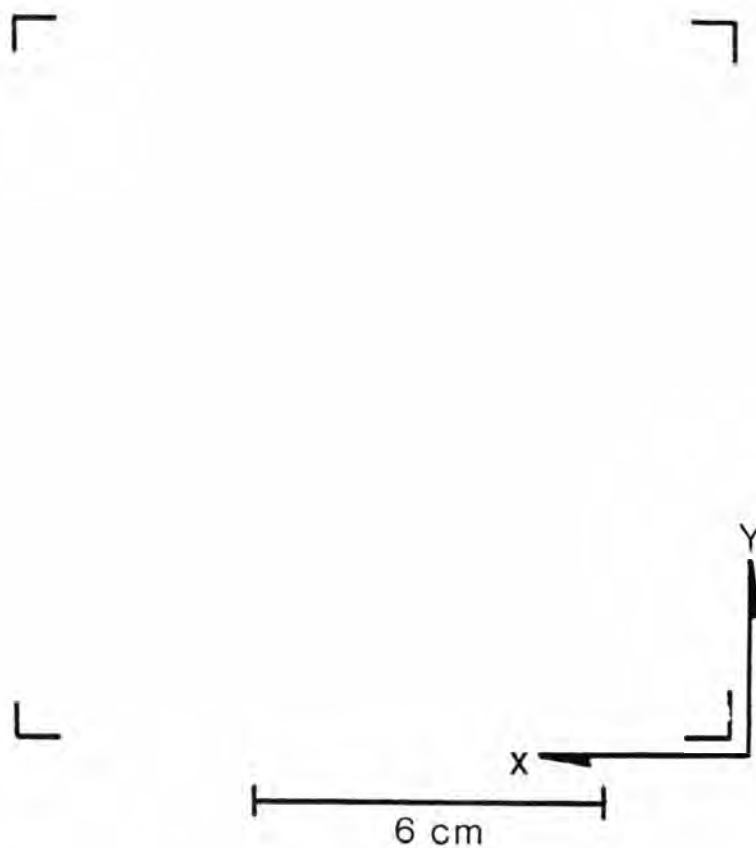


Figure 12. Brown phyllitic schist containing plagioclase clasts (white streaks). The surface shown is slightly oblique to the XY plane, which is sub-parallel to the bedding plane, and as a result shows bedding structure defined by increased plagioclase clasts content. Note the planar calcite filled extension veins formed perpendicular to the mineral lineation.

and graphite in the carbonate-poor interbeds suggests that these rocks are semi-pelitic (semi-aluminous) fine-grained sediments. The presence of chloritoid locally indicates that the sediments range to pelitic or aluminous compositions.

Rock Units in the Central Part of the Field Area

Rock units in the central part of the field area (Fig. 6) differ in protolith, structure, and metamorphism from the rocks to the west of the Le Conte fault just described. The rock units in the central part of the field area are part of the Napeequa unit of Tabor et al. (in press). The rock types include quartz biotite schists and variants, metagabbros, ultramafics, and minor amphibolite (Fig. 6). The rocks are metamorphosed to the amphibolite facies. These rocks are dominantly mylonitic like the Cascade River Schist west of the fault, although they are more complexly folded and disrupted and are not traceable (Fig. 6).

Quartz Biotite Schists

Quartz biotite schists are the dominant lithology of the Napeequa unit observed in field area. These schists are tannish-gray to brown or black, with the darker schists containing more biotite and graphite (Fig. 13). The rocks are strongly-aligned and well-foliated mylonites, which are commonly banded with thicker poorly fissile layers and thinner strongly fissile layers (Fig. 13b).

These schists contain biotite (10-45%), commonly in a graphitic matrix of quartz (30-75%) and subordinate albite, or more commonly oligoclase (0-15%)(Fig. 13). Plagioclase clasts are rare, in contrast to the metaclastites in the Cascade River units in the western and northeastern parts of the field area. Plagioclase clasts were observed in only two samples, both of which are near the Le Conte fault and along the

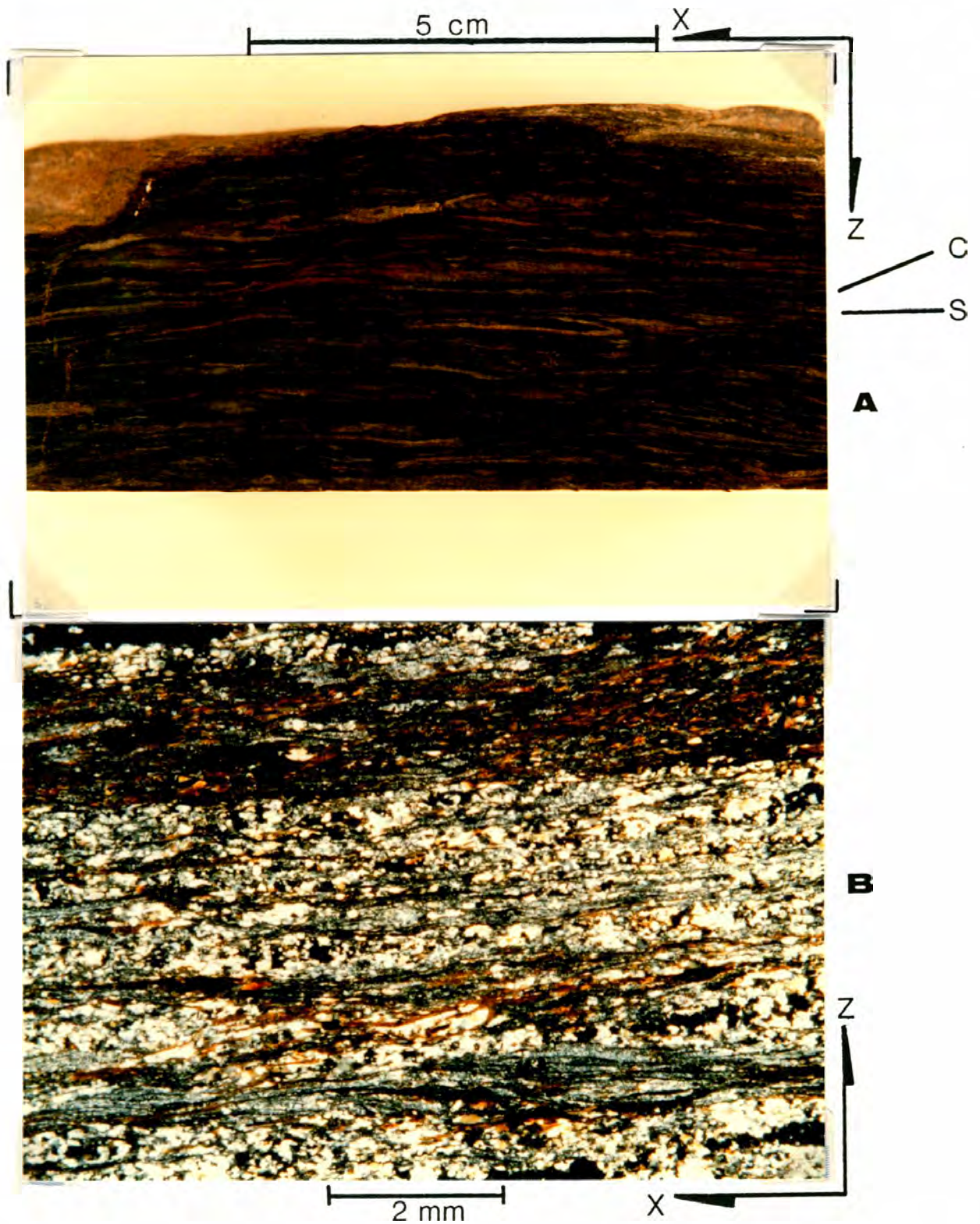


Figure 13. A) Quartz biotite schist of the Napeequa unit with S-C surfaces indicating dextral shear and the dark color characteristic of the schists in the central part of the field area (60). B) Photomicrograph of a quartz biotite schist showing the spaced mylonitic surfaces and the abundance of biotite (150).

western part of the Napeequa unit. Other constituents include white mica (0-20%), chlorite (0-20%), .5-2 mm in diameter almandine garnet (0-5%) and graphite (0-10%). The dominant chlorite is Mg chlorite, although Fe chlorite is found in association with retrogressed biotite, particularly next to cross-cutting C surfaces. Accessory minerals include calcite, sphene, rutile, ilmenite, magnetite, apatite, tourmaline, and rare pyrite.

The biotite schists grade into calcareous interlayers and into micaceous quartzites or quartzite. Abundant white mica (20%) and garnet, and rare clinozoisite, occur in the subordinate more aluminous varieties of these schists. These compositional variations occur perpendicular to the foliation over a scale of meters, and probably reflect bedding. The relatively high quartz content in these schists together with associated basic and ultrabasic rocks suggests the protolith was an impure chert.

Amphibolites

Amphibolites are a minor lithology in the central part of the field area and commonly occur as discrete layers within the quartz biotite schists. The amphibolites contain hornblende, plagioclase, and epidote. Less commonly constituents include minor quartz, chlorite, sphene, and opaques. Whole rock geochemical analysis of one thin amphibolite layer (Fig. 45b) suggests that these rocks are calc-alkaline basalts of oceanic affinity (Fig. 7, Table 1). One thick amphibolite layer is observed in the Napeequa unit. This unit differs from the thin layers by its greater percentage of quartz (greater than 20%) and lack of biotite. Whole rock geochemical analysis of one sample suggests that this layer is a tholeiitic andesite (Fig. 7, Table 1). This layer may be a Cascade River unit metavolcanic layer which has been imbricated into the Napeequa unit along a shouldering zone adjacent to the northeastern margin of the Hidden Lake pluton.

Ultramafic Rocks

Ultramafic bodies range in size and shape from centimeter scale pods or layers which line faults, to layers that are meters in thickness (Fig. 6). Generally, the foliation and outline of the ultramafic bodies are concordant with the foliation in the adjacent schists.

Ultramafic rock types include serpentinites, tremolite schists, and forsterite bearing talc schist. The serpentinites are fine-grained and vary from massive, or mat textured (Fig. 14a), to well-foliated (Fig. 14b). The antigorite-rich serpentinites are blue-green on fresh surfaces, and brown on weathered surfaces (Fig. 15a). The serpentinites commonly contain antigorite (60-90%), veins or grains of magnesite (3-10%), and accessory chromite (or magnetite)(Fig. 14). Ghosts of probable forsterite grains are outlined by magnetite "dust". Just north of the Hidden Lake pluton, an extensive ultramafic layer contains a relict high-grade core containing partially serpentinized forsterite (30%), talc (50%), antigorite (12%), and opaque (8%)(Fig. 15). The forsterite is interpreted to be metamorphic (see Metamorphic Section), although a primary origin cannot be discounted without forsterite composition data. The light greenish blue ultramafites, which have a substantial tremolite and/or talc content, are restricted to the foliated varieties, suggesting that silica enrichment (metasomatism) predated or accompanied deformation. Thin talc-rich layers are common along faults. Noteworthy are the talc-lined faults immediately to the northeast of the Hidden Lake pluton along a possible shouldering zone. Tremolite commonly occurs as monominerallic layers ("Blackwall").

Metagabbro

Two extensive bodies of foliated to semi-massive metagabbros occur in

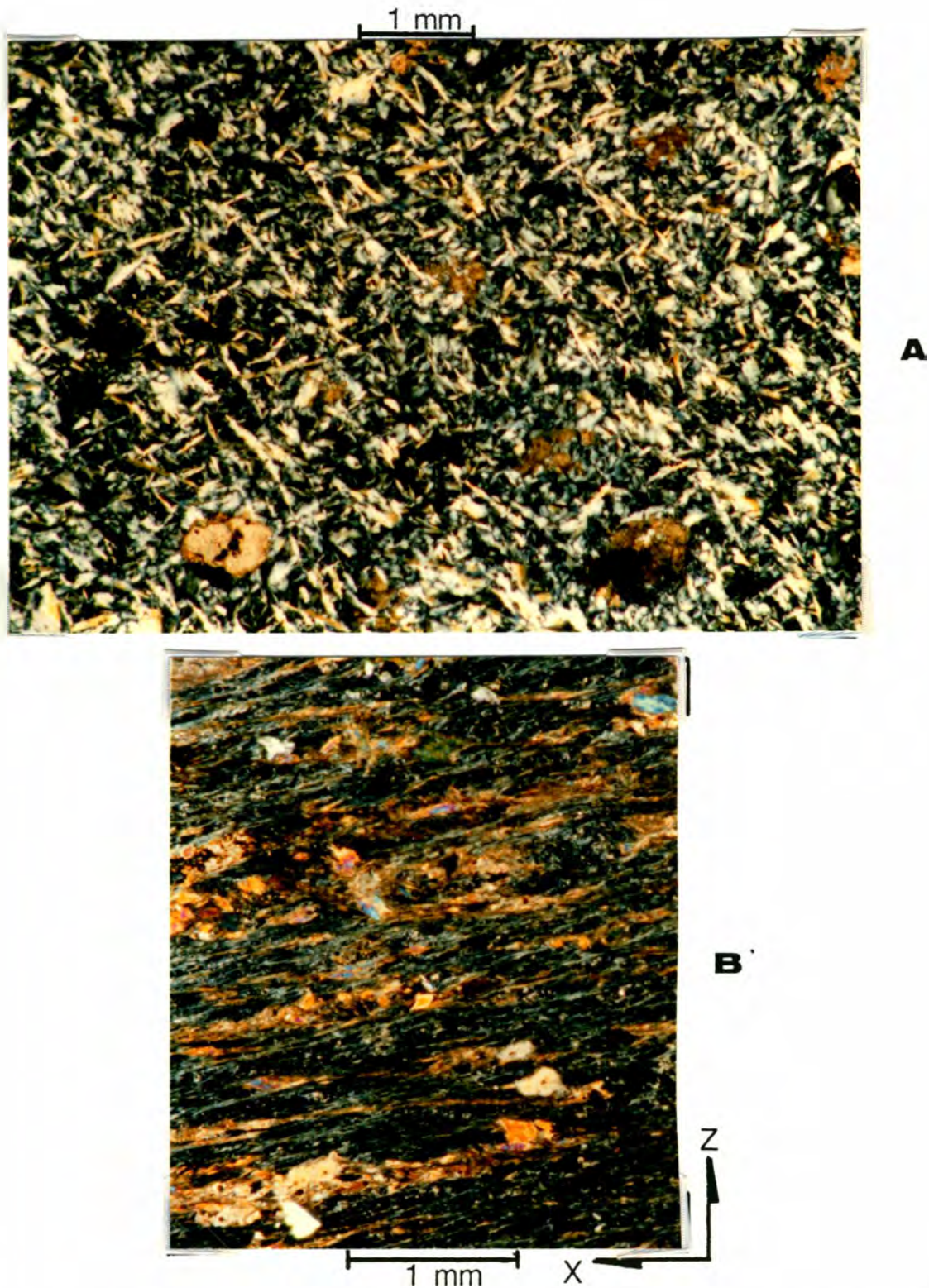


Figure 14. A) Microphotograph of a serpentinite containing mat-textured antigorite, magnesite, and chromite (145). B) Well-foliated serpentinite containing antigorite, talc, and opaque (225). Upgrade to the east the serpentinites give way to forsterite-talc bearing ultramafite probably due to deserpentinization.

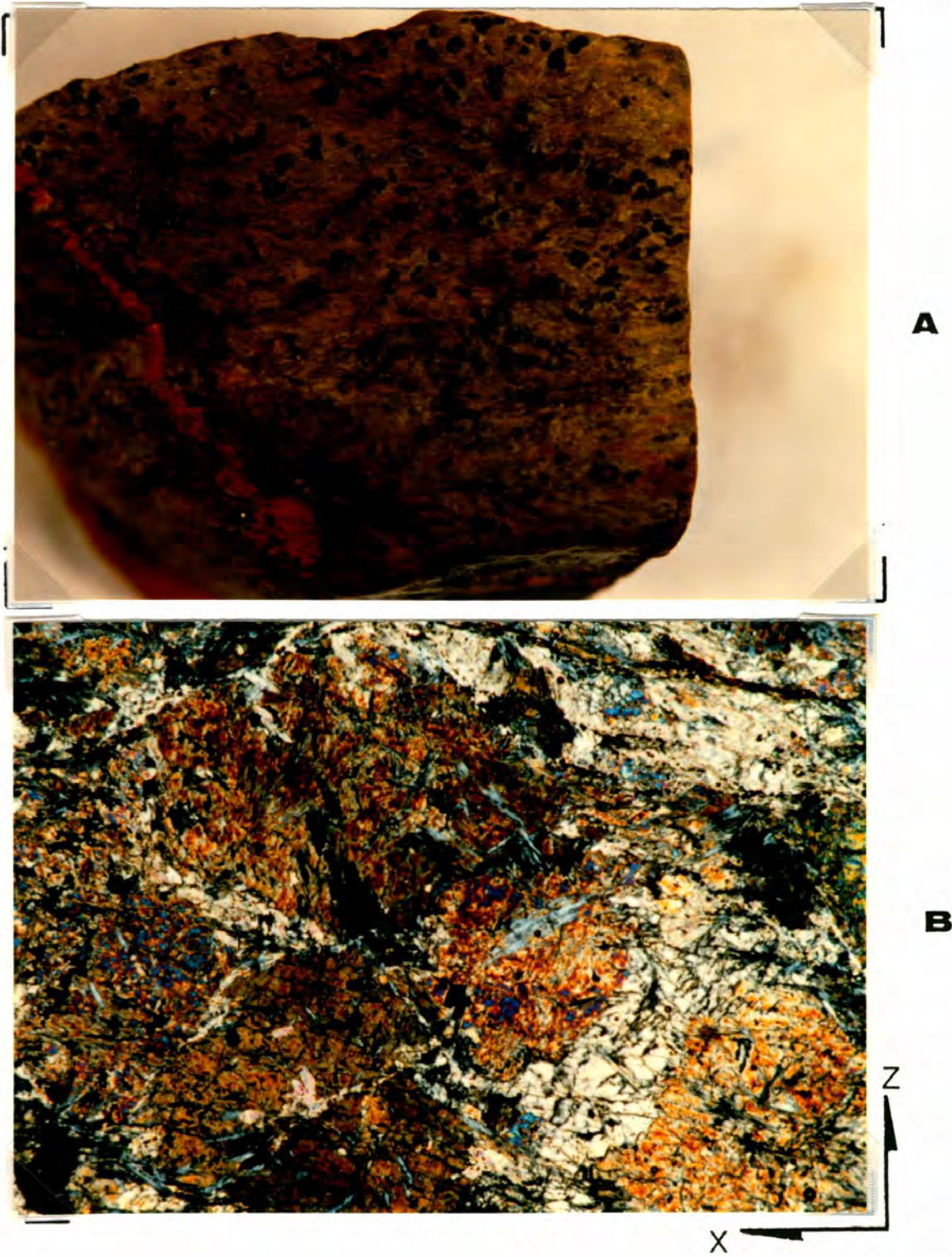
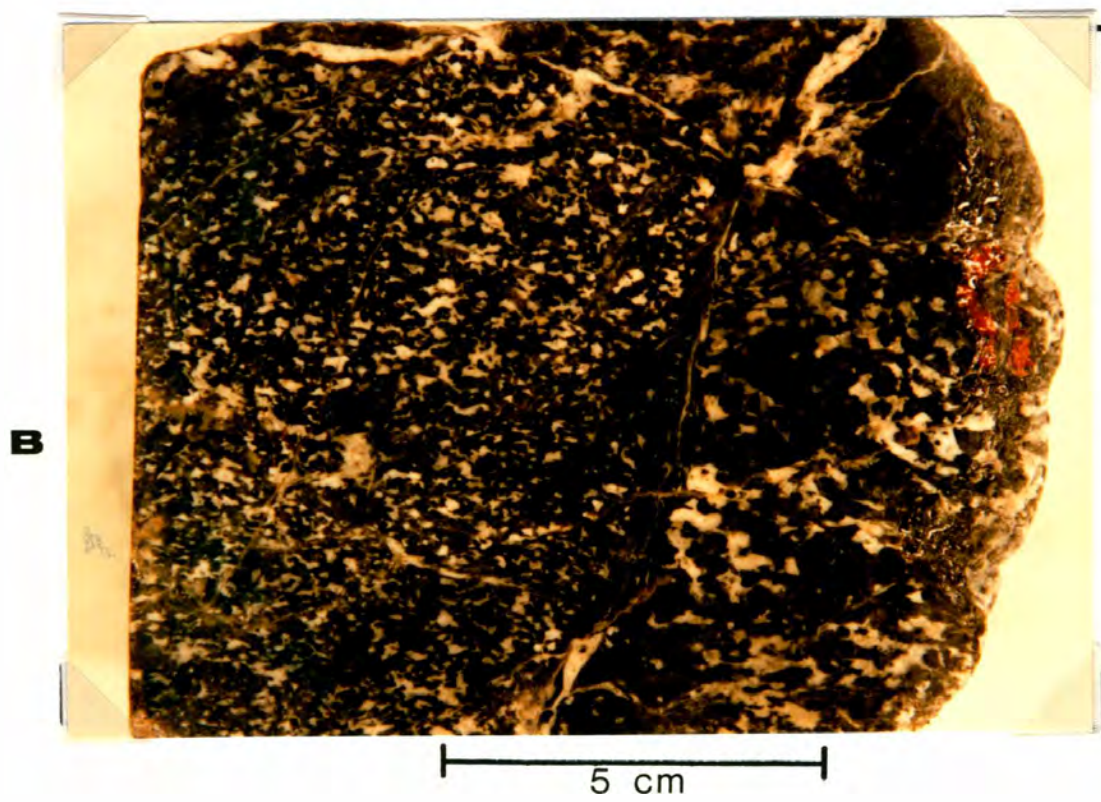
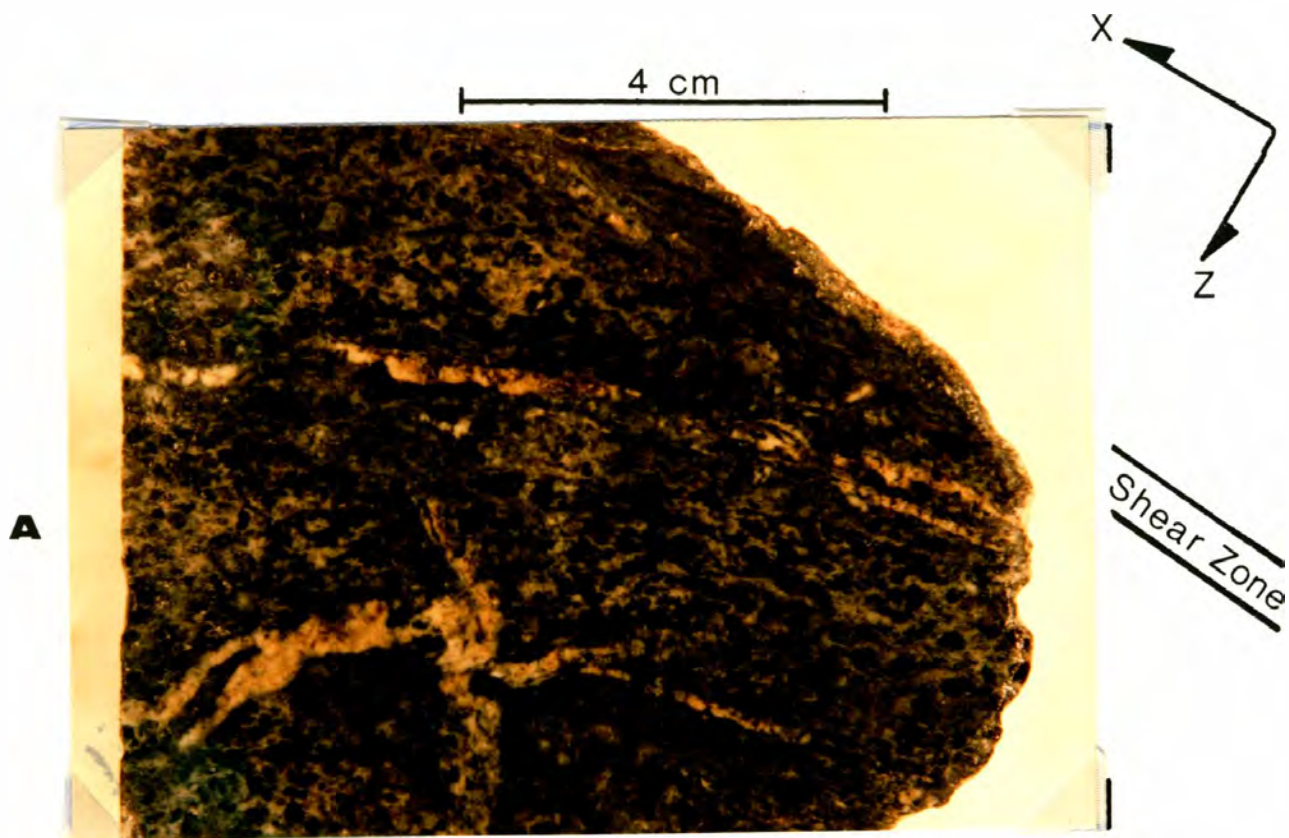


Figure 15. A) Forsterite bearing ultramafite, displaying characteristic brown weathering and forsterite porphyroblasts (25d). B) Photomicrograph of the above hand sample showing talc and antigorite replacing forsterite.

Figure 16. A) Metagabbro in the Napeequa unit from just below the Cascade River Road. Note the coarse grain size, except in small-scale shear zones (top right)(44). B) Metagabbro in the Napeequa unit from just north of the Hidden Lake pluton (157). This body occurs next to a possibly cogenetic ultramafic layer (Fig. 15).



the field area, one just below the Cascade River Road, and another just north of the Hidden Lake pluton (Fig 6). These bodies are spatially associated with, and are possibly genetically related to, ultramafic bodies. A good example of this relationship is found along the northeastern margin of the Hidden Lake pluton where a layer of 30 m thick ultramafite and 30 meter thick metagabbro occur together (see Plate 1). These lithologies may be cogenetic and of ophiolitic origin.

The metagabbros are light to dark green, and contain medium to coarse-grained amphibole porphyroblasts in a plagioclase-rich matrix (C.I. = 60-80)(Fig. 16). The dark green metagabbros, which lack visible grains, are strongly sheared. The pods and layers of coarser-grained material attest to the once coarser-grained nature of this unit.

The metagabbroic body west of the Hidden Lake pluton (Fig. 6) contains 2-4 mm in length tremolitic hornblende (50-60%), with interstitial plagioclase (10-20%), epidote (10%), and minor biotite, prochlorite, sphene, and calcite (44; Fig. 16a). The body directly north of the Hidden Lake pluton contains tremolitic hornblende (60%), plagioclase (15%), and zoisite (25%)(25c.1; Fig. 16b).

These two bodies are interpreted to be metamorphosed gabbros due to the abundance of Ca-amphibole and plagioclase, lack of quartz, low silica content (Fig. 7, Table 1), and medium- to coarse-grain size versus the fine- to medium-grain size of the amphibolites. Whole rock geochemical analysis of one metagabbro, although possibly complicated by cumulate origin, suggests a calc-alkaline arc-affinity (Fig. 7, Table 1).

Rock Units in the Northeastern Part of the Field Area

The northeastern part of the map area contains a homoclinally layered sequence of metasedimentary and metavolcanic rock units which strike to the northwest and dip steeply to the southwest (Fig. 6). These rock

units, in order of decreasing abundance are: locally conglomeratic quartzo-feldspathic schists, mica schists, amphibolites, quartz mica schists, calcareous schists, calcareous amphibolites, minor marbles and graphitic mica schists (Fig. 6). These rock types conform to Tabor et al. (in press) Cascade River unit (Fig. 4). These rocks generally contain a granoblastic, medium- to coarse-grained fabric, with a strong foliation, and a weakly developed mineral lineation. Garbenschiefer (Fig. 20b) textures are common in amphibolite, mica schist, and graphitic mica schists. This contrasts with the finer-grained mylonitic rocks observed in both the Neepequa and Cascade River units in the central and western part of the field area (see Structure Section). The rocks of this area are in the kyanite-staurolite zone of the middle amphibolite facies (see Metamorphic Section).

Quartzo-Feldspathic Schists

The extensive quartzo-feldspathic unit is distinguished by the occurrence of plagioclase clasts. The unit is locally conglomeratic containing cobble, pebble, and rare boulder sized clasts, with tonalite to quartz diorite (Fig. 17b), dacite and minor black garnet-bearing metasedimentary compositions. Minor schist and quartzite clasts are reported by Tabor (1961) in a similar unit along strike. The unit is coarse-grained, poorly sorted, and compositionally immature. Graded bedding structures are defined by the decreasing content and size of plagioclase and conglomerate clasts, and increasing muscovite content, towards the top (from quartzo-feldspathic schists to mica schists; Fig 18). These structures, assuming normal grading, suggests that younging is to the southwest.

The matrix is composed of granoblastic quartz (20-25%), calcic

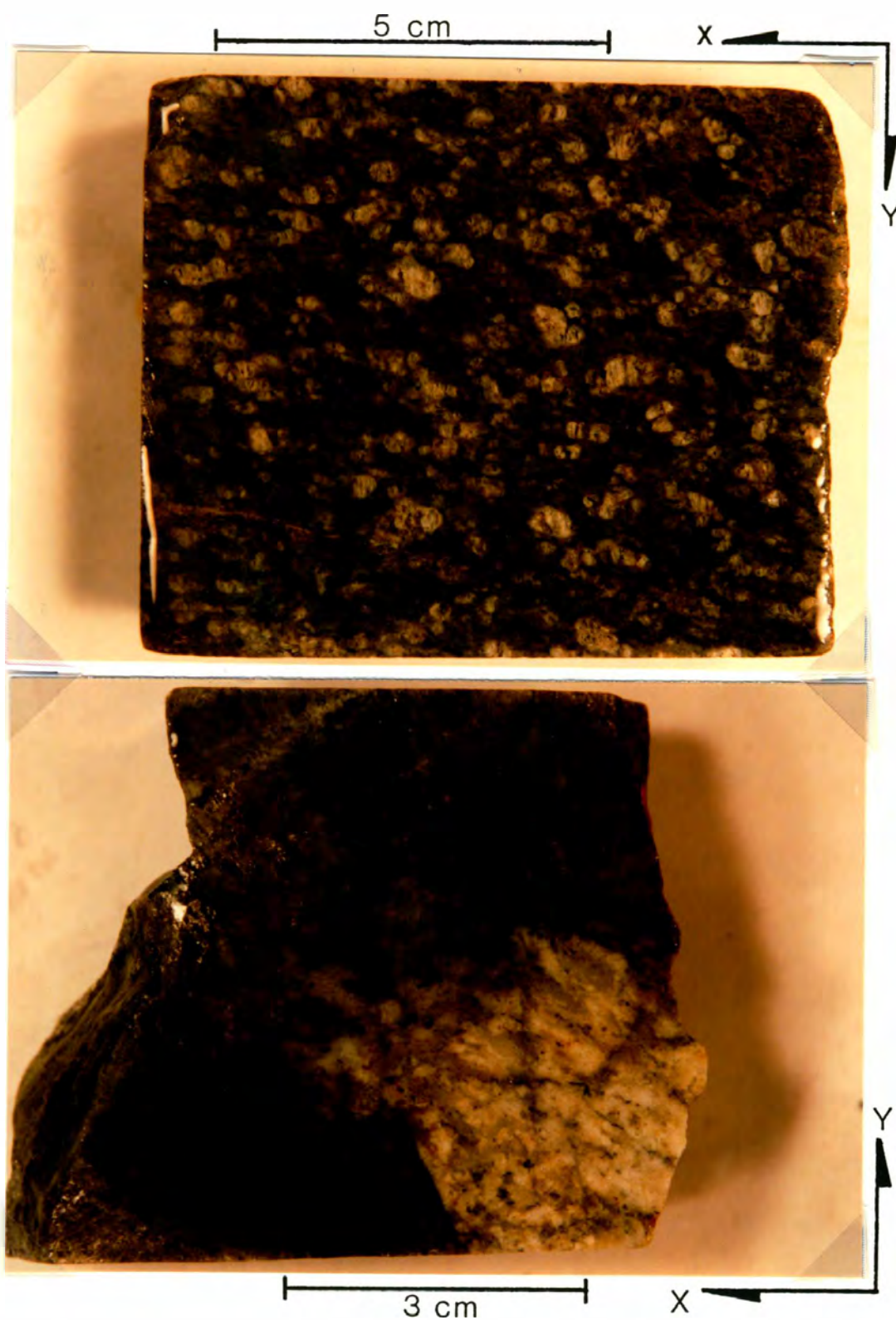


Figure 17. A) Photo showing stretched plagioclase clasts in a typical quartzo-feldspathic schist of the Cascade River unit and biotite mineral lineation (922b). B) Granitic clast in a mica schist (132). This mica schist is a interbed within the quartzo-feldspathic unit.

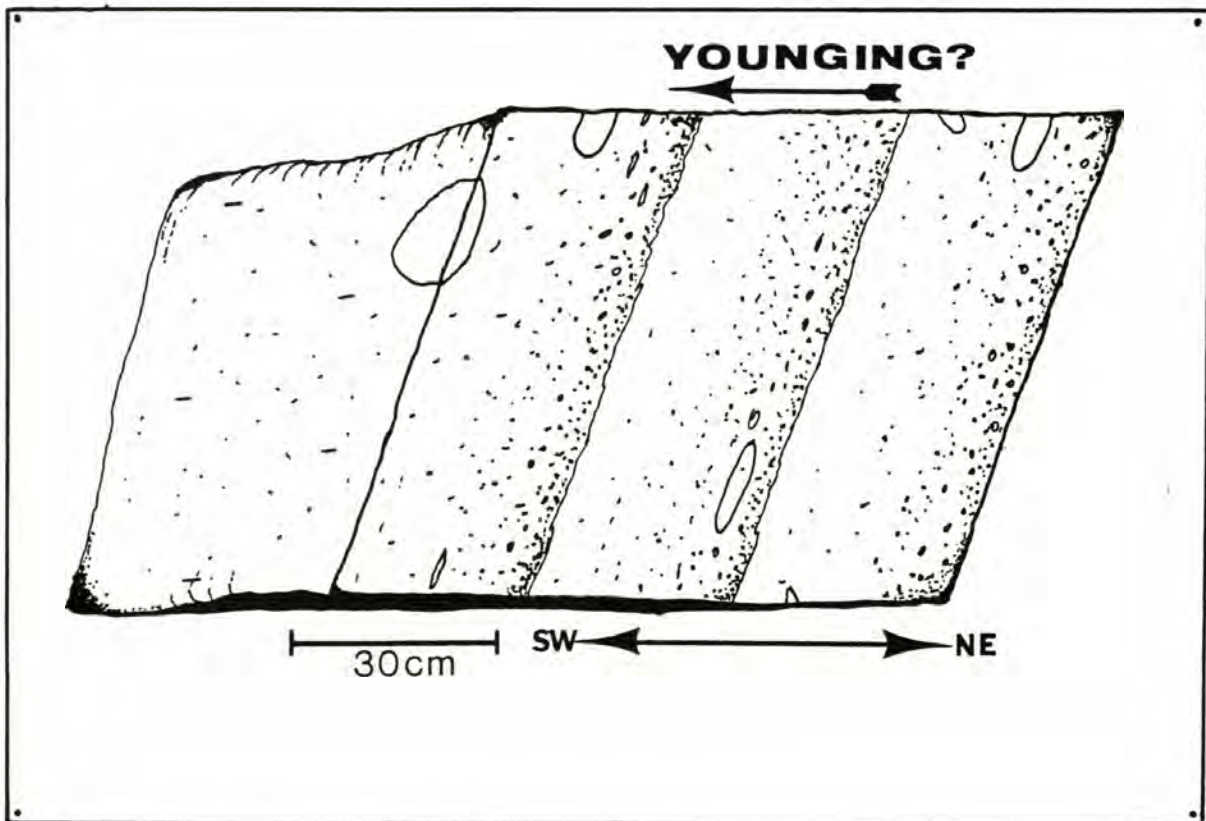


Figure 18. Field Sketch showing graded bedding structures in the locally conglomeratic quartzo-feldspathic unit. These primary structures are defined by the decreasing content and size of plagioclase and conglomerate clasts, and increasing muscovite content, towards the top.

oligoclase (20-25%), and subangular to angular plagioclase clasts (20-30%). Other phases include muscovite (10-30%), biotite (0-20%), and 1 mm in diameter almandine garnet (0-10%). Accessory phases include ilmenite, magnetite, sphene and rutile. Retrogressed biotite, resulting in minor pennite and K-spar, is common in cross-cutting shear zones in the northeastern part of the field area (See Structure Section). Carbonate and epidote are found in cross-cutting veins which are spatially related to retrogression of the biotites.

The protolith of this unit is a poorly sorted arkosic to volcanic conglomerate. The unit is interbedded with 1) Thin to thick (cm to 1-2 meter) layers of micaceous schists (below); 2) Thin (cm's-meter) calcareous amphibolites (Fig. 22) and ortho-amphibolites (below); and 3) 1-3 meter thick concordant foliated plagioclase-porphyr hornblendic mafic dikes, which define an injection zone.

Mica Schists

These rocks are well-foliated and commonly contain large porphyroblasts of 2mm-3cm in length hornblende (0-30%), and 1mm-3cm in diameter garnet (0-30%). The matrix is composed of plagioclase (20-40%) (An 20-49), and quartz (10-20%), with biotite (10-15%), less commonly with muscovite (0-30%) and chlorite (0-15%)(Fig 19, 48a,b,f,g). One occurrence each of staurolite and kyanite occur in the garnet and muscovite bearing aluminous varieties. Accessory minerals include epidote (0-5%), calcite, rutile, sphene, magnetite, and ilmenite.

The mica schists are intermediate in composition between the quartz mica schists and the quartzo-feldspathic schists. These schists are distinguished from quartzo-feldspathic schists by the lack of plagioclase clasts. The mica schists occur as separate, thick, mappable layers, and as interbeds, some with kyanite and staurolite, within the extensive

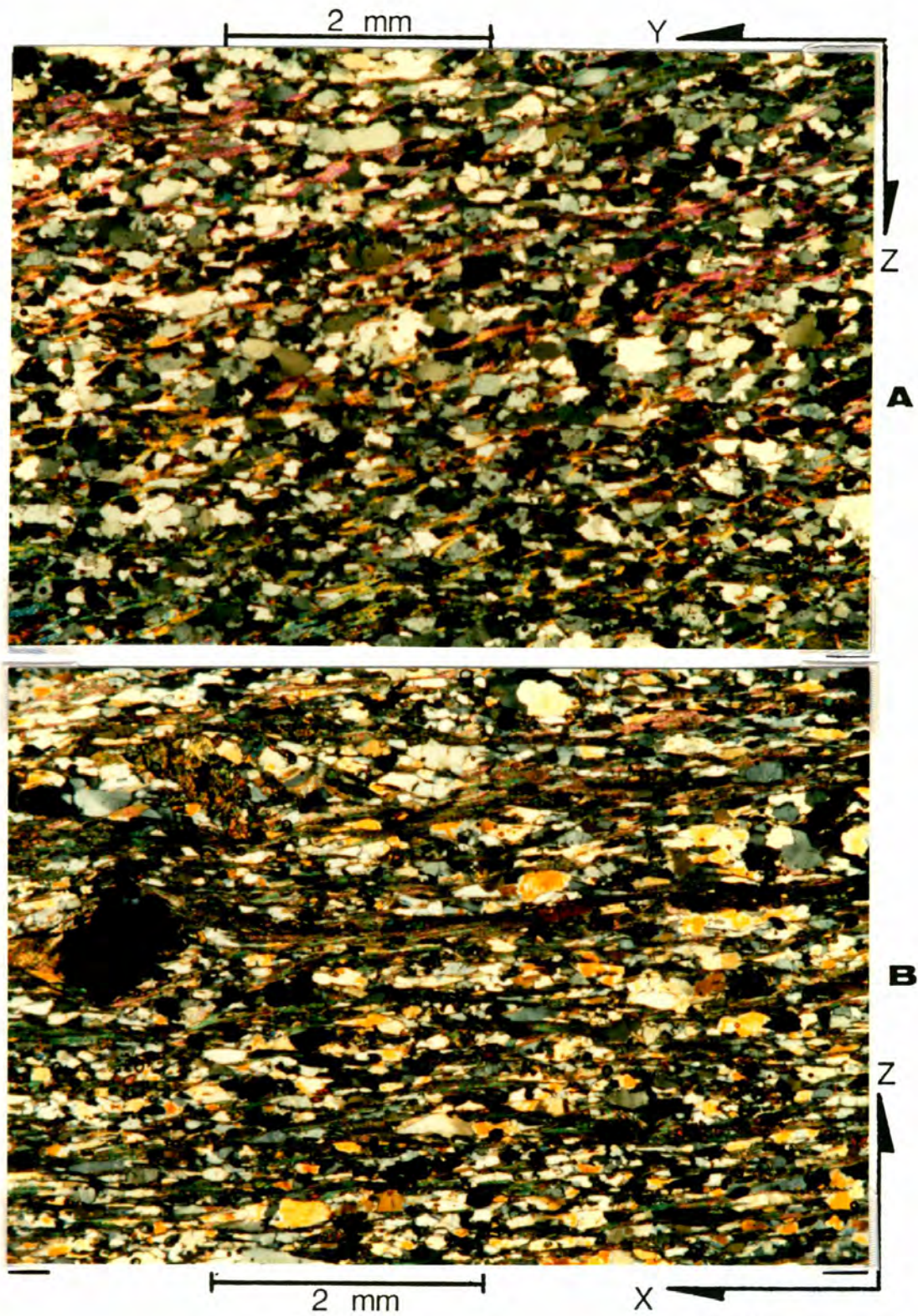


Figure 19. Photomicrograph of a mica schist (132) showing a typical S1 foliation (see Structure Section) defined by muscovite, biotite and elongate, slightly undulose, quartz and oligoclase grains.

conglomerate bearing quartzo-feldspathic unit.

This unit encompasses a relatively wide range of metasedimentary protoliths. The lack of medium-grained plagioclase clasts suggests a finer-grained feldspathic to pelitic protolith, varying from rare pelites to immature siltstones. The hornblende-rich varieties probably have a mafic igneous component (metatuffaceous or volcanoclastic?).

Amphibolites

Amphibolite layers in the northeastern layered sequence are thick (10's of meters) and are divided into quartz-rich (quartz greater than 20%) and quartz-poor (quartz 0-10%) varieties. Both varieties commonly contain dark and leucocratic layering on a centimeter to meter scale, which reflect volcanic or volcanoclastic interbeds. These rocks are moderately- to well-foliated, and contain weak- to well-aligned, coarse-grained (2 mm to 2 cm in length) hornblende prisms on the foliation surface (Fig. 20).

The quartz-poor unit contains quartz (0-7%), plagioclase (25-45%), hornblende (30-55%), biotite (5-35%), chlorite, epidote (0-7%), and opaques. The quartz-rich unit contains quartz (25-35%), plagioclase (5-20%), and hornblende (30-50%). Biotite is absent and epidote is abundant (10-25%) in the quartz-poor unit. The leucocratic layers, in the thicker layers of both sub-units, contain more quartz and plagioclase and less mafic phases (Fig 20a).

Whole rock geochemical analysis of four quartz-poor amphibolites indicate that these metavolcanics are calc-alkaline basalts to andesites with an arc-affinity (Fig. 7, Table 1). No quartz-rich amphibolites were analyzed, but they presumably represent a more siliceous volcanic protolith (e.g. dacites).

Quartz Mica Schists

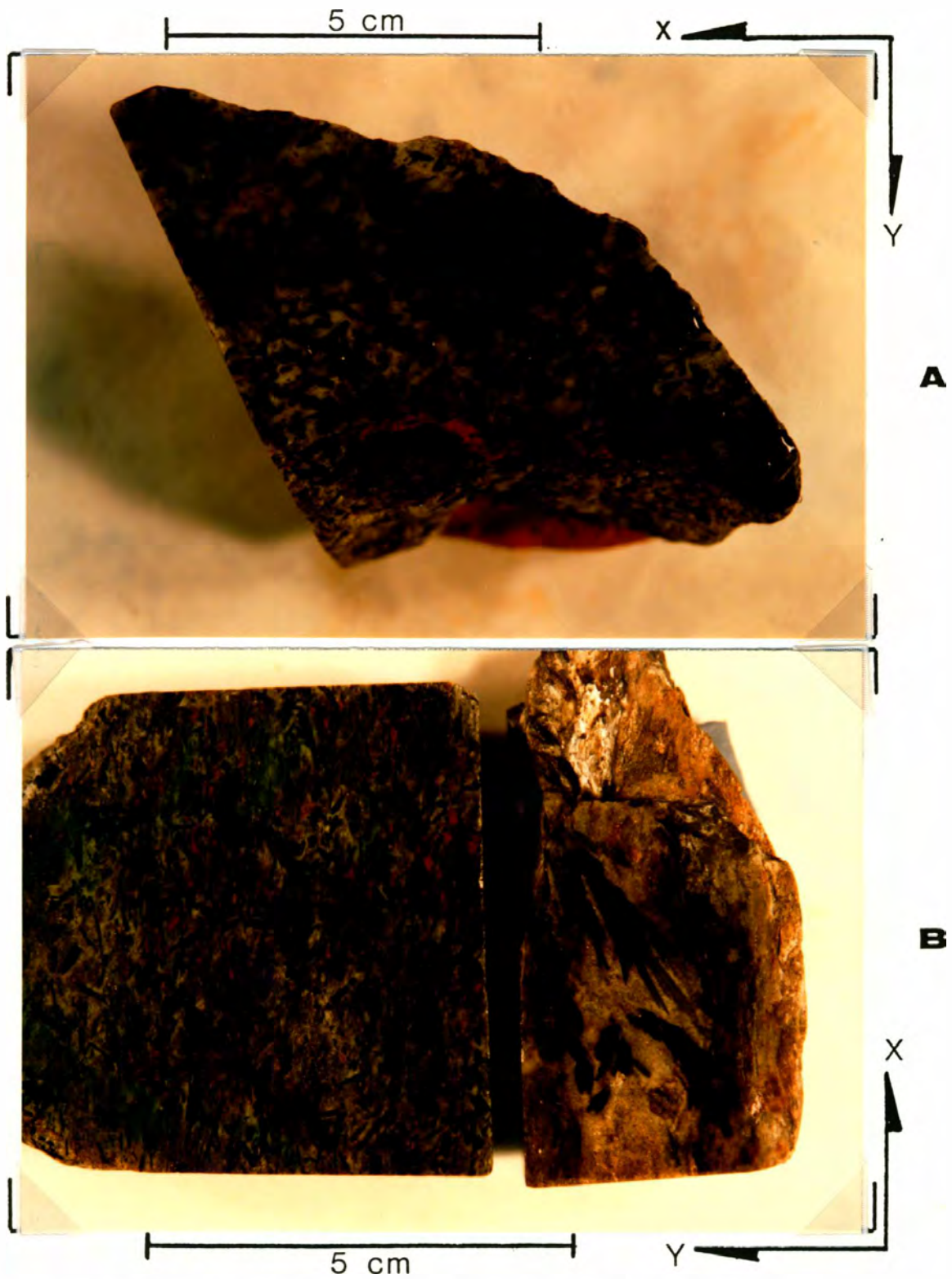


Figure 20. A) Quartz-poor amphibolite (meta-dacite, 6) with garbenschiefer texture. Note the poorly aligned nature of these samples on the S1 surface (see Structure Section). B) Photo of a leucocratic quartz-rich amphibolite (meta-andesite, 188), and garbenschiefer in a mica schist.

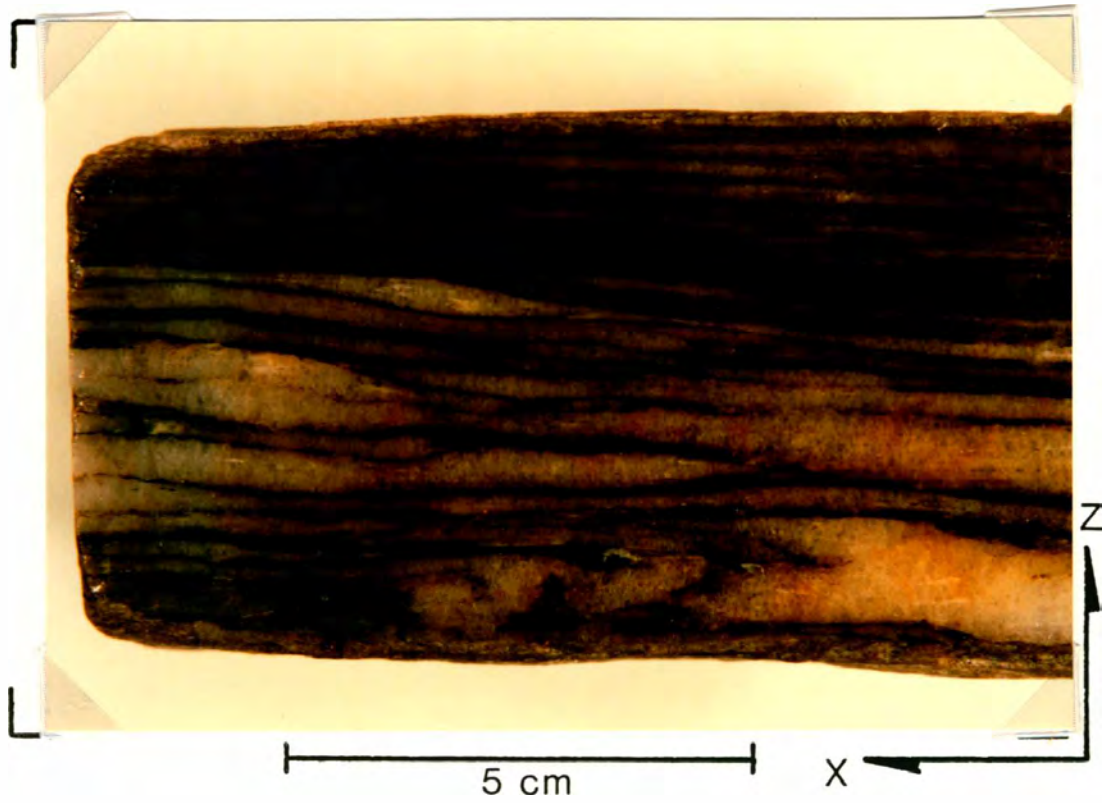


Figure 21. Quartz mica schist showing the well-developed pure quartz layers separated by dark, biotite-rich layers, which probably reflect bedding.

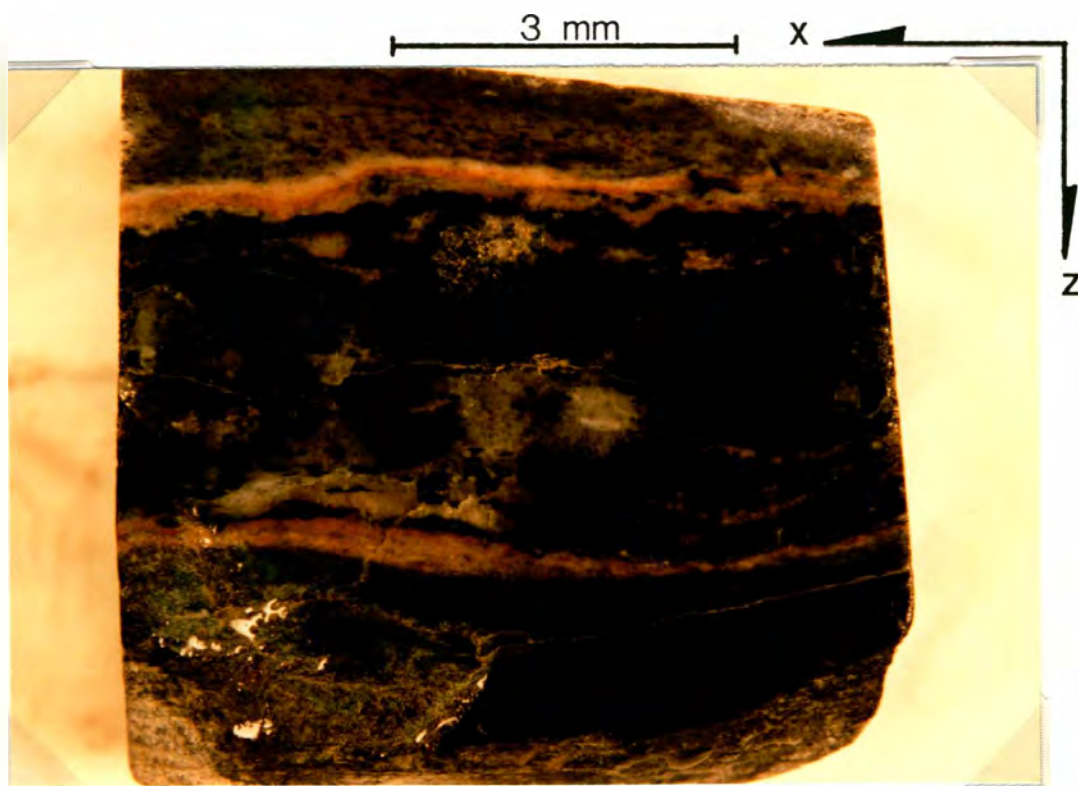


Figure 22. Thin calcareous amphibolite layer within a kyanite bearing mica schist interbed of the quartzo-feldspathic unit (183b).

The quartz mica schists are well-foliated, medium-grained, and show segregation or primary layering (Fig. 21). The matrix is composed of quartz (10-80%), oligoclase (An 20)(7-45%), biotite (10-35%), muscovite (3-10%) and rare chlorite. Subordinate plagioclase and biotite-rich interlayers occur between more quartz-rich, thicker layers. Commonly this unit contains coarse-grained porphyroblasts (2mm-1cm) of almandine garnet. Accessory minerals include magnetite, ilmenite, and rutile.

The inferred protolith for the quartz-rich varieties is an impure ribbon chert. The biotite-rich quartzo-feldspathic interlayers possibly represent a more immature protolith with a volcanic or volcanoclastic detrital influence. These quartz schists are similar in composition to the quartz biotite schists observed in the nearby Napeequa unit. The unit is included in the northeastern Cascade River unit since: 1) the unit dips to the southwest parallel to the other rock units in the northeastern area; and 2) the unit is partially interbedded with the pelitic graphitic schist unit and thus appears to be in stratigraphic continuity with the homoclinal northeastern Cascade River sequence.

Calcareous Amphibolites, Calcic Mica Schists and Marble

This unit includes a calcareous amphibolite, calcic mica schist and a thin marble layer. One marble bed occurs in this calcareous package on the ridge south of Marble Creek and on the ridge between the two Sibley Creeks. Two beds occur at the headwaters of the southern fork of the Sibley drainage. It is not clear whether these represent two separate beds, or the same bed structurally repeated, since the second bed occurs in an imbricated zone.

The calcic amphibolites contain carbonate and epidote-rich laminae (1-5mm), between thicker, hornblende-rich layers. The hornblende-rich layers contain hornblende (50%), calcic plagioclase and epidote (35%),

quartz (10%), and calcite (5%). The hornblende-poor layers contain hornblende (5%), calcic plagioclase and epidote (35%), quartz (20%), and abundant calcite (25%). Less common phases include muscovite, chlorite, clinozoisite and plagioclase clasts. Accessory minerals include rutile, opaque, and sphene. The calcic mica schists contain calcic plagioclase (20-40%), biotite (25%), epidote (3-5%), quartz (20%), calcite (5-25%), and opaque.

The abundance of carbonate, epidote, and quartz suggests that the protolith for the calcareous schist and amphibolite is a calcareous sediment with a probable volcanic or volcanoclastic component (marl), in association with a thin limestone (marble) bed.

Graphitic Mica Schists

This unit is only observed along the western part of the northeastern Cascade River unit. It is in part interbedded with the quartz mica schists (Fig. 6). These distinctive rocks are black, well-foliated, and strongly fissile (Fig. 23). These rocks contain quartz (15-30%), oligoclase (10-20%)(An 28), white mica (40-50%), biotite (0-7%), graphite (0-7%), and coarse-grained, euhedral, 2-5mm in diameter garnet porphyroblasts (5-20%). Fine-grained (1 mm in diameter) staurolite occurs in one sample. Biotite is common, although not abundant, and occurs as discrete porphyroblasts, or as a replacement product in hornblende. Hornblende (0-2%) is restricted to the more biotite- and oligoclase-rich rocks. The coarse-grained (1-3 cm in length) and radiating nature of the hornblende in garbenschiefer texture, observed in many of the hornblende bearing units in the northeastern area, contrasts markedly with the well-aligned smaller porphyroblasts (less than 5 mm), observed in mylonites of the central and western parts of the field area (see Structure Section).

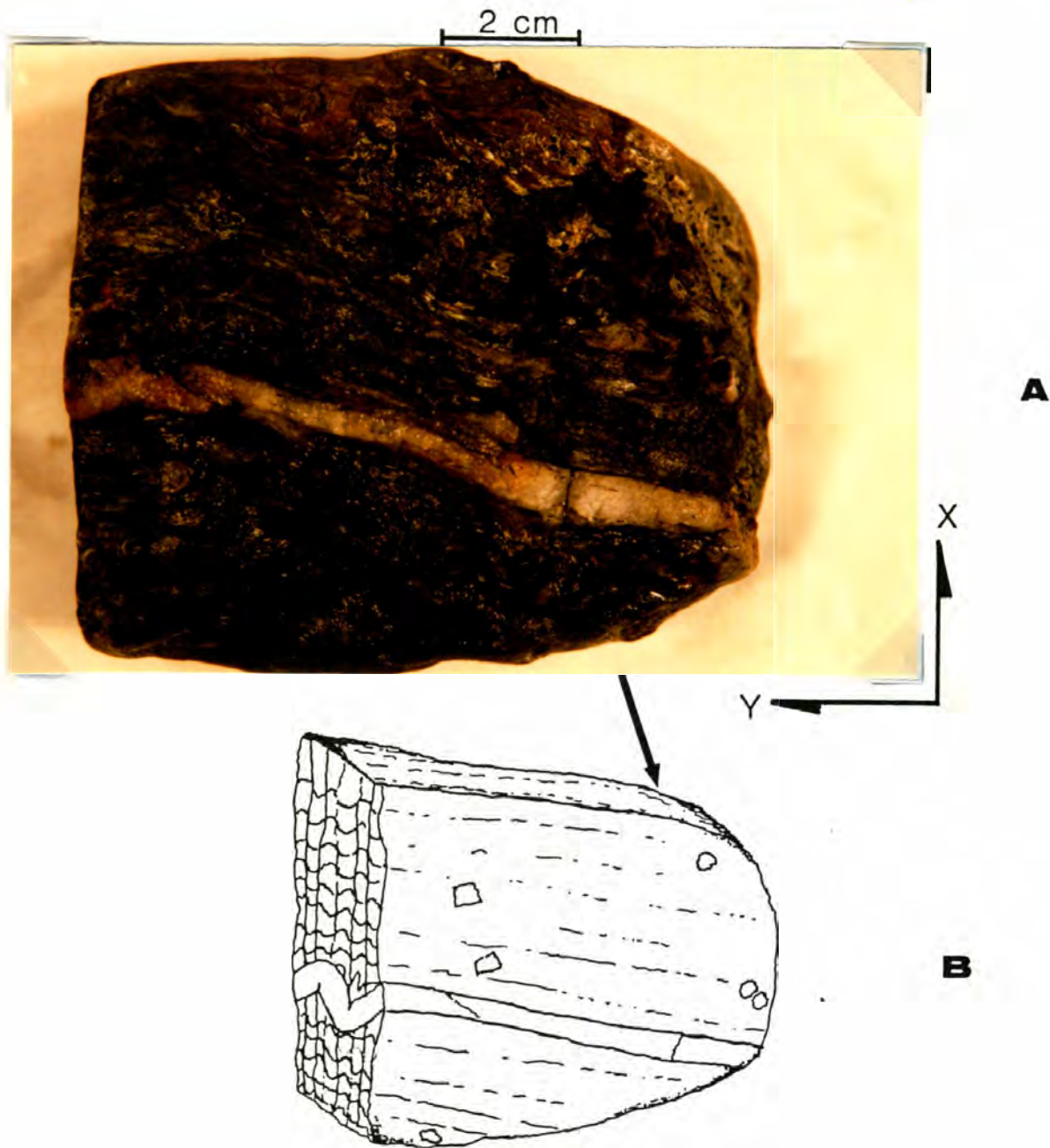


Figure 23. A) Graphitic mica schist cut parallel to the axial planar cleavage and perpendicular to the previous penetrative micaceous cleavage. Pelitic rocks such as these are rare in the study area and constitute only a small percentage of the Cascade River Unit (124). B) Sketch showing the orientation of the photo and the axial planar cleavage associated with these schists (see Structure Section).

The abundance of muscovite, graphite, garnet, and the one occurrence of staurolite indicates that the protolith of this unit is a shale (pelite). The graphitic mica schists, quartz mica schists, and a quartz-rich amphibolite layer occur in a transition zone between the western part of the northeastern Cascade River unit and the Napeequa unit (Fig. 6, 38 B-B').

Discussion

Possible Depositional Environment for the Cascade River Unit which occurs West of the Le Conte Fault

Many of the attributes of the Cascade River Schist suggest near-arc eugeosynclinal deposition (Tabor, 1961; Misch, 1966). The Chemical compositions of the metavolcanic rocks in the Lookout Mountain area (Cary, pers. comm.), directly north of the study area, are dominantly andesitic, but range from basaltic to rhyolitic with a calc-alkaline, island arc affinity (Table 1). An arc environment is also suggested by the geochemistry of the Cascade River Schist metasediments (Babcock and Misch, 1988).

The metaconglomerate unit appears to be derived from a volcanic and plutonic provenance (Fig. 24). Rapid deposition in a high energy environment, proximal to the source region, is suggested by the relatively angular plagioclase clasts, poor sorting, compositional immaturity, and the occurrence of boulder sized clasts reported elsewhere (Cary, pers. comm.; Tabor, 1961).

The metamarl-semipelite-pelite unit is interpreted to represent a more distal, lower energy depositional environment (Fig. 25), as suggested by its inferred protolith which is finer-grained, better sorted, and commonly carbonate rich. The occurrence of plagioclase clasts in some of the layers of this distal facies suggests some of these rocks received the

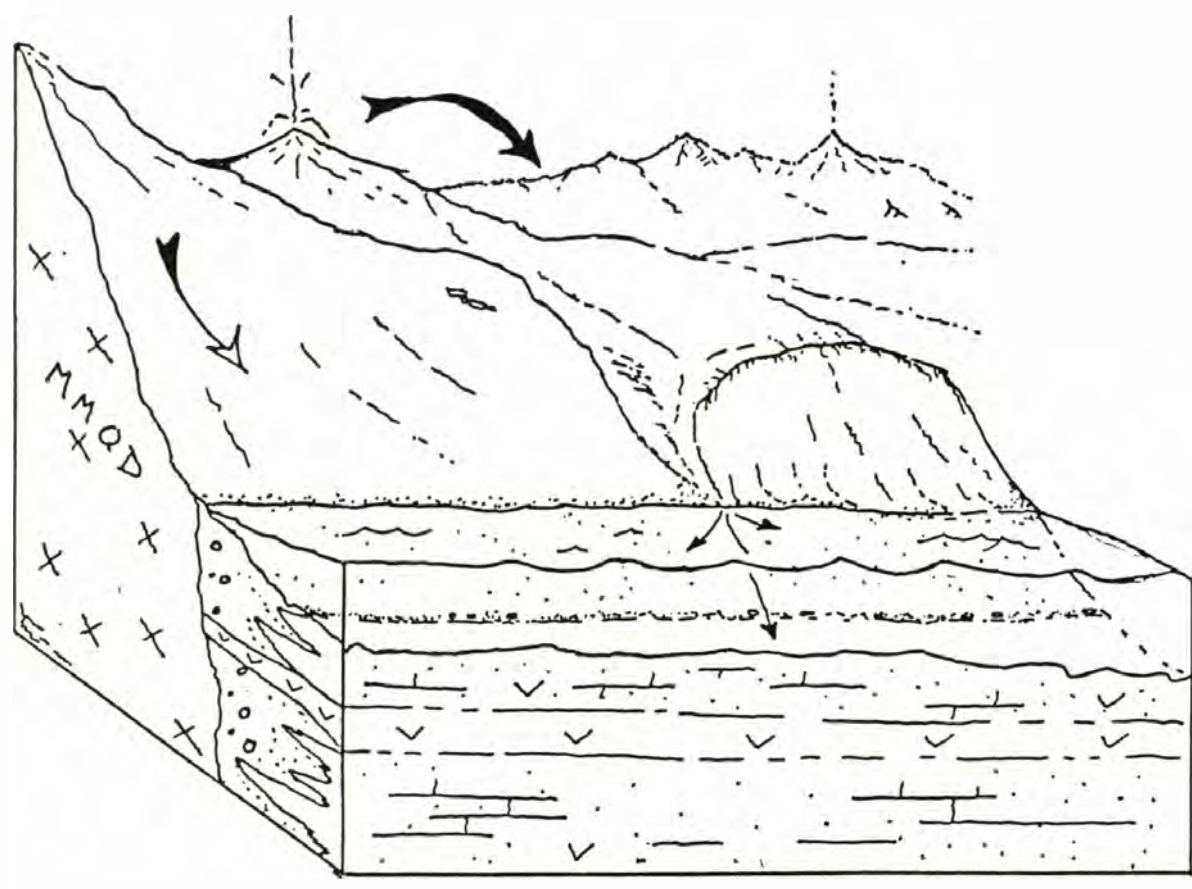


Figure 24. Possible depositional environment for the rock units west of the Le Conte fault. The overall metasedimentary package next to the Marblemount Meta-Quartz Diorite appears to be a fining outward sequence with proximal conglomerates, tuffs, and flows, grading to more distal semipelites, marls and minor limestone pods and pelites.

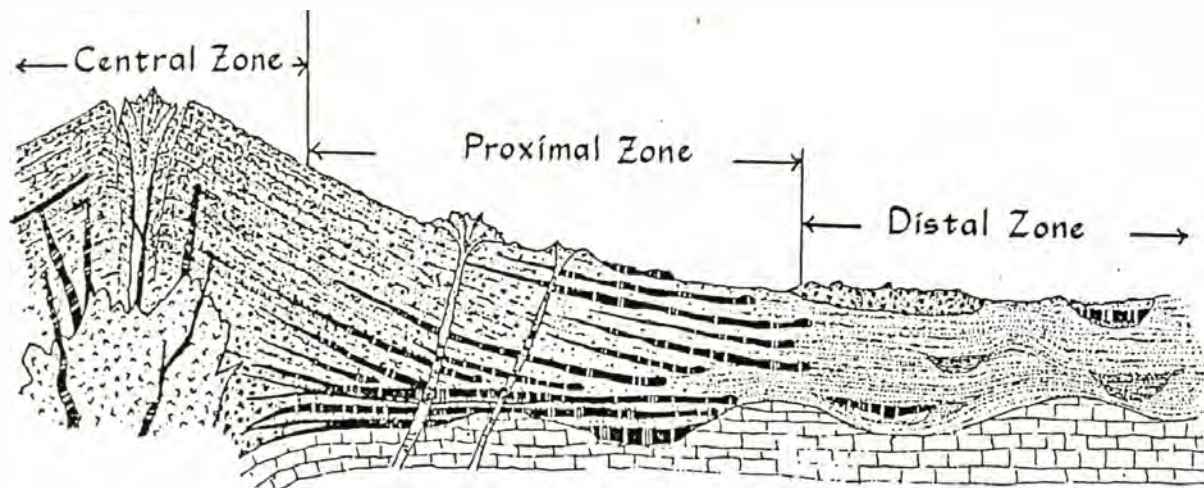


Figure 25. Principal facies variations in the volcanic rocks related to a central vent volcano (from Williams and McBirney, 1979). Proximal facies contain broad thick lavas, lahars with angular blocks up to approximately 10 meters in diameter, tephra (lapilli to coarse ash range), zones of weathering and soil development between lava flows, clastic debris reworked by water, and ignimbrites. Distal facies contain volcanic and volcaniclastic rocks interlayered with shallow water sediments and organic debris (marls) and conforms more closely to conventional stratigraphic relationships than the proximal facies.

same plagioclase clast input as did the metaconglomerate unit. The plagioclase clasts may be volcanic (tuffaceous) or detrital (clastic or volcanoclastic) in origin. Tuffaceous debris sporadically influenced the distal facies as indicated by the occurrence of the metatuff bed along the western margin of the metamarl-semipelite unit and the occurrence of thin metatuffaceous interbeds (Fig. 11).

Relationship Between the Western Cascade River Unit and the Marblemount Meta-Quartz Diorite

The contact between the Marblemount Meta-Quartz Diorite (MMQD) and the Cascade River Schist (CRS) in the field area is strongly sheared, which has masked the primary nature of the contact (see Structure Section). There are three hypotheses concerning the nature of the MMQD-CRS contact: (1) The MMQD is older than, and basement for, the CRS, and thus the MMQD-CRS contact is unconformable (Misch, 1966). This is suggested by the similarity of the plutonic clasts in the metaconglomerate unit to the MMQD. (2) The MMQD is younger and intrudes the CRS (Cater, 1982). This hypothesis is suggested by outcrop features in the the Holden area to the southwest. (3) The MMQD-CRS represents a coeval volcanic arc package, complete with sub-arc plutonics (MMQD) and supra-arc sediments and volcanics (CRS). Cary (pers. comm.) and Fugro Inc. (1979) reported intermixing of greenschist and MMQD along the contact, and suggest that the MMQD and the basal CRS represent a coeval magmatic suite.

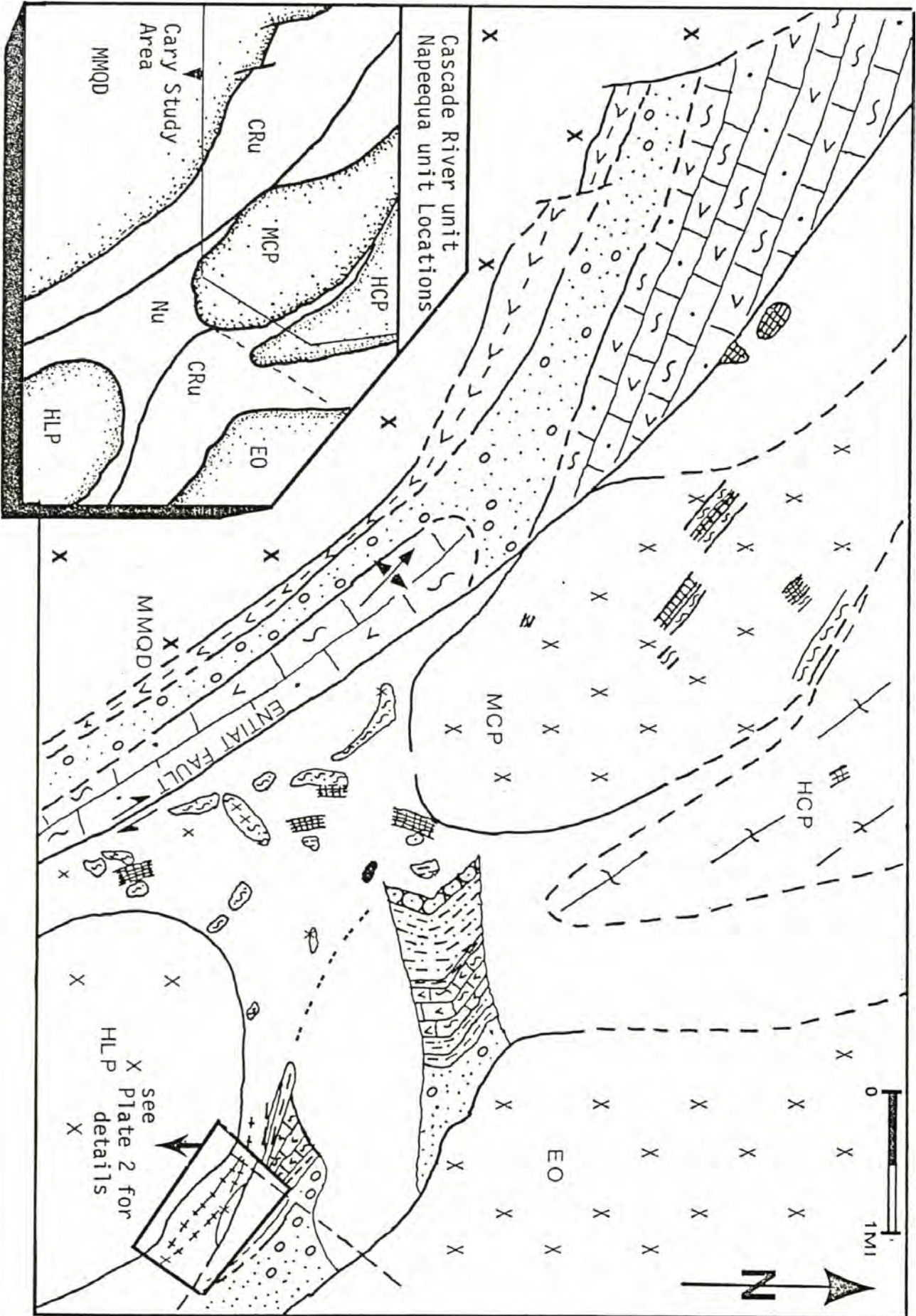
The most recent evidence supports the third hypothesis. The age of the Cascade River Schist appears to be about 220 Ma based on recent a U-Pb analysis (by J.S. Stacey) of zircon collected by Jeff Cary (Cary, pers. comm.) from a metarhyolite bed adjacent to the Marblemount Meta-Quartz Diorite. This is the same age obtained for the adjacent Marblemount Meta-Quartz Diorite (Mattinson, 1972). This age, taken with arc-related

aspects of the western Cascade River unit metasediments and volcanics, and the proximity of the MMQD to these lithologies, suggests a coeval parentage. Apparently the volcanism was active while the MMQD was exposed and being eroded, and the MMQD clasts were intermixed with the volcanic clasts (Fig. 24). Possibly the sub-arc plutonic body intruded to a shallow level of the arc. It is also conceivable that the contact between the sub-arc plutonics and supra-arc volcanics and sediments could be both unconformable and intrusive at different sites along the arc.

Correlation of the Rock Units in the Western Cascade River Unit

Cary (pers. comm.) has mapped a tuff, conglomerate, and pelite petrofacies directly to north in the Lookout Mountain area (Fig. 26). These rock units are on strike and correlative, respectively, with the greenschist, metaconglomerate, and metamarl-semipelite-pelite units observed west of the Le Conte fault in my study area. Tabor (1961) also describes rock types along strike to the southeast of my study area, which appear to correlate with the rock units in the western part of the study area (Fig. 27). The greenschist, metaconglomerate, and metamarl-semipelite units in the western part of the field area correlate with the "transitional", metaconglomerate, and calcic mica schist units mapped by Tabor (1961) to the south along the western side of the Cascade River Schist belt (Fig. 27). Tabor (1961) describes the calcic mica schists and phyllitic schists as being rich in calcite, epidote, plagioclase clasts, and graphite, in association with marble intercalations. This rock is very similar to the metamarl-semipelite unit in composition, the occurrence of marble pods, and lithologic positioning relative to the metaconglomerate unit. The units in both Cary's and Tabor's areas are 50-100% thicker than in the study area (Fig. 26, 27). Possible explanations include tectonic thinning resulting from dextral subhorizontal shear,

Figure 26. Combined geological maps of the Lookout Mountain (Cary, in progress)-Sibley Creek area (this study). Symbols are the same as in Figure 6. The Napeequa unit (Nu) west of the Le Conte fault contains distinctive ultramafite and quartz biotite schist, which are not clearly traceable versus the Cascade River unit (CRu). Cary does not report any metagabbro within his study area. Cary's area is delineated by the fine line in the index. X = ultramafite too small to be mapped



transpressive offset along the Le Conte fault (see Structure Section), and/or to primary depositional differences along strike.

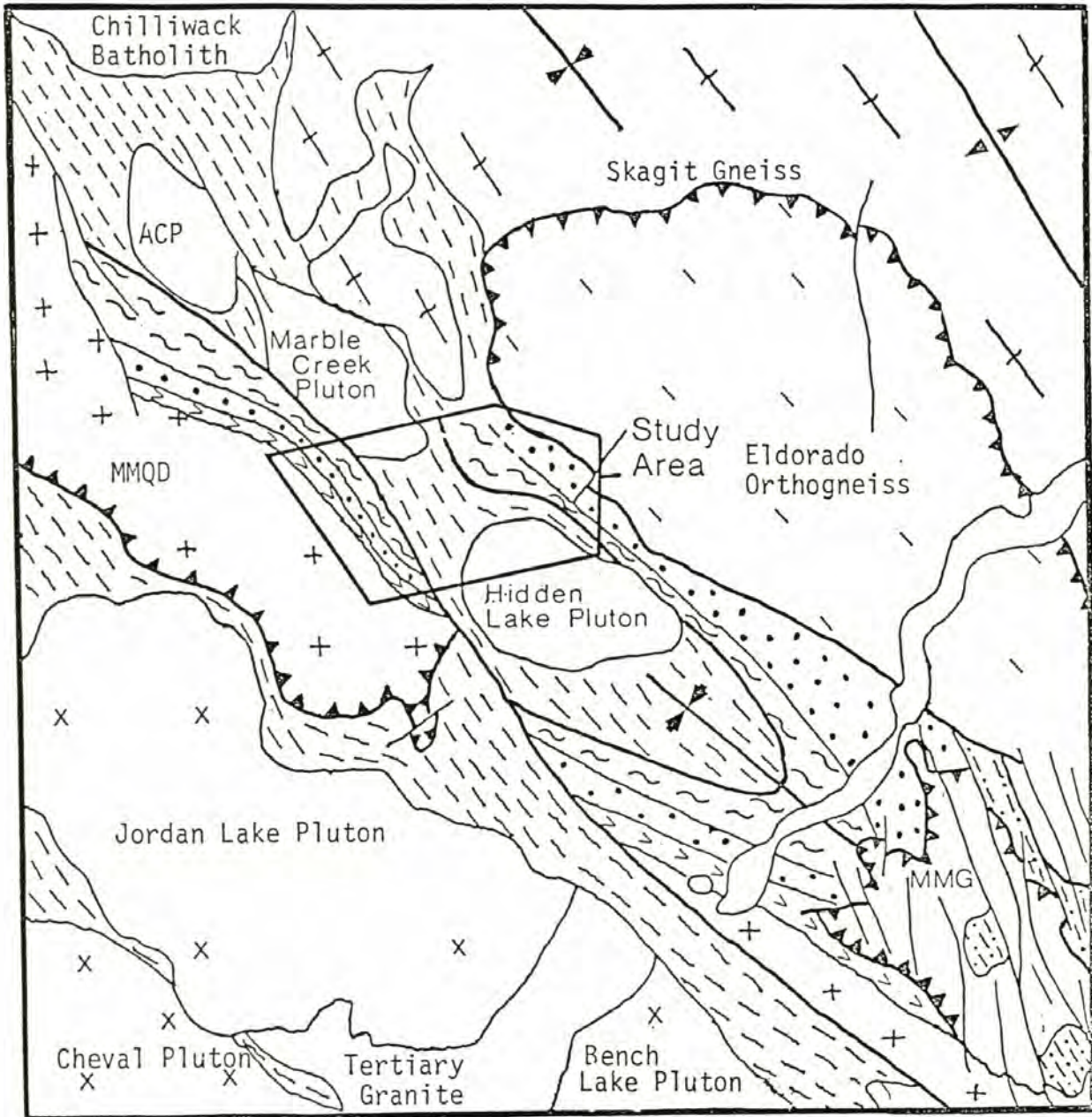
Correlation of the Rock Units in the Northeastern Cascade River Unit

The homoclinal Cascade River unit in the northeast part of the field area is on strike with, and bears a strong resemblance to, the lithologies described by Tabor (1961), and observed by the author and E.H. Brown in the vicinity of Mount Johannesburg. In this area a stratigraphy can be recognized where locally conglomeratic quartzo-feldspathic schist passes southwestward into interlayered amphibolite, metamarl, marble, and metapelites. This sequence correlates with the northeastern homoclinal Cascade River sequence in the study area (Fig. 27). Tabor (1961) reports that a calcic mica schist layer occurs along the western side of Mount Johannesburg, southeast of the metaconglomerate unit, and that a few thick beds of marble are associated with the northeastern part of this calcareous unit. One, or possibly two, marble beds occur in the northeastern part of the study area, thus correlative units appear to have the same relative positions on a regional scale. Other probable correlative units described by Tabor (1961) in the Mount Johannesburg area include amphibolite layers and black, fine-grained mica schist.

Correlation of the Central Napeequa Unit

The Napeequa unit within the field area consists of quartz biotite schists (and variants), ultramafite, minor amphibolite, and two metagabbroic bodies, which, in contrast to the rocks of the Cascade River unit, are not mappable. The inability to trace these units in the study area is due to limited exposure, and discontinuity resulting from intense faulting and folding. Cary (pers. comm.) and Tabor et al. (in press) indicate that rock types of the Napeequa unit are continuous beyond the

Figure 27. Regional geologic map showing the distribution of the Cascade River and Napeequa units of the Chelan Mountains terrane. The map is modified from Tabor, et al. (in press) to include the generalized and traceable metavolcanic, metaconglomerate, and metamarl-semipelite-pelite layers in the Cascade River unit.

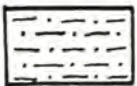


From Tabor (et al., in press)

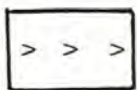
0 10 km



Quartz biotite schist (and variants), ultramafite, metagabbro and amphibolite



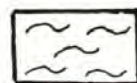
Undifferentiated



Metavolcanic unit



Metaconglomerate unit



Metamarl-semipelite-pelite unit

with additions Napeequa Unit

Cascade River Unit

study area (Fig. 27). The rock types to the north of my study area include amphibolite, quartzo-feldspathic schist, quartzite, and subordinate ultramafite, calc-silicate and marble, with the ultramafite commonly occurring as roof pendants in the Marble Creek pluton (Cary, pers. comm.). Tabor et al. (in press) indicate that the Napeequa unit continues to the south of my study area, where it terminates as a plunging fold, around which the western and northeastern Cascade River units probably merge (see Structure Section; Hypothetical Macroscopic Fold to the South of the Field Area).

Comparison of the Western and Northeastern Cascade River Units

The western and northeastern Cascade River units in the study area are similar in lithology and stratigraphy (Fig. 28), although the facing direction appears to be reversed. Both areas contain metaconglomerate dominated by felsic and granitic clasts, metamarl, metavolcanic layers, metasemipelite and metapelites. Metamorphic differences obscure the comparison. However, the overall similarities, and convergence of the distal lithologies to the south, strongly suggest that these parts of the Cascade River unit are structurally related (see Structure Section). Another possibility is that the separate areas represent two parts of the same basin (e.g. failed marginal basin between an arc and remnant arc).

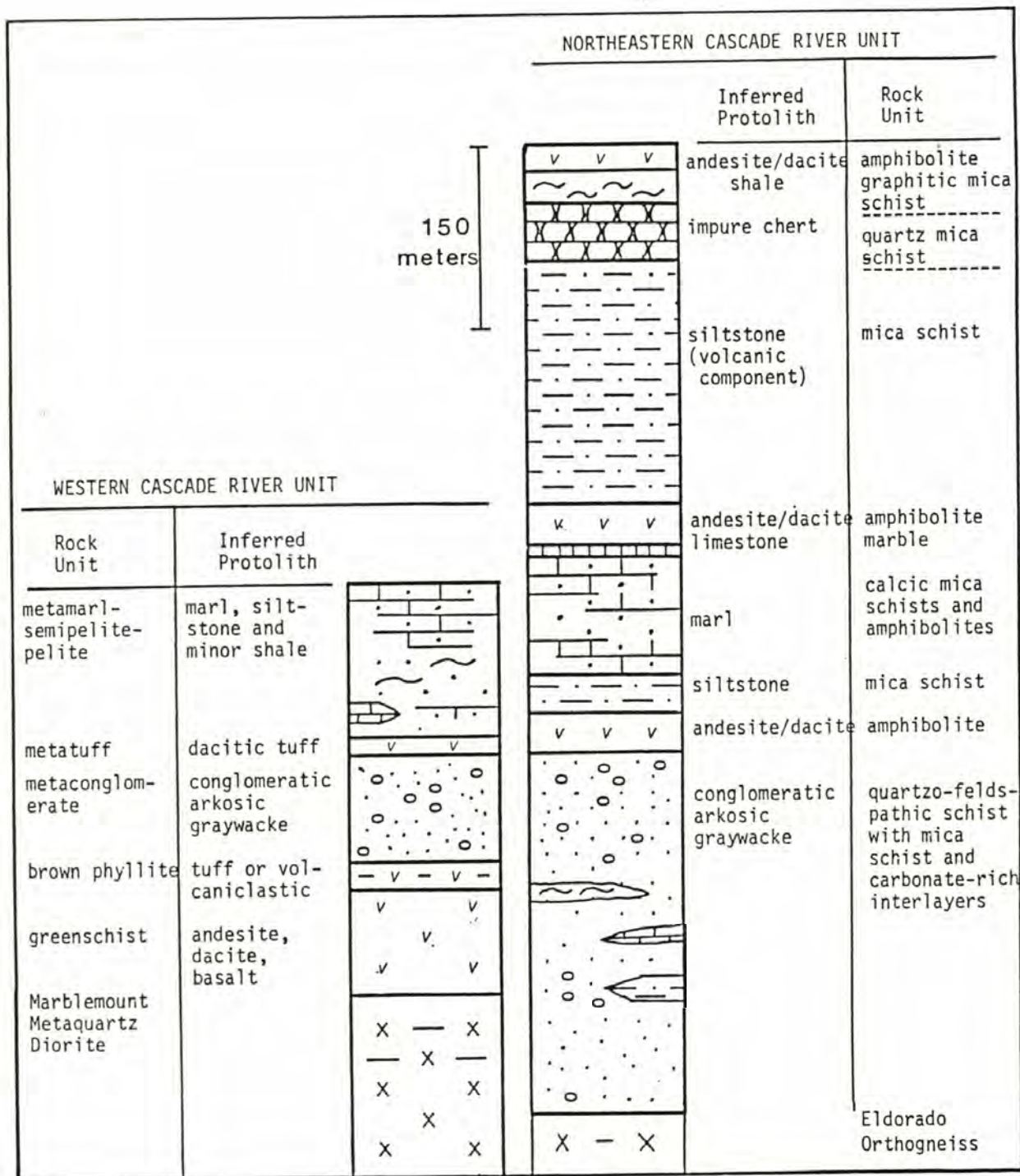


Figure 28. Generalized stratigraphic columns for the western and northeastern Cascade River units.

METAMORPHIC SECTION

Introduction

Metamorphic mineral assemblages and geothermobarometry of the Cascade River Schist (CRS) indicate that the metamorphic grade in the field area increases to the northeast across the structural trend. The same pattern is observed along the Skagit River (Misch, 1966, 1968, 1971), where the metamorphic grade increases northeastward from the greenschist facies, through the albite epidote and epidote amphibolite facies, culminating in epidote-free sillimanite bearing Skagit Paragneisses. Mapped metamorphic zones and facies in the study area include the biotite zone of the greenschist facies, the garnet zone of the uppermost greenschist and lower amphibolite facies, and the staurolite-kyanite zone of the middle amphibolite facies. These three facies correspond approximately to the western, central, and northeastern parts of the field area described in the rock units section.

Mineral Assemblages

Introduction

Mineral assemblages in metamorphosed semipelites, pelites and basites demonstrate that the CRS west of the Le Conte fault is in the greenschist facies. The CRS directly east of the fault is in the lower epidote amphibolite facies, and increases to middle epidote amphibolite facies in the northeastern part of the area (Fig. 29). Critical mineral assemblages are given in Table 2. A complete listing of the mineral assemblages are given in Appendix 1.

Greenschist Facies Mineral Assemblages

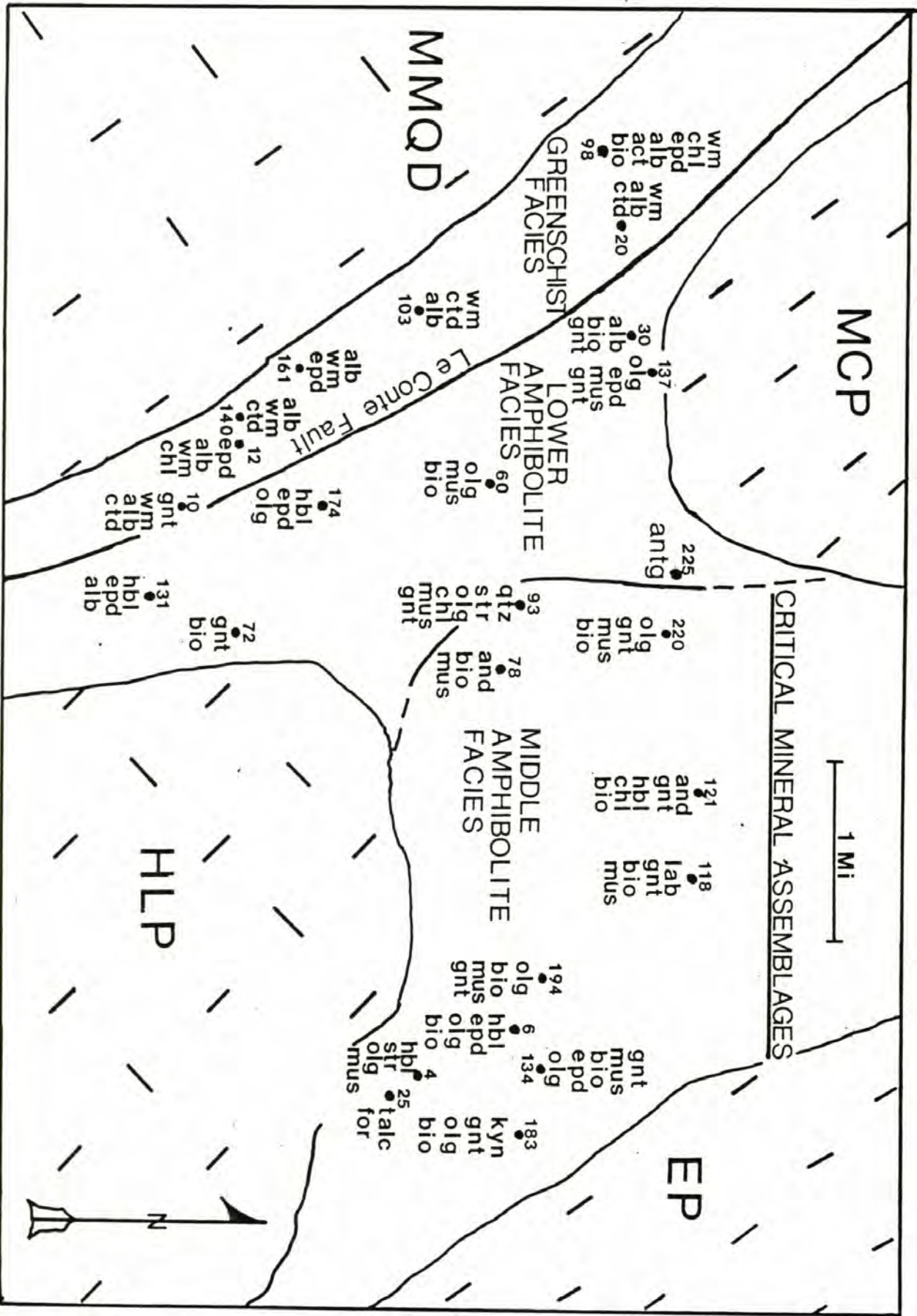
The meta-semipelites west of the Le Conte fault contain the assemblage quartz + albite + white mica, commonly with chlorite and biotite (Table 2). The rare pelites contain quartz, albite, white mica

Table 2. Type Sample Mineral Assemblages (locations given in Figure 29)

Type Sample-	Greenschist Facies							Lower Amphibolite Facies						
	12	15	10b	103	140	209	98	60	*30	137	72	131	179	225
	SP	SP	P	P	P	P	B		SP	SP	SP	B	B	UM
Protolith-quartz	X	X	X	X	X	X	x	X	X	X	X			
plagioclase	00	X	x	x	x	x	x	16	00	20	x	00	15	
epidote	x		x	x	x		X					x	x	
clinozoisite										x				
chlorite	X		x	r		r	r		r	r	R			
biotite			x	x		x	x	x	x	x	x	x		
white mica	x	X	X	X	X	X		X	x	X				
chloritoid			x	x	x	x								
garnet			X						x	x				
actinolite							X							
hornblende												X	X	
tourmaline	x	x		x	x	x		x						
magnetite			x				x							
ilmenite		x							x					
rutile		x		x				x	x	x				
sphene	x			x	x							x		
opaque				x	x	x		x		x			x	x
calcite	X				x									
graphite		x	x					x	x	x	x			
antigorite														X
magnesite														X
Middle Amphibolite Facies														
Type Sample-	220*	121*	118*	93b*	78	194*	184*	134*	183	183b	4	124	6	25
	SP	SP	SP	SP	SP	SP	SP	SP	P	P	P	P	B	UM
Protolith-quartz	X	X	X	X	X	X	X	X	X	X	X	x	x	
k-spar								r		r				
plagioclase	21	32	49	28	32	23	30	27		30				
epidote						x	x		x	x	x		x	
clinozoisite		x												
chlorite		x	r	x			R	x	R	r	x			
biotite	X		X	X	X	X	X	X	x	x		x	X	
muscovite	X	X	X		X	X		X	X	X	X	X		
garnet	x	x	X	X		x				x		X		
kyanite										X				
staurolite									x		x	x		
hornblende		X	X	x			x				x		X	
tourmaline		x		x						x		x		
ilmenite	x	x	x	x		x	x	x		x		x		
rutile	x	x	x	x		x	x	x	x					
sphene									x				x	
opaque									x		x			
calcite			x										x	
graphite				x								x		
antigorite														r
forsterite														X
talc														X

Protoliths- semipelite (SP), pelite (P), basite (B), ultramafite (UM).
 X,x = greater and less than approximately 10% (respectively)(R,r = retrogressive products). * = geothermobarometry sample.

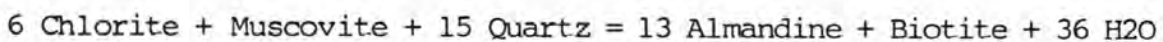
Figure 29. Map showing the locations of the critical assemblages and metamorphic facies. Abbreviations- white mica (wm), muscovite (mus), chloritoid (ctd), albite (alb), oligoclase (olg), andesine (and), labradorite (lab), epidote (epd), biotite (bio), chlorite (chl), garnet (gnt), actinolite (act), hornblende (hbl), staurolite (str), kyanite (kyn), antigorite (antg) and forsterite (fors). The garnet isograd occurs along or just west of the Le Conte fault. The oligoclase isograd occurs along, or just east of, the Le Conte fault. The staurolite isograd could be drawn at the boundary between the lower and middle amphibolite facies. The general lack of strongly aluminous metasediments in the lower amphibolite facies (Napeequa unit) may result in the displacement of this isograd to the east.



(muscovite?), with three occurrences of chloritoid, and one chloritoid + almandine (#10b) suggesting proximity to the garnet zone at that locality (Fig. 29). The metabasites contain actinolite to actinolitic hornblende + albite + epidote + quartz + biotite + chlorite and white mica reflecting biotite zone conditions (Fig. 29, Table 2).

Lower Amphibolite Facies Mineral Assemblages

The meta-semipelites directly east of the Le Conte fault contain quartz + albite (or oligoclase) + biotite, minor white mica (probably muscovite), and commonly almandine. The Le Conte fault is interpreted to mark the boundary between the greenschist and lower amphibolite facies in the field area. This structure marks the beginning of abundant non-retrogressed biotite, almandine, and oligoclase + epidote within the field area (see Structure Section; Timing of Metamorphism and Deformation). A possible reaction leading to the production of almandine is (Thompson and Norton, 1968):



The abundance of almandine and biotite, and the paucity of chlorite and muscovite in these samples, relative to the semi-pelites across the fault in the greenschist facies, may be evidence for this type of reaction; and/or, the abundance of biotite over other micas reflects the relatively low aluminum and high ferromagnesium content of these oceanic metasediments (See Rock Units Section). The first appearance of key minerals such as staurolite and kyanite may be displaced to the northeast due to the low Al bulk composition of the Napeequa metasediments (Fig. 29, Table 2). These minerals first appear in the metapelites of the northeastern Cascade River unit.

Middle Amphibolite Facies Mineral Assemblages

Mineral assemblages in metapelitic units in the east-northeastern part of the field area are indicative of the staurolite-kyanite zone of the middle amphibolite facies. The pelites contain quartz + oligoclase to andesine + muscovite + garnet, commonly biotite, one occurrence of kyanite, and two occurrences of staurolite. The metabasites contain hornblende, epidote, oligoclase, and commonly biotite (Fig. 29; Table 2). A northeasterly directed metamorphic gradient is also suggested by the increase in porphyroblasts and matrix average grain-size from the greenschist to the middle amphibolite facies (Table 3).

Table 3. Upgrade Grain Size Variations

	<u>Greenschist-Lower Amphibolite Facies</u>	<u>Middle Amphibolite Facies</u>
Garnet	1 - 2 mm (diameter)	2 mm - 1 cm (diameter)
Ca-Amphibole	1 - 2 mm (length)	2 mm - 2 cm (length)
Matrix	fine- to medium-grained	medium- to coarse-grained

Petrogenetic Grid

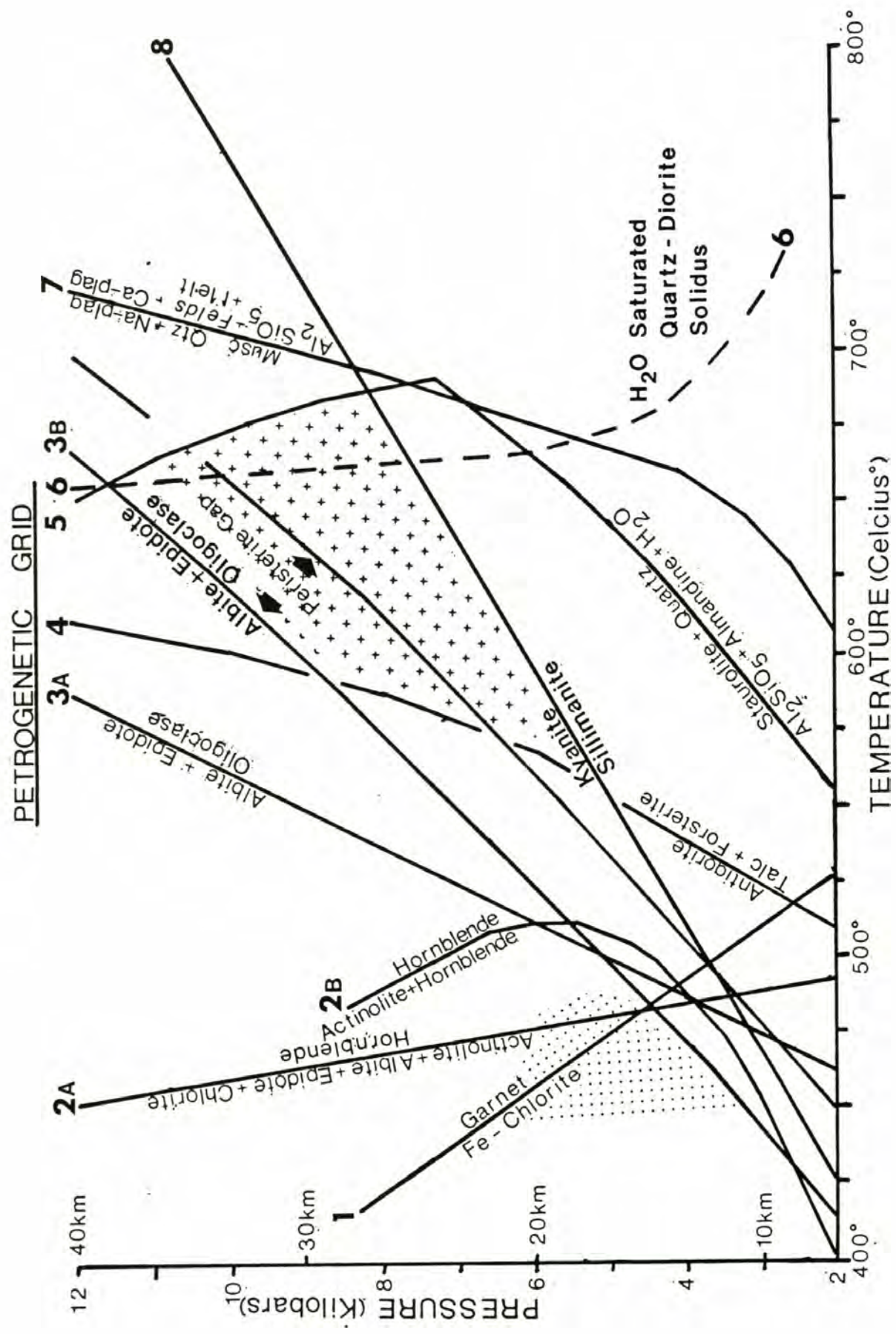
Introduction

The index minerals in the study area include garnet, actinolite-hornblende, talc + forsterite, albite-oligoclase, staurolite + quartz, staurolite + hornblende, kyanite + hornblende, and kyanite. The stability fields of these minerals, and mineral assemblages, have been investigated by many workers and are summarized in a petrogenetic grid (Fig. 30).

Upper Greenschist Facies Equilibria

Garnet Stability- The stability field of almandine garnet was estimated by Brown (1978) using the relative order of appearance of minerals in terranes crystallized along different P-T paths, published work on O 18/16 fractionation, Mg/Fe distribution coefficients, sphalerite composition, experimentally studied reactions, and thermodynamic calculations. The one garnet observed west of the Le Conte fault is

Figure 30. Petrogenetic grid containing published reaction lines for the key equilibria in the field area. Reaction lines were derived from Brown, 1978 (1, 2A, 3A), Maruyama (et al., 1983)(2B, 3B), Pigage and Greenwood (1982)(5), Holdaway (1971)(8), Piwinski and Wyllie (1970)(6), Huang and Wyllie (1975)(7). Reaction line 4 was determined using the PTXss program of Berman (unpublished). The stippled pattern corresponds to the P-T region estimated for the greenschist facies, using the single occurrence of garnet, the hornblendic nature of the actinolite, and the occurrence of albite, which suggest proximity to reaction lines 1, 2A, and 3B, respectively. The crossed pattern corresponds to the P-T region estimated for the middle amphibolite facies, using the occurrence of oligoclase to bytownite + epidote, kyanite, hornblende, talc + forsterite, and staurolite + quartz. The different slopes and intercepts of the temperature axis reactions 3A and 3B demonstrate the ambiguities involved with the P-T estimates using the petrogenetic grid approach.



almandine-rich (#10b; Appendix 3) and therefore crystallized at or above the stability limit of almandine (greater than 450–500 C). This one occurrence adjacent to the Le Conte fault, together with the lack of garnet in the other metapelites and metasemipelites west of the Le Conte fault, and the abundance of garnet east of the fault suggests: 1) the Le Conte fault is in part a post-metamorphic structure; and 2) the rocks west of the Le Conte fault were metamorphosed to P-T conditions proximal to the garnet reaction line (Fig. 30). These conclusions are also supported by the Ca-amphibole and plagioclase compositions bordering the fault.

Greenschist-Amphibolite Facies Transitional Equilibria

The boundary between the greenschist and amphibolite facies is traditionally drawn where actinolite and albite + epidote are eliminated in favor of hornblende and oligoclase + epidote. This boundary is defined by reactions which form more calcic plagioclase and hornblende-rich amphibole at the expense of epidote, albite, and chlorite. The transition between these facies is complicated by the occurrence of a peristerite gap between albite and oligoclase and immiscibility between actinolite and hornblende.

Actinolite-Hornblende Transition- The Ca-amphiboles west of the fault vary from actinolite to hornblende, with most being actinolitic hornblende (Fig. 31, Appendix 3). Misch and Rice (1975) report a probable immiscibility gap (based on Al content) between tremolite and hornblende at or near the oligoclase isograd in the Skagit section. No such gap (based on Si or Al) is evident in the present study area. The compositions also span the proposed compositional gap of Maruyama et al. (1983) who attributes the lack of such a gap to a low FeO/MgO whole rock ratio. Ca-amphiboles just east of the fault are hornblende (Si less than 7.25), and indicate that the greenschist-amphibolite boundary occurs along

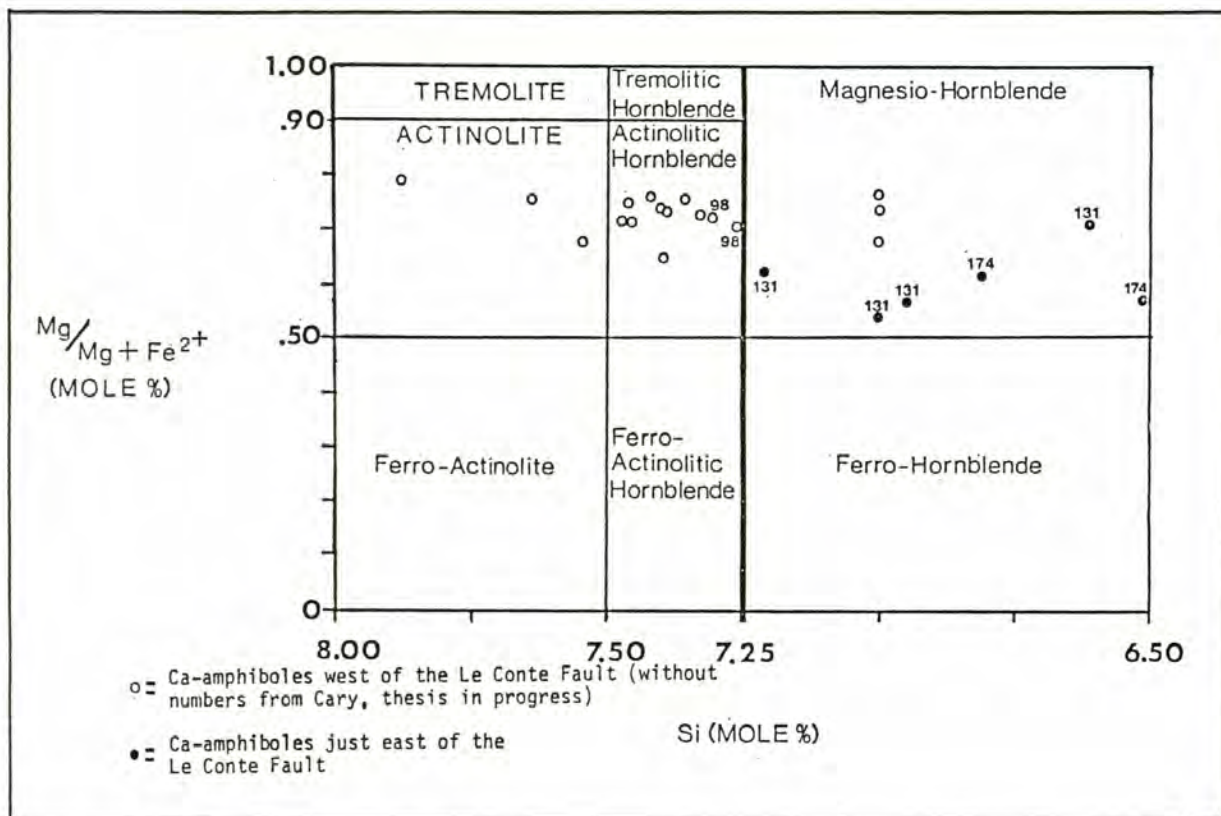


Figure 31. Compositions of the Ca-amphiboles, based on the classification scheme of Leake (1979), which indicate that the greenschist-amphibolite facies boundary is structurally controlled by the Le Conte fault.

the Le Conte fault.

Albite-Oligoclase Transition- Albite (An less than 5%) + epidote occurs west of the Le Conte fault (Table 1, Figure 29), whereas oligoclase + epidote (#137 & 179), and albite + epidote + hornblende (#131) coexist east of the fault. The oligoclase isograd is interpreted to occur at, or just east of, the Le Conte fault, or a narrow belt of albite amphibolite facies is possible just east of the fault (Fig. 29). Misch (1979) states that a narrow belt of albite-epidote amphibolite facies occurs along the western boundary of the amphibolite facies along strike to the north-northwest in the Skagit section.

Middle Amphibolite Facies Equilibria

The stability of hornblende, oligoclase, staurolite + quartz, talc + forsterite, kyanite, and staurolite + hornblende places semi-quantitative constraints on the P-T region occupied by the middle amphibolite facies (Table 2, Fig. 29). The stability limits of several of these minerals and minerals pairs are exceeded in the Skagit Gneiss, indicating that temperature increases to the northeast (Misch, 1971).

Staurolite + Quartz Stability- The upper temperature stability limit of staurolite + quartz is 650 C at 8-10 kb, assuming a high Fe/Mg ratio in staurolite (Pigage and Greenwood, 1982), and that Fe and Mg are not fractionated between staurolite and garnet (Brown and Forbes, 1986)(Fig. 30). The stability of staurolite + quartz is exceeded upgrade in the Skagit Gneiss where staurolite is only found as inclusions in garnet (Misch, 1968; Whitney, 1987).

Talc + Forsterite Stability- Ultramafic assemblages in the field area include antigorite + magnesite in the lower amphibolite facies and forsterite + talc + antigorite in the middle amphibolite facies, with

antigorite being a retrogressive product of forsterite. Reactions constraining these assemblages include:

(1) Antigorite = 18 Forsterite + 4 Talc + 27 H₂O (steep positive slope and intercepts 600 C at 9 Kb).

(2) Talc + Forsterite = 5 Enstatite + H₂O (steep negative slope and intercepts 650 C at 9 Kb.).

The assemblage forsterite + talc suggests temperatures between 600-650 C for the middle amphibolite facies (assuming a low Fe content), which is in agreement with the temperatures suggested by the stability of staurolite + quartz. Higher grade assemblages in the Skagit Gneiss include: forsterite + anthophyllite; anthophyllite + tremolite + chlorite + talc; forsterite + talc + chlorite; and forsterite + enstatite + chlorite (Whitney, 1987).

Kyanite and Staurolite + Hornblende Stability- The presence of kyanite in the middle amphibolite facies suggests that pressures were greater than 6-8 kb, assuming temperatures of 600-700 C for this facies (Holdaway, 1971)(Fig. 30). Also, the coexistence of staurolite + hornblende (#3; Fig. 48a), and hornblende + kyanite (#183b), are indicative of high pressure metamorphism (Selverstone, et al., 1984). Whitney (1987) also reports that staurolite + hornblende coexist in the Cascade River Schist directly to the north of the these samples in the Marble Creek Area.

Geothermobarometry

The Thermometer used in this study is based on the distribution of Mg and Fe between garnet and biotite (Ferry and Spear, 1978). The barometer used in this study is based on the distribution of Ca and Fe in the GRIPS assemblage (Garnet, Rutile, Ilmenite, Plagioclase, Silica; Bohlen and Liotta, 1986), and the total aluminum content of magmatic hornblende

(Hammarstrom and Zen, 1986; Hollister, et al., 1987). Mineral compositions (Appendix 3) were determined by E.H. Brown using the electron microprobe at the University of Washington.

Geothermometry

Garnet-Biotite Temperatures- The Fe-Mg distribution coefficient (Kd) between garnet and biotite is dominantly temperature sensitive and thus valuable for geothermometry (Ferry and Spear, 1978). The temperature (T) and distribution coefficient (Kd) are related by:

$$T(K) = -12,454 - .057 P(Kb) - 3RT \text{ LN}(Kd) / -4.662$$

Temperatures in the range of 494 to 653 C (+/- 50 C) are obtained using garnet rim-biotite compositions in rocks of the middle amphibolite facies, assuming an ideal solution model and pressures of 8 kb. An ideal solution model ignores the effects of Ca and Mn substitutions in garnet, and Ti and Al(4) substitutions in biotite. Ferry and Spear state that garnet-biotite geothermometry may be useful without correction for additional components if the mole fraction of Ca + Mn is less than .20. Significant amounts of Ca and Mn in garnet result in an underestimation of the metamorphic temperatures. Newton and Haselton (1981) recommend that only garnets with Mn less than 1/3 Mg be used, with the assumption that Mn mixes ideally with all other components. Samples #184 and 220 contain the largest molar fractions of Ca and Mn, and highest Mn/Mg ratio and give the lowest and most unreasonable temperatures (Table 4).

Table 4. Ferry and Spear Temperatures Uncorrected for Ca and Mn
X CaMn = (Ca + Mn)/(Ca + Mn + Fe + Mg) less than .20 and Mn/Mg less than .33

<u>Sample #</u>	<u>X CaMn</u>	<u>Mn/Mg</u>	<u>Temperature (C) (8Kb)</u>
#194	.17	.55	573 (+/- 50 C)
#93b	.18	.06	559
#134	.18	.37	646
#118b	.20	.32	653
#184	.30	1.04	520
#220	.35	1.40	494

The relatively high amounts of Ca and Mn in all these garnets indicate that nonideal solution models are needed. Exceptions may include samples 134 and 118. These samples meet the stipulated requirements, give reasonable ideal solution model temperatures (Fig. 30), and unreasonably high non-ideal solution model temperatures (Fig. 32). This study has applied the nonideal solution models of Ganguly and Saxena (1984) and Berman (unpublished) for garnet, and were plotted using the P-T-Xss program of Berman (unpublished). Both garnet models result in similar upward revisions from the temperatures estimated using the ideal solution model of Ferry and Spear (Table 5). The "preferred" column in Table 5 gives the average of: 1) the three reasonable ideal Ferry and Spear ideal solution temperatures (Table 4; #93, 134, 118); 2) the two reasonable nonideal Ganguly and Saxena temperatures (Table 5; #220, 194); and 3) drops the retrogressed sample (#184). This "preferred" temperature agrees with the temperature estimated using the petrogenetic grid (Fig. 32).

Table 5. Garnet-biotite Temperatures (C)

Sample #Nonideal.....		Ideal.....		"Preferred"
	Ganguly	and Saxena	Berman	Ferry and Spear		
93b	693		691	559 +/- 50 C		559
220	678		620	494 "	"	678
194	647		675	573 "	"	647
184	583		528	520 "	"	-
134	770		770	646 "	"	646
118b	800		760	653 "	"	653
						637

Geobarometry

GRIPS- The GRIPS barometer (Bohlen and Liotta, 1986) is based on the reaction: Garnet (Gr1,Alm2) + 2 Rutile = 2 Ilmenite + Anorthite + Quartz. All samples contain ilmenite in the matrix and as inclusions in the garnet (#194, 134, 118b, 93b and 121). Rutile occurs in the matrix of samples 184, 134, 118b, and occurs as inclusions in garnet in samples 184 and

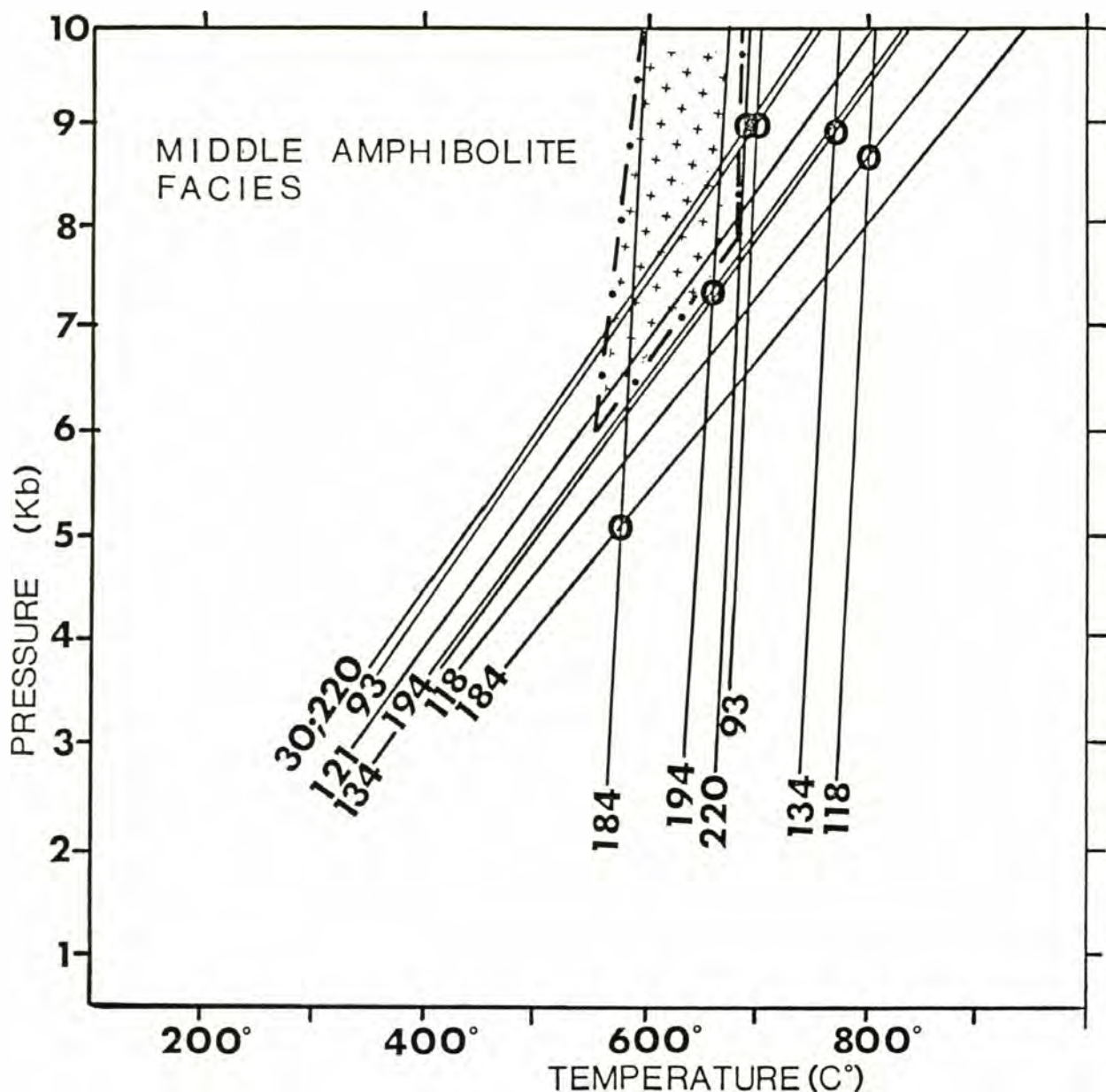


Figure 32. Geothermobarometric results for the middle amphibolite facies using the garnet-biotite thermometer of Ferry and Spear (1978) and the GRIPS barometer of Bohlen and Liotta (1986). These results were obtained using the computer program "P-T-Xxx88" from Berman (personal communication) and based on the non-ideal solution model of Ganguly and Saxena (1984) for garnet (Garnet-biotite and GRIPS), and Berman (unpublished) for plagioclase (GRIPS). The pattern of crosses is the P-T region estimated for the middle amphibolite facies using the petrogenetic grid approach. Circles represent the intercepts of the non-ideal GRIPS and garnet-biotite lines. No garnet-biotite temperatures were estimated for samples 30 and 121. Temperatures are ± 50 C and pressures are ± 1 kb.

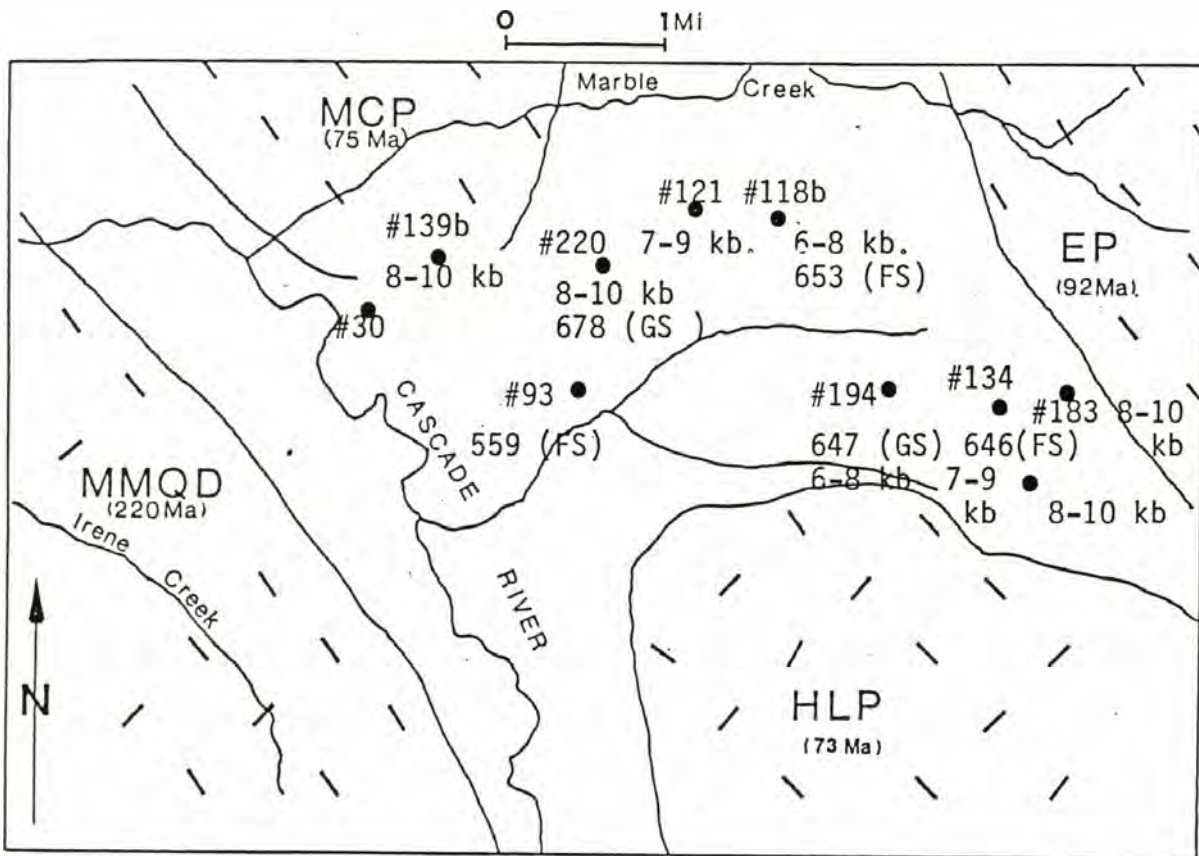


Figure 33. Location and P-T estimates for the geothermobarometric samples, and the high pressure assemblages of hornblende + staurolite (4) and hornblende + kyanite (183). Abbreviations next to the temperatures refer to the calibrations of Ferry and Spear (FS) and Ganguly and Saxena (GS). Assuming reasonable temperatures for the amphibolite facies samples 30 and 121 also suggest pressures of 8-10 kb.

118b. Ilmenite and rutile were considered to be pure. Maximum and minimum pressures can be inferred from rutile and ilmenite assemblages, respectively. Sample #184 lacks ilmenite and gives a low and anomalous pressure estimate (Fig. 32). Pressures of 8-10 kb \pm 1 Kb were obtained for the other 7 samples using both an ideal and non-ideal (Fig. 32) solution model for garnet (Ganguly and Saxena, 1984; Berman, unpublished) and plagioclase (Furman and Lindsley, 1988).

Aluminum in Hornblende- The aluminum content of magmatic hornblende is pressure sensitive in granitic rocks (Hammarstrom and Zen, 1986; Hollister et al., 1987). Hollister et al. (1987) conclude that the pressure of solidification of calc-alkaline plutons containing the buffering assemblage of quartz, plagioclase, orthoclase, biotite, magnetite and sphene can be estimated to \pm 1 kb using hornblende rims. The Marble Creek pluton contains this buffering assemblage, and yields pressure of 9-10 (\pm 1) kb using rim compositions (Table 6; Appendix 3).

Table 6. Pressure Results for the Marble Creek pluton (#139b)

	Hbl'd Rim	Hbl'd Core
Pressure (Zen, et al.)-	9.3 Kb	6.7 Kb
Pressure (Hollister et al.)-	10.0 Kb	7.1 Kb
Total Aluminum (mole %)-	2.77	2.11

Summary of the P-T Estimates

Greenschist Facies

The one occurrence of almandine garnet and the abundance of actinolitic hornblende in the greenschist facies suggests proximity to the garnet-in and hornblende-in reaction lines, and thus pressures of 3-6 kb and 400-475 C for this facies (Fig. 30). The abundance of albite + epidote indicates temperatures below the oligoclase-in reactions line. Cary (pers. comm.) using the crossite component (Na M4) of actinolite (Brown, 1977) obtained pressures of 3-4 Kb for the greenschist facies, which is in agreement with the pressures inferred using the petrogenetic

grid approach.

Lower Amphibolite Facies

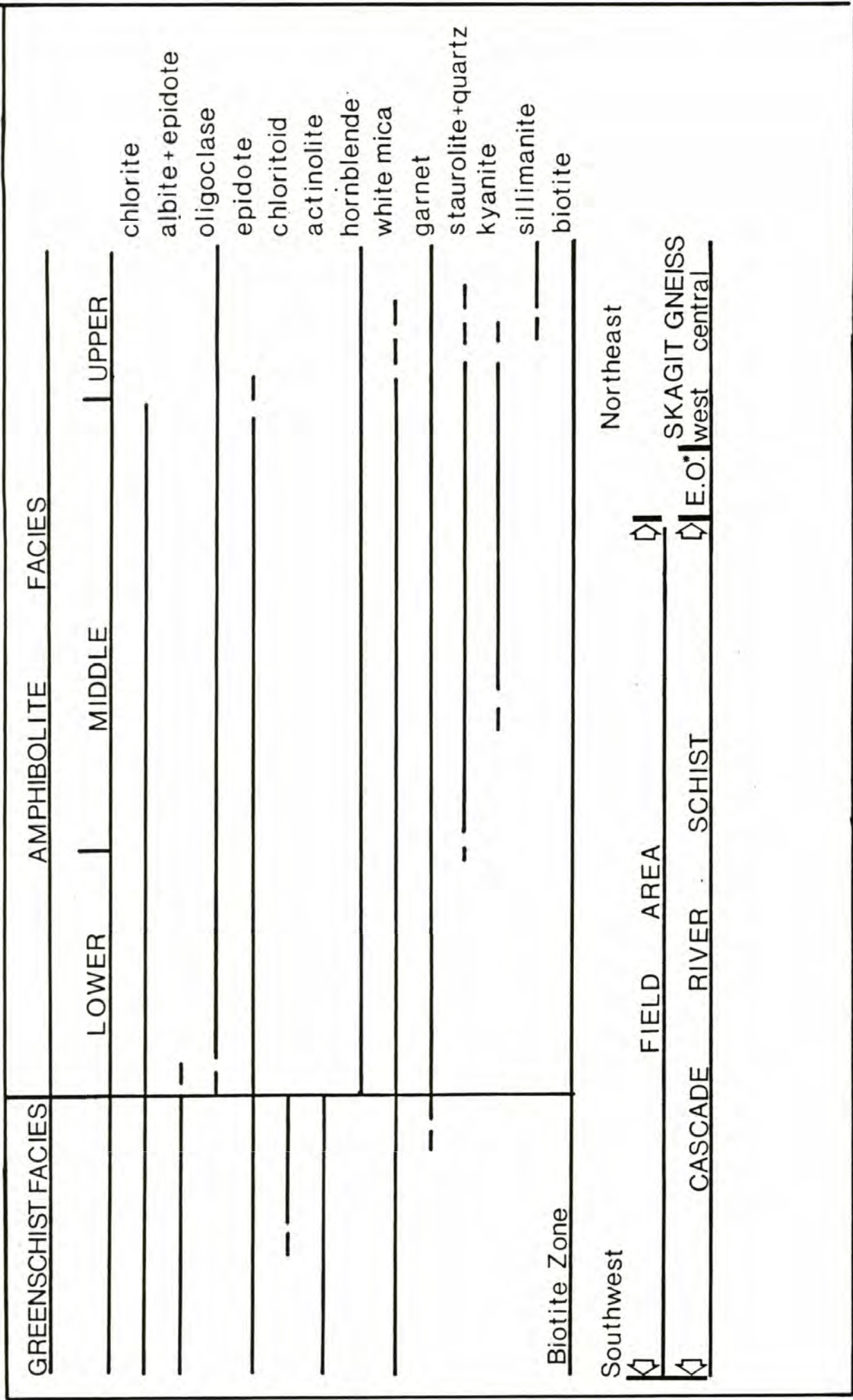
Geobarometry and mineral assemblage data suggest that a substantial increase in pressure and temperature occurs along the Le Conte fault or at the greenschist-amphibolite break. The occurrence of hornblende (Fig. 31), garnet and the proximity to the oligoclase isograd, suggests temperatures above 500 C (Fig. 30). The fact that garnet, oligoclase + epidote, and hornblende all appear at the boundary between the greenschist and amphibolite facies may suggest pressures of 4-6 Kb for the lower amphibolite facies (Fig. 30). However, the coincident first appearance of these key index minerals is probably the result of late-to-post metamorphic offset along the Le Conte fault, which has truncated the original gradient and structurally juxtaposed the first appearance of these minerals. The one occurrence of almandine garnet just west of the fault in the field area, and the existence of an albite amphibolite facies along Skagit River (Misch, 1979), suggest that the paragenetic sequence is garnet, hornblende, and then oligoclase. This paragenetic sequence suggests pressures higher than 5 Kb for the lower amphibolite facies (Fig. 30). The high pressures of solidification for the Marble Creek pluton suggests that the high pressure metamorphism extends to the Le Conte fault. The pluton intrudes and contains roof pendants of lower amphibolite facies rock types (Cary, pers. comm.; see Rock Units)(Fig. 29), and is interpreted to reflect the peak metamorphic pressures of this facies. These pressures contrast with the moderate pressures estimated for the greenschist facies and suggests that a pressure differential of 3-6 kb exists across the Le Conte fault.

Middle Amphibolite Facies

The occurrence of hornblende, oligoclase (to labradorite) + epidote, kyanite, staurolite + hornblende, staurolite + quartz, and forsterite + talc suggests pressures of 8-10 kb and temperatures of 575-675 C for the middle amphibolite facies (Fig. 30). The agreement between the mineral equilibria (kyanite, staurolite + hornblende) and the GRIPS barometer pressure estimates is strong evidence for high pressure metamorphism. However, temperatures estimated for this facies are poorly constrained due to: 1) uncertainties in the positioning of the staurolite + quartz and talc + forsterite stability fields due to uncontrolled chemical variables; and 2) the generally scattered garnet-biotite temperatures. The preferred P-T region is given in Figure 30, although temperatures as high as 700 C and as low as 550 C cannot be ruled out. The temperatures are constrained to be between 575-675 C (at 9 kb), assuming the oligoclase-in (Maruyama, et al., 1983) and staurolite-out (Pigage and Greenwood, 1982) reaction lines are essentially correct, which is in agreement with the "preferred" (Table 5) average garnet-biotite temperature of 630 +/- 50 C (Fig. 32).

Comparison with the Amphibolite Facies in the Skagit Gneiss- Whitney (1987) reports temperatures of 720 C and pressures of 9 Kb for the sillmanite bearing Skagit paragneisses. These upper amphibolite facies rocks are above the stability field of staurolite + quartz since staurolite is only found as inclusions in garnet (Yardley, 1978). Whitney reports temperatures of 650 and pressures of 9 Kb for the staurolite bearing Skagit paragneisses, which suggests that the upper stability limit of staurolite + quartz of Pigage and Greenwood (1982) is essentially correct (650 C at pressures of 8-10 kilobars; Fig. 30). The Skagit Gneiss is also evidenced to be metamorphosed at higher temperatures by the absence of epidote (Misch, 1971) and muscovite (Yardley, 1978; Fig. 30

Figure 34. The stability ranges of key index minerals from the greenschist facies in the western Cascade River Schist belt, through the lower, middle, and upper amphibolite facies in the eastern Cascade River Schist belt and into the central part of the Skagit Gneiss. The data are compiled from: albite + epidote (this study; Misch and Rice, 1975), oligoclase + epidote (this study; Misch and Rice, 1975), epidote (Misch, 1968), chloritoid (this study), actinolite and hornblende (this study; Cary, pers. comm.; Misch and Rice, 1975), white mica (Yardley, 1978), garnet (Misch, 1968; this study), staurolite + quartz (Misch, 1968; Yardley, 1978; this study), kyanite (Misch, 1968; this study), biotite (Misch, 1968; this study), sillimanite (Misch, 1968; Yardley 1978).



line #7), and the occurrence of enstatite (greater than 650 C at 9 Kb) and anthophyllite bearing ultramafic rocks (Fig. 34). Misch (1979) maps a northwest trending epidote-out isograd to the northeast of the study area, which separates the middle amphibolite facies of the CRS and western Skagit Gneiss from the upper amphibolite facies in the central Skagit Gneiss.

Misch proposed (1968) that the migmatitic gneisses formed in the core of a "thermal anticline"; a northwest trending complex antiform defined by gross metamorphic pattern and foliation (Haugerud et al., 1987). Evidence presented by Misch (1979, 1975, 1971), Whitney (1987), and this study indicates that the central part of the Skagit Gneiss reached the highest temperatures. Whitney (1987) states that, "there is not enough data to evaluate Misch's proposal that the metamorphism of the Skagit Gneiss was regionally isobaric, but the presence of coexisting staurolite and hornblende in the CRS suggests that high pressures were attained there as well." Barometric and mineral assemblage data presented in this study support the interpretation that the amphibolite facies metamorphism in the CRS and the Skagit Gneiss was approximately regionally isobaric to the Le Conte fault (in the study area).

Age of Metamorphism

Little constraint can be placed upon the upper time limit of metamorphism, although the metamorphism is presumably not much older than the abundant 90 Ma plutons (i.e. 92 Ma Eldorado Orthogneiss; Mattinson, 1972). The minimum age of metamorphism in the field area is constrained by the K-Ar biotite ages of 38-48 Ma on the Hidden Lake pluton, Eldorado Orthogneiss and Cascade River Schist (Haugerud et al., 1987; Mattinson, 1972), which are evidence for cooling through the 280-300 C (+/- 50)

isotherm (Hunziker, et al., 1984). K-Ar biotite ages determined throughout the Crystalline Core indicate that the orogen was uplifted progressively later towards the Skagit Gniess (Brown and Talbot, manuscript).

Structure Section

Introduction

The structural geometry of the study area is complex, containing two major, syn-to-late metamorphic, penetrative phases of deformation (D1 and D2), and three minor localized deformations.

Domain Analysis

The various phases of deformation are differentially developed in different parts of the area, so for ease of analysis the area has been divided into three domains (A, B and C), with domain C being sub-divided into two sub-domains (domains C1 and C2)(Fig. 35). Each domain shows a relatively homogeneous structural style, history, metamorphic grade and general protolith composition (Table 7). The foliation in the field area strikes to the northwest and dips steeply to the southwest, although northeast dips are common as a result of later folding (Fig. 37A). Lineations in the field area define a broad northwest to southeast girdle, with a preponderance of shallow lineations (Fig. 37B). Both these structural elements, show a more homogeneous structural style when plotted on a domain scale (Fig. 35, 36).

The Description of the Penetrative Deformational Events (D1 and D2)

The first penetrative deformational event (D1) is defined by a well-developed foliation, scattered mineral lineation, and oblate ellipsoidal or flattened strain markers. Overprinting this first deformation to varying degrees is the second deformation, which is evident in localized to broad shear zones. This superimposed shear is found dominantly in domains A, B and C1, and thus the fabrics related to the first deformation are mainly evident in domain C2.

Table 7. General Domain Characteristics

<u>Analysis</u>	<u>Domain A</u>	<u>Domain B</u>	<u>Domain C1</u>	<u>Domain C2</u>
L1 Lineation Plunge	-	-	-	steep
L2 Lineation Trend	NW	NW	WNW-ESE	NW-SE
L2 Lineation Plunge	shallow	shallow to moderate	shallow	shallow
Foliation Dip	SW (NE) (Steep)	NE-SW (shallow-steep)	N-S (steep to moderate)	SW (NE) (steep)
Foliation Type	S2	S2	S2	S1 + S2
Open "Later" Folds	yes	yes	no	no (only western C2)
Flinn Plot Fields	constriction	-	-	flattening
Porphyroblast Extension (%)	0-100%	0-30%	0-100%	0-30% (D2 shear zones)
Kinematic Indicators	dextral	variable	sinistral	dextral
Dominant Deformation	D2 +(later folds)	D2 +(later folds)	D2 +(shoulering zone)	D1 + D2
Metamorphic Grade	greenschist (biotite zone)	lower amphibolite (garnet zone)	----upper amphibolite---- (staurolite-kyanite zone)	
Temperature	400-500 C (grid)	450-650 C (grid)	-----630 C +/- 50 C----- (grid + thermometry)	
Pressure	3-6 Kb	9 Kb +/- 1 Kb	-----8-10 kb-----	
Unit	Cascade River	Napeequa	Napeequa (+Cascade River)	Cascade River

The First Deformation

First Foliation (S1)- The dominant structure resulting from the first deformational event is a foliation. S1 is defined by the parallel alignment of phyllosilicates (biotite, chlorite and white mica; Fig. 19), granoblastic lenses of quartz and plagioclase (Fig. 21), splays of hornblende in garbenschiefer texture (Fig. 20), and flattened clasts.

The S1 foliation in domain C2 strikes to the northwest and dips steeply to the southwest (Fig. 35). This domain contains a non-repeated, "on-end", stratigraphic section of the Cascade River unit (Fig. 38 B-B'). Field observations indicate that both the S1 foliation (Fig. 18) and S2 (Fig. 11) are parallel to bedding.

First Folds (F1)- The calcareous amphibolites in domain C2 contain similar style isoclinal F1 folds (Fig. 39). The axial planes to the folds are parallel to the S1 foliation in the adjacent feldspathic quartz mica schists. The asymmetry in these folds indicates vergence to the northeast. If large-scale isoclinal folding is responsible for the parallel development of bedding and the S1 foliation, then the axial plane for this larger structure in the field area would also dip steeply to the southwest parallel to the S1 foliation. The lack of repetition of the marker beds or units in domain C2 suggests that the scale of these isoclinal folds (if they exist) are very large. Also, many of the mapped rock units in domain C2 are traceable outside the field area to the southeast, suggesting that the postulated large-scale folds are upright (See Discussion).

First Lineation (L1)- A weakly developed L1 mineral lineation is contained on the S1 surface (Fig. 20), which, like S1, is preserved in domain C2. L1 is defined by the weak alignment of hornblende (Fig. 40a, 20), micas, lenses of granoblastic matrix material (Fig. 19), and clasts.

Figure 35. Lower hemisphere, stereographic (Schmidt), equal area projection of the poles to the foliations (S1 and S2) for domains A, B, C1 and C2 (composite projection Figure 37A).

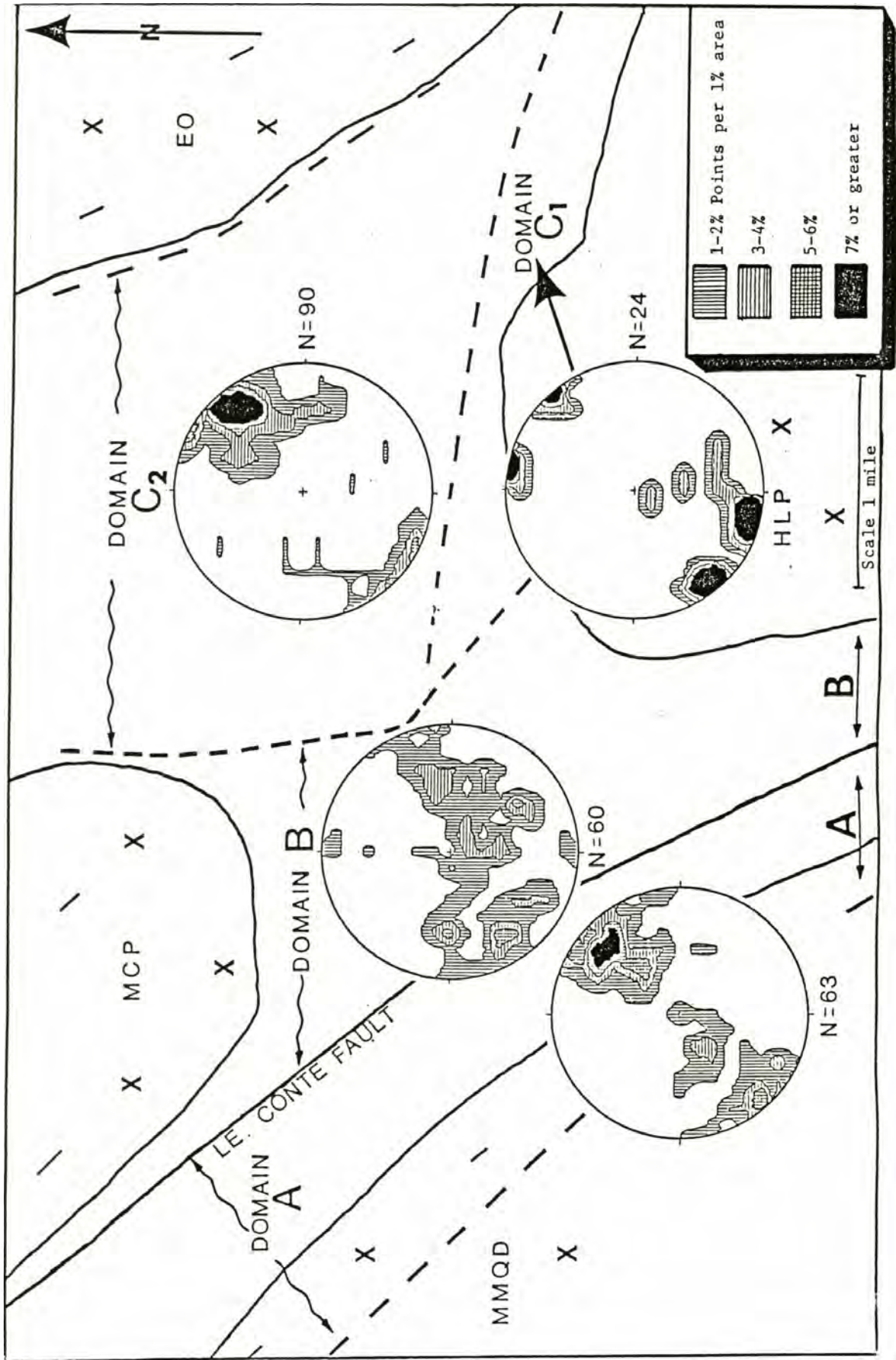


Figure 36. Lower hemisphere, stereographic (Schmidt), equal area projection of the lineations (L1 and L2) for domains A, B, C1 and C2 (composite projection Figure 37B).

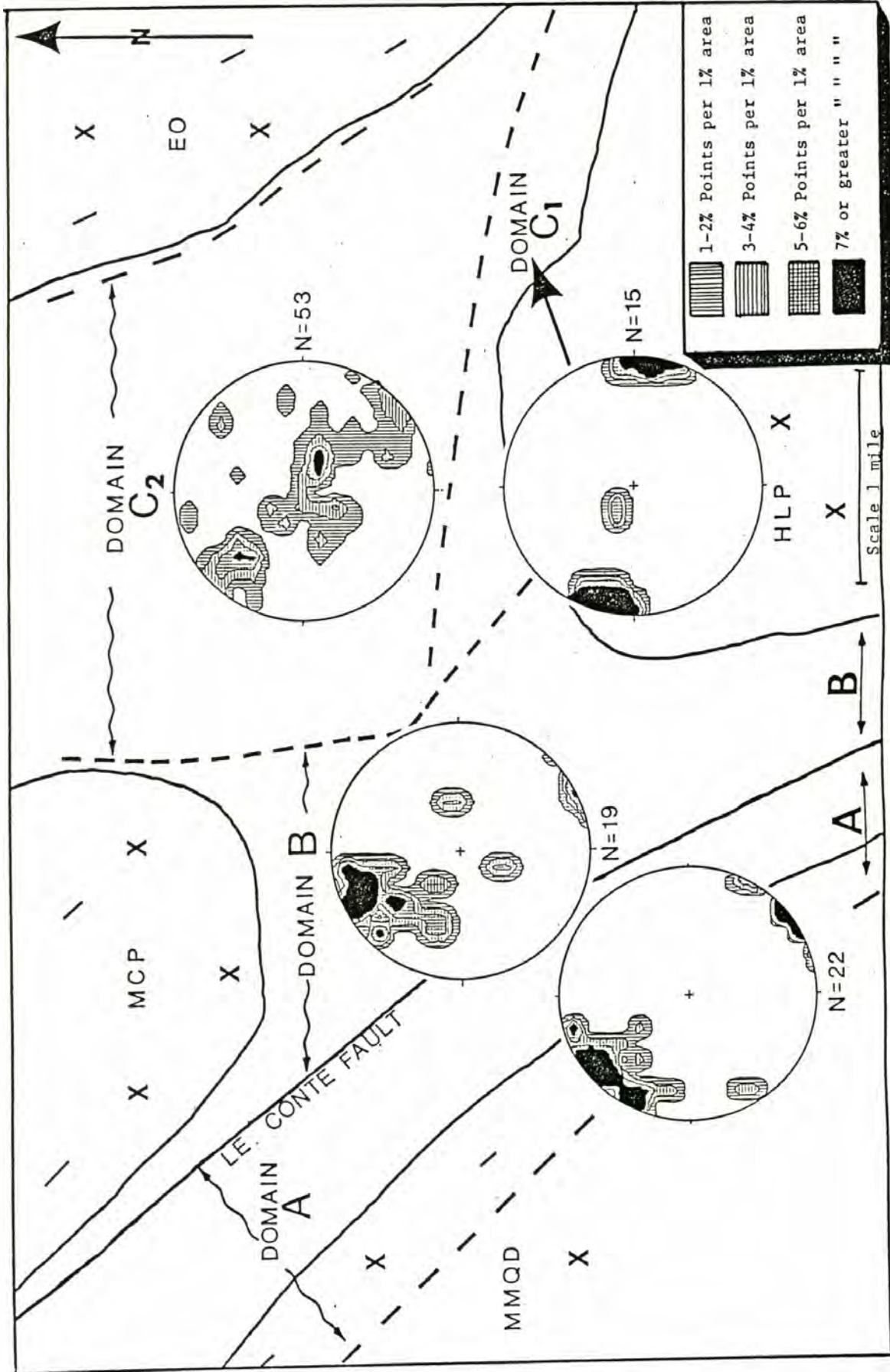


Figure 37. Lower hemisphere stereographic (Schmidt) equal area projections. A) The S1 + S2 (total S; poles to the foliation) for the field area. B) The L1 + L2 (total L) for the field area. C) The poles to the foliations (S) for domains A, B and western domain C2, which shows a girdle distribution. D) The L2 lineations for domains A and B plunge shallowly to the northwest, whereas the L2 lineations in domain C1 plunge shallowly to the west-northwest and east-southeast. This rotation in trend is probably due to the deflection of the D2 fabric during intrusion by the post-D2 Hidden Lake pluton. E) Concentric and parallel type open to tight mesosopic folds axes plunge shallowly to the northwest. F) Poles to the symmetric, extension veins in domain A. G) Poles to the lamprophyre dikes in domain C and the Hidden Lake pluton. These dikes are steep and strike to the north-northeast and east and are the result of east-west extension.

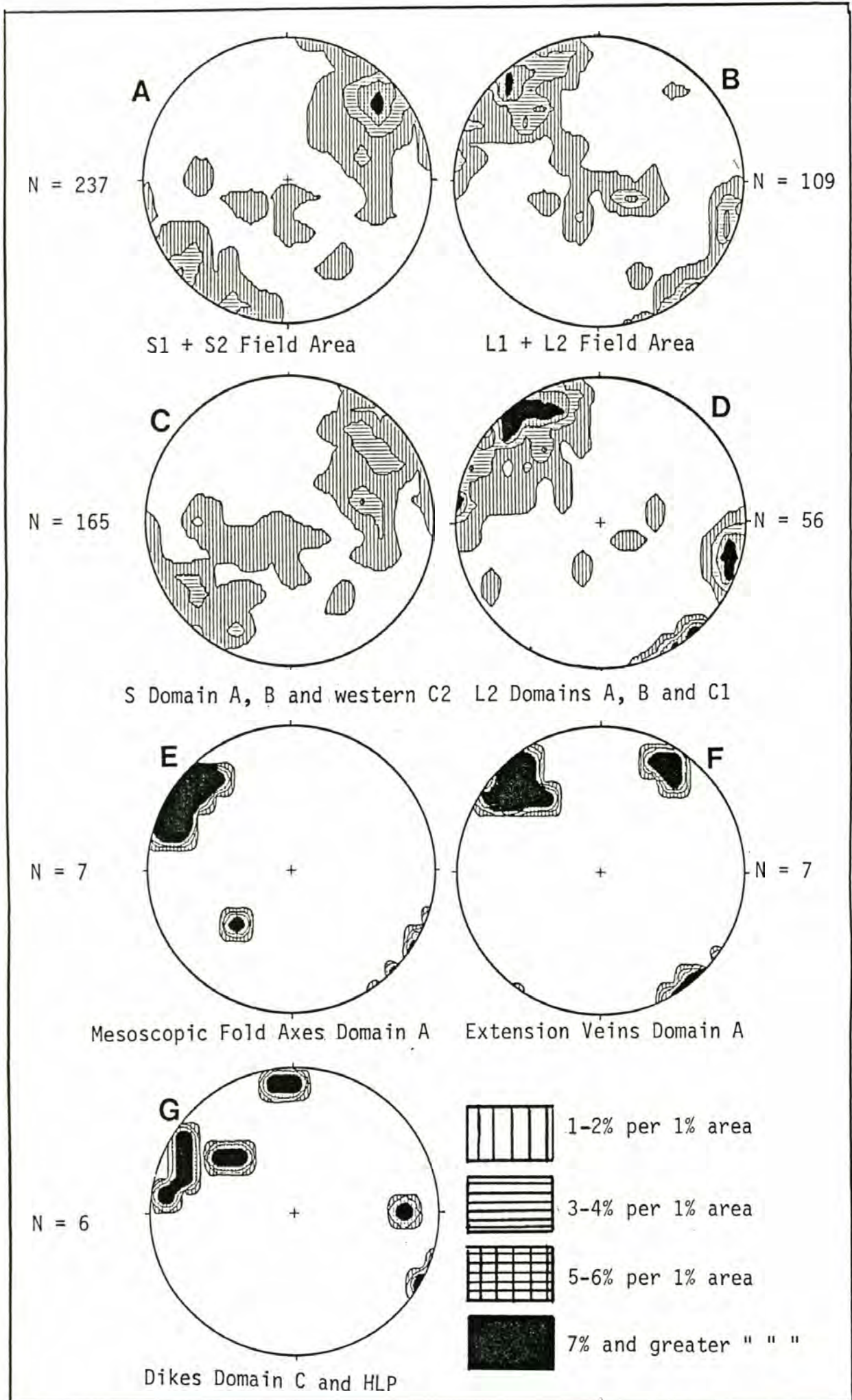
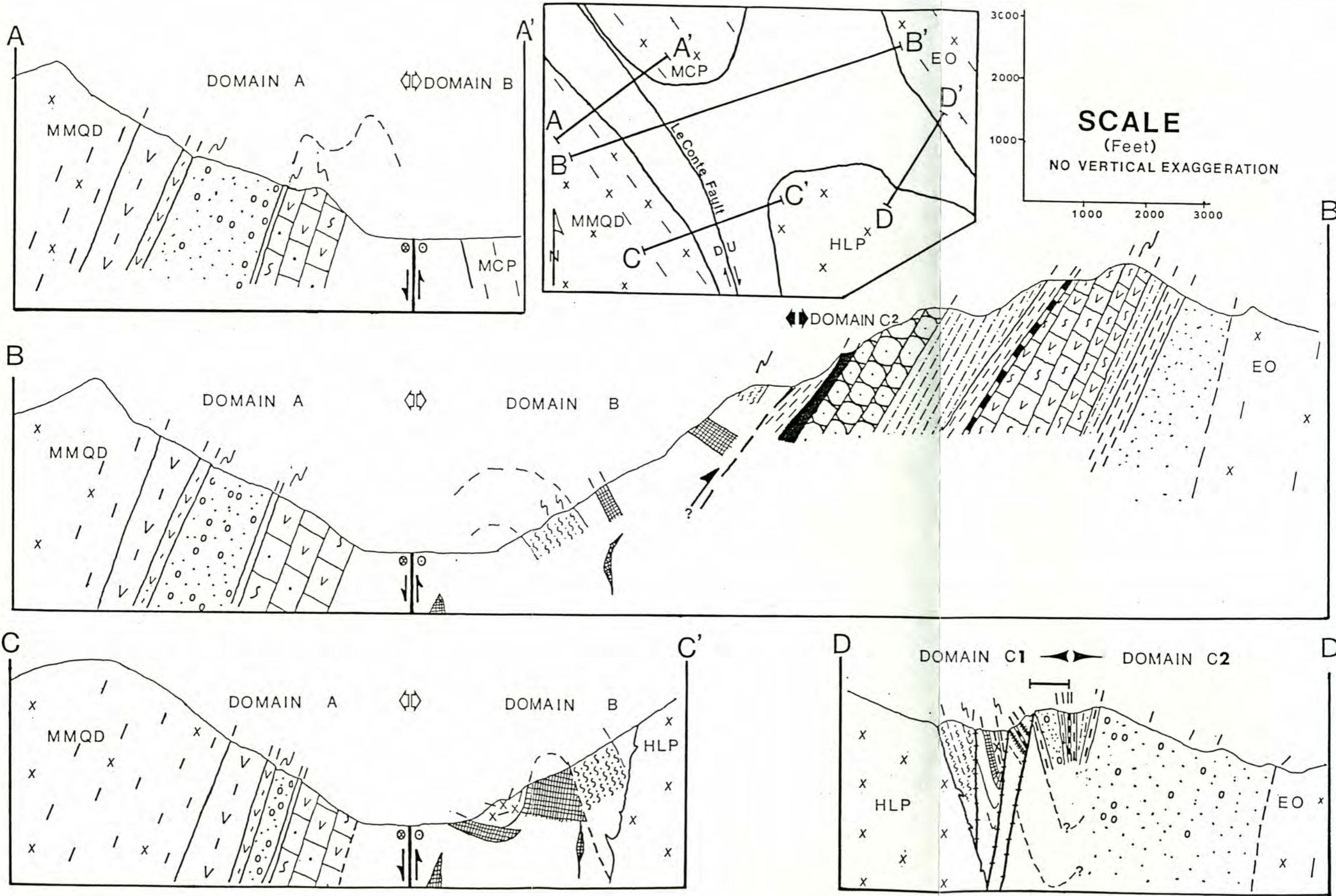


Figure 38. Cross-sections A-A', B-B', C-C' and D-D' (symbols given in Figure 6). The S and Z symbols shown above the cross-sections are parasitic, asymmetric, upright, mesoscopic scale, tight to open folds which give the sense of vergence to inferred macroscopic folds. The bar symbol above D-D' shows the region of consistently sinistral kinematic indicators in domain Cl.



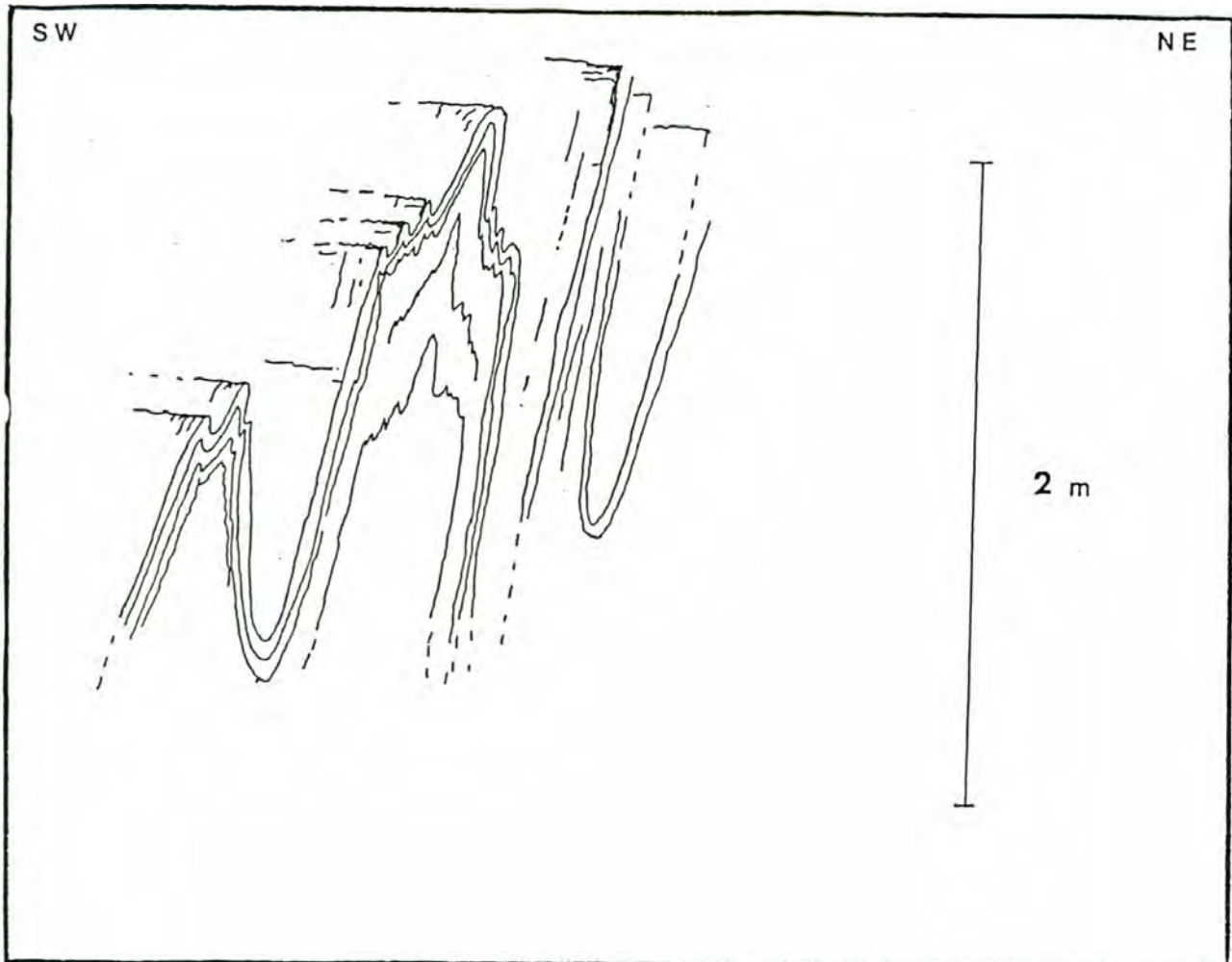
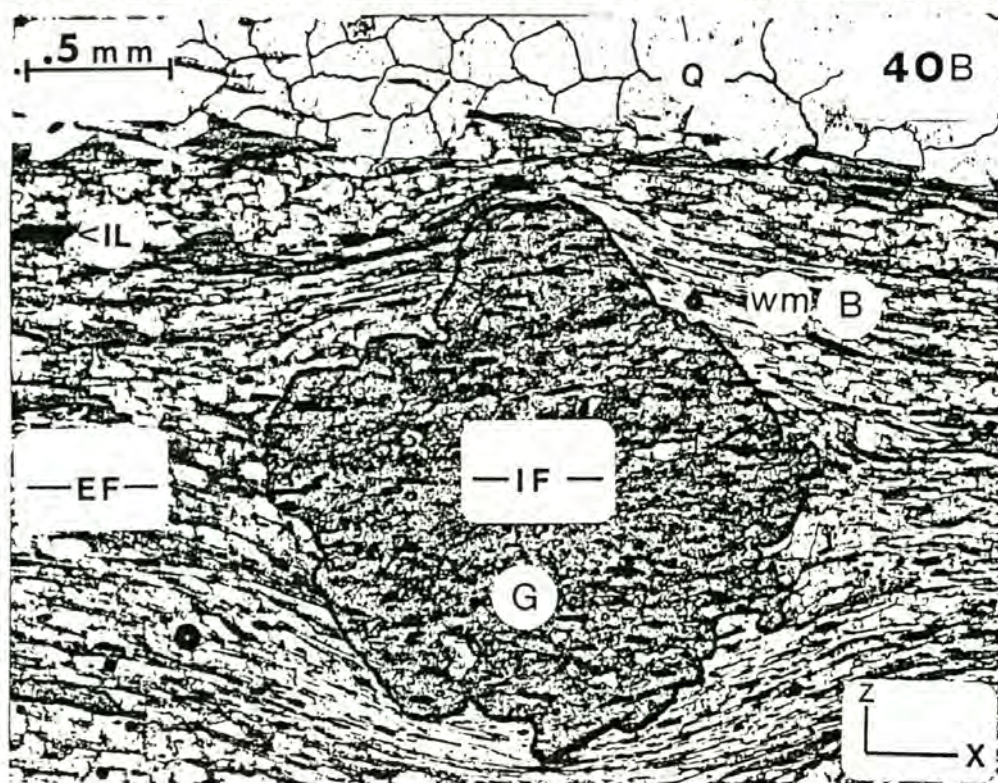
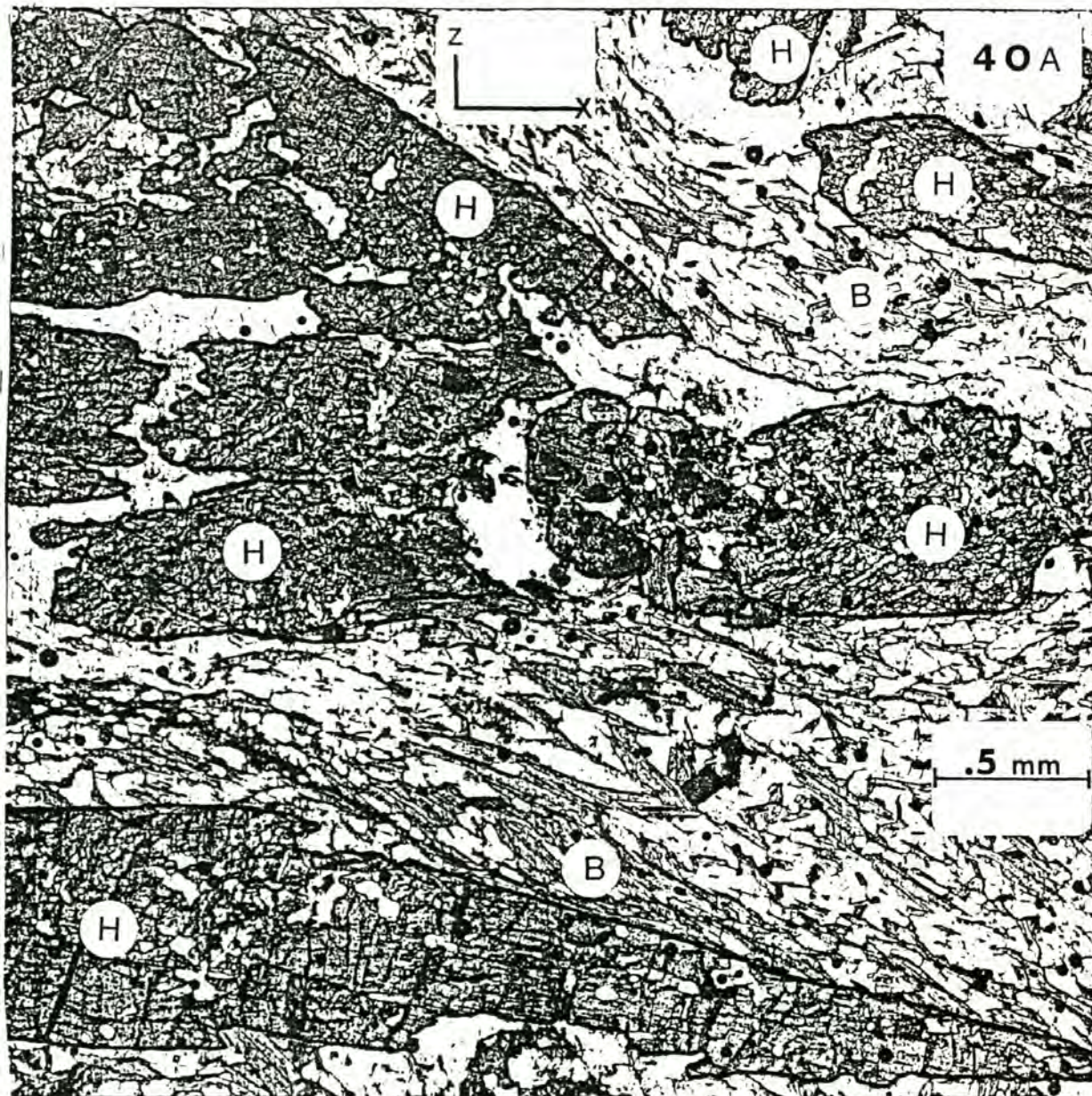


Figure 39. Field sketch of a upright F1 folds observed in the calcareous amphibolites in domain C2 (trend of the fold axes is northwest). These folds may mimic a much larger antiformal structure with vergence to the northeast.

Figure 40. A) Microfiche enlargement of a leuco-amphibolite (6) from domain C2 showing weakly aligned L1 hornblendes, and a few slightly attenuated hornblendes. These tectonites are in direct contrast to the well-aligned and stretched hornblendes in D2 tectonites (see Figure 45B). B) Microfiche photo of a quartz mica schist from domain C2 (220) showing the planar internal fabric (IF) in garnet, which, in this sample, parallels the external foliation (EF).



Garbenschiefer textures are restricted to domain C2 (Fig. 40b). The lineations in domain C2 define a girdle (Fig. 36). This girdle has two maxima: steeply to moderately plunging mineral L1 lineations, and sub-horizontal L2 lineations observed in cross-cutting shear zones.

The axial ratios of 50 clasts from one sample of metaconglomerate in domain C2 plot in the oblate ellipsoidal strain field, suggesting that D1 is a flattening deformational event (Fig. 41). This finding agrees with the relatively weak development of L1 lineations, and strongly developed S1 foliations. The oblate spheroidal clasts in the measured sample are slightly elongate in the down-dip direction parallel to the L1 mineral lineations, providing a link between the L1 mineral lineations and the strain data.

Timing of D1 With Respect to Metamorphism- The high grade minerals that define the D1 fabric formed during or after the first deformation and before the commonly retrogressive second deformation. In D1 tectonites hornblende (Fig. 48a) and garnet (Fig. 40b) porphyroblasts contain a planar internal fabric, or lack syn-tectonic rotational features (e.g. snowball textures). This geometry suggests that porphyroblast growth occurred after the formation of the internal fabric, and that either 1) the porphyroblast growth was synchronous with an irrotational shearing event, or 2) the porphyroblasts overgrew an earlier schistosity during a static growth period. The first scenario is favored due to 1) the weak alignment of the L1 mineral lineations, 2) the deformation (i.e. bending) of L1 hornblende prisms and 3) the common discordance of the internal and external fabrics in porphyroblasts of some D1 tectonites. Thus it appears that irrotational shear preceded and outlasted porphyroblast growth. This assumes that the internal fabric in the porphyroblasts is an early aspect

of the first deformation and that continued flattening affected the porphyroblasts during (or after) deformation.

The Second Deformation

Superimposed upon the D1 deformation is a dextral strike-slip shear fabric (D2), evident in domains A, B and C1 (Fig. 37d), and in isolated shear zones in domain C2.

Second Foliation (S2)— The D2 tectonites commonly contain a sheared or granulated matrix and both S and C surfaces. The S2 foliations are defined by micas, sheared matrix layers (Fig. 9, 13b) and in domain A by the XY plane of conglomerate clasts (Fig. 8). Layers of less-sheared material, bounded by more sheared material, are observed in domains A, B and C1 (Fig. 13b). The inhomogeneous nature of D2 shear is observed both at the thin-section and outcrop scale, particularly in domain B, where strongly sheared layers occur between less strained to granoblastic zones (Fig. 13b). Domain C2 is interpreted to be a mega-augen region around which the D2 shear was largely partitioned, and suggests that the inhomogeneity of shear occurs at a large-scale.

The S-C mylonites are found dominantly in domains A, C1, and discrete domain C2 shear zones, whereas ribbon quartz mylonites dominate domain B. This phenomenon may be due to: 1) The rheological difference between the dominant metasedimentary protoliths of these domains (i.e. the quartz-rich biotite schists of the Napeequa unit in domain B versus the commonly mica-rich metasedimentary protoliths of the Cascade River unit in the other domains); or 2) a differential strain affect within the large-scale shear zone.

The S2 foliations strike to the northwest and dip steeply to the southwest (Fig. 35). North to north-northeast shallowly dipping S2 foliations, and northeast moderately to steeply dipping S2 foliations in

domains A, B, and northeastern domain C2, are the result of later folding (Fig. 35).

Second Lineation (L2)- Both mineral and stretching lineations are observed in D2 shear zones. The L2 mineral lineations are defined by the alignment of phyllosilicates (biotite, chlorite and white mica). The L2 stretching lineations are defined by the alignment and stretching of conglomerate pebbles (Fig. 8), plagioclase clasts (Fig. 9, 17a, 48d,i,j), Ca-amphiboles (Fig. 45b), idiomorphic epidotes (Fig. 43, 48j), staurolites (Fig. 48a), and strain shadows adjacent to garnets (Fig. 48h) and other porphyroblasts. Quartz fibers in domain A indicate that the stretching direction is parallel to the mineral elongation direction, since the fibers are straight and parallel to the stretching lineation (Fig. 45a). The amount of extension, recorded as boudinage of porphyroblasts, varies across the area. The porphyroblasts in domains B generally show only 5-10% extension (Fig. 45b, 47), versus domains A (Fig. 43) and C1 (Fig. 48a,j), which generally show up to 100% extension. This variation demonstrates the inhomogeneous nature of the D2 shear. For example, much of the shear strain in domain B was probably taken up in the incompetent serpentinite bodies thus reducing the bulk strain state of the schists, amphibolites, and the resultant porphyroblast extension.

L2 mineral and clast lineations in domain A, and in D2 shear zones in domain C2, consistently plunge shallowly to the northwest (Fig. 36). Mineral lineations in domain B plunge shallowly to moderately to the northwest (Fig. 36). Mineral lineations in domain C1 consistently plunge shallowly to the west-northwest or east-southeast (Fig. 36). The more westerly trend of the L2 lineations in domain C1 (Fig. 37d) may be due to:

- 1) the counterclockwise rotation of the L2 lineations about a vertical

axis due to the shouldering and warping of the D2 fabric by the probably post-tectonic Hidden Lake pluton; or 2) deflection of the D2 around a pre-tectonic Hidden Lake pluton.

Second Deformational Strain Analysis- The metaconglomerate unit in domain A contains extremely stretched "cigar" shaped or prolate ellipsoidal clasts (Fig. 8), with $X : Y : Z = 20+ : 2 : 1$ and K values = 2-6 (Fig. 41). Constrictional strain is suspected for the D2 tectonites in domains B, C1, and in D2 shear zones in domain C2. This is evidenced by the sub-parallel orientation of the L2 stretching lineations throughout the field area, although the magnitude of strain is variable as suggested by the different degrees of porphyroblast extension.

Figure 41 displays the contrasting nature of the flattening observed in domain C2 and the stretching characteristic of domain A. The consistent orientation and strong development of the stretching lineations in domains A, B and C1 is in direct contrast to the predominantly steeply plunging, weakly developed mineral and clast lineations observed in domain C2; although isolated shear zones in domain C2 do contain the sub-horizontal stretching lineation and S-C mylonites. This suggests that: 1) domain C2 is largely outside the influence of the D2 strain regime; and 2) the D2 shear regime overprinted most of the D1 S-tectonites resulting in L-S tectonites with distinctive stretching lineations.

Second Deformation Kinematics- The orientation of the X axis and XY plane of the D2 bulk strain ellipse in general plunges shallowly to the northwest and dips steeply to the southwest, respectively, as deduced from the orientation of the L2 and S2 fabric elements. D2 is a non-coaxial or rotational deformation, as indicated by the rotation of passive markers, such as porphyroblasts, and has resulted in a variety of kinematic indicators. These include S-C mylonites, biotite "fish", and shear

asymmetric conglomerate clasts, and rotated porphyroblasts (Passchier and Simpson, 1986; Simpson and Snoke, 1983). The kinematic indicators are observed on the X-Z plane of thin-sections derived from oriented hand-samples. The indicators give a consistent dextral sense of shear in domain A (Fig. 42, 44, 48d,e,i,) and in isolated shear zones in domain C2 (Fig. 48g) and consistently sinistral sense of shear in domain C1 (Fig. 47, 48b,f,j,k, Table 8). Kinematic indicators in domain B are scarce (Fig. 13a).

Table 8. Summary of Kinematic Analysis

<u>Domain</u>	<u>Dextral</u>	<u>Sinistral</u>	<u>Total</u>
Domain A	17	1	18
Domain B	2	1	3
Domain C1	3	13	16
Domain C2	10	0	10

These indicators, along with the sub-horizontal stretching lineations and the steep S2 shear foliation, indicate that domain A, and isolated shear zones in domain C2, are dominated by a dextral, strike-slip shear. The apparent consistency of the kinematic indicators suggest that D2 was not the result of pure shear since a significant component of pure shear would result in inconsistent shear indicators.

The anomalous sinistral sense of shear in domain C1 could be due to: 1) later overturning of the D2 shear fabric by folding; or 2) an R2 riedel antithetic shear zone related to the D2 dextral shear regime. Folding and/or faulting synchronous with Hidden Lake pluton emplacement folding and/or faulting may have overturned the D2 fabric, and consequently the dextral kinematic indicators (Fig. 49, 38D-D' see bar symbol for the location of the indicators). The folding interpretation is supported by the occurrence of conglomerate bearing quartzo-feldspathic schists on both sides of the possible synform (Fig. 38D-D'), which, along with the foliation orientation, suggests synformal repetition.

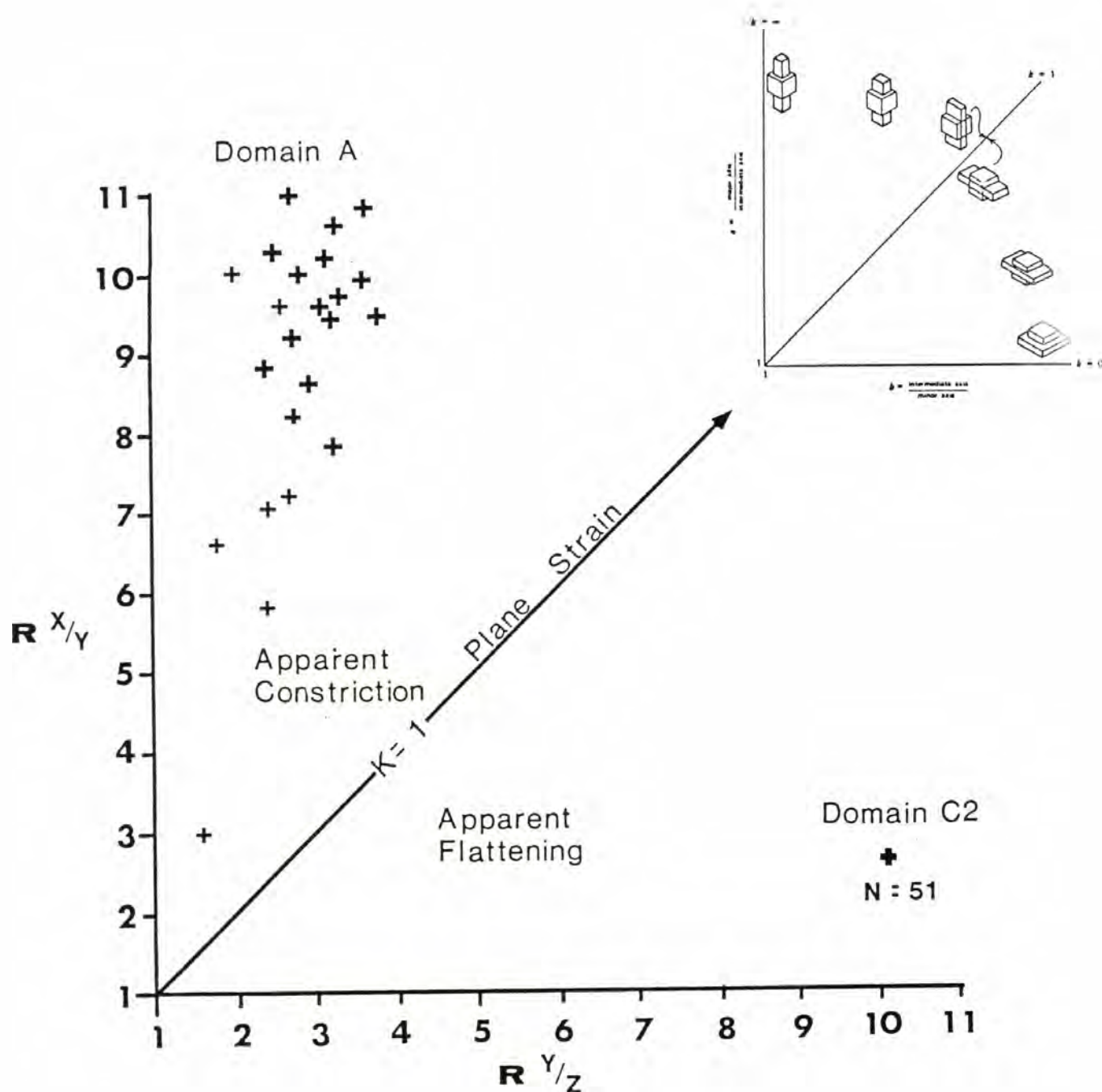
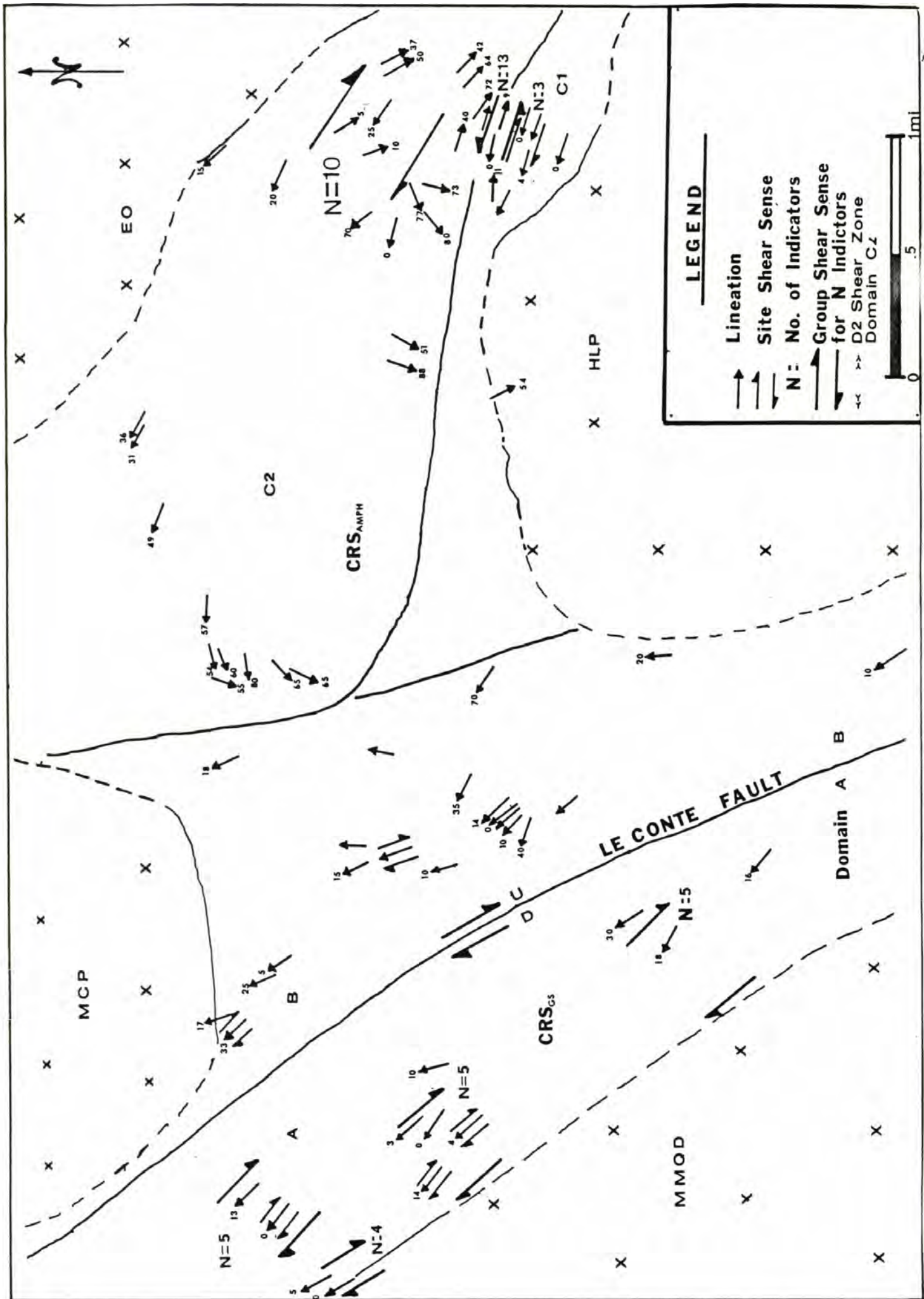


Figure 41. Flinn plot of conglomerate clast axial ratios. The average of 51 clasts in a conglomerate bearing quartzo-feldspathic schist sample from domain C2 show flattening; whereas several clasts from different parts of domain a consistently show constriction. Flattening and constriction strain patterns agree with the types of fabrics (S and L-S tectonites) observed in D1 and D2 tectonites, respectively.

Figure 42. Kinematic indicator map for the field area, supplemented by key lineations. The kinematic indicators from domains A and D2 shear zones in domain C2 show a very consistent dextral sense of shear. Fewer and less consistent indicators were observed in domain B. Kinematic indicators from domain C1 give a consistent sinistral sense of shear, which may be due to the folding or overturning of the D2 fabric (see Figure 49 for overturning model).



Timing of D2 with Respect to Metamorphism- The second deformation is late-syn- to late-metamorphism since all the key metamorphic minerals in the D2 shear zone(s) are deformed by this deformation (Table 9). The pre-tectonic nature of the porphyroblasts in the D2 tectonites is evidenced by: 1) the boudinage of actinolite, hornblende (Fig. 45b), garnet (Fig. 46), staurolite (Fig. 48a), and idiomorphic epidote (Fig. 43, 48j) porphyroblasts; 2) the shearing (biotite fish; Fig. 48b,f,g,j,k) and chloritization of biotite (Fig. 48b, 47), and garnet; 3) the strain shadows adjacent to garnet (Fig. 48h); 4) the serpentinization and boudinage of metamorphic forsterite (Fig. 15b); and 5) the lack of recrystallization of cataclastic, fine-grained, quartzo-feldspathic matrix (Fig. 9, 13b), particularly in domain B where the mylonitized matrix layers occur between granoblastic layers, indicating that deformation outlasted or was later than crystallization.

Table 9. Petrographic Evidence For Late-Metamorphic D2 Shear

<u>Characteristic</u>	<u>Minerals</u>
(1) Internal S that is discordant to the shear foliation	Hornblende, Actinolite, Garnet
(2) Minerals boudinaged (stretched) and/or rotated into the N.W. stretching direction.....	Hornblende, Actinolite, Epidote, Garnet, Plagioclase Staurolite
(3) Mylonitic Matrix.....	Quartz, Plagioclase
(4) Mica Fish.....	Biotite, White Mica
(5) Strain Shadows behind porphyroblasts.	Hornblende, Biotite fish, Epidote, Garnet and Actinolite

The earlier S1 foliation, in D2 shear zones, may be represented by:

1) the planar internal schistosity in hornblende and garnet porphyroblasts discussed above; and/or 2) the S surfaces in the S-C mylonites. In D2 tectonites the internal fabric in porphyroblasts is commonly oblique to the external foliation (Fig. 48a), which suggests that the porphyroblast growth is late-to-post tectonic with respect to the internal fabric (S1), but pre-tectonic with respect to the external fabric (S2). The S and C

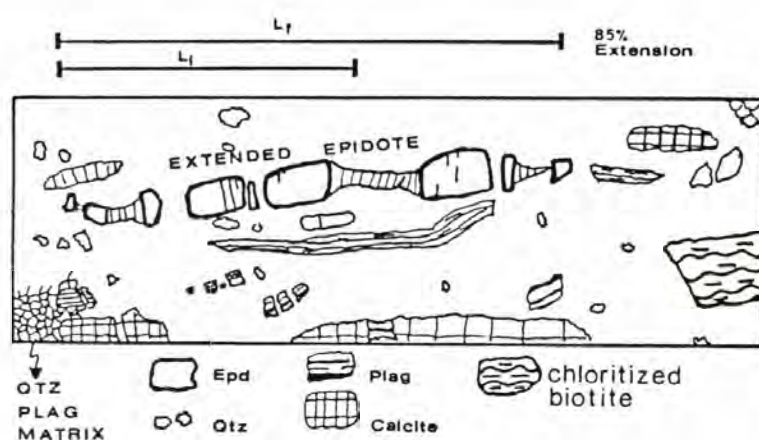
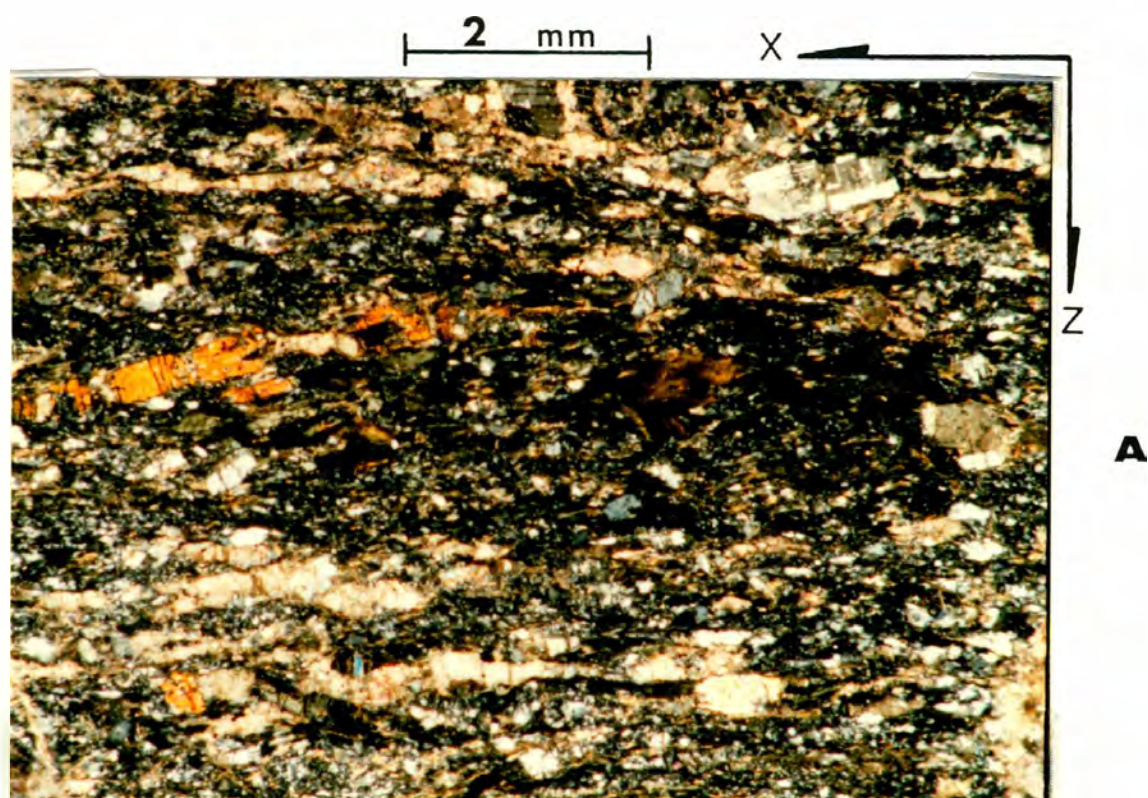


Figure 43. A) Photomicrograph showing the boudinage of idiomorphic epidote prisms (upper middle) and plagioclase clasts (upper right) in domain A (metamar1, 100). These porphyroblasts are stretched in a sub-horizontal direction. B) Sketch of the photo showing the 85% extension calculated from the initial and final lengths of idiomorphic epidote prism.

Figure 44. A) Sketch (54b) showing the S and C surfaces and the dextral sense of shear in a mylonite from the metaconglomerate unit in domain A (54b) (NOTE- SHEAR SENSE IS REVERSED SINCE THE SAMPLE IS DERIVED FROM THE BOTTOM OF A ORIENTED HAND-SAMPLE). B) Microphotograph of the above sample (54b). Note the intense granulation of the quartzo-feldspathic matrix which is characteristic of the D2 tectonites.

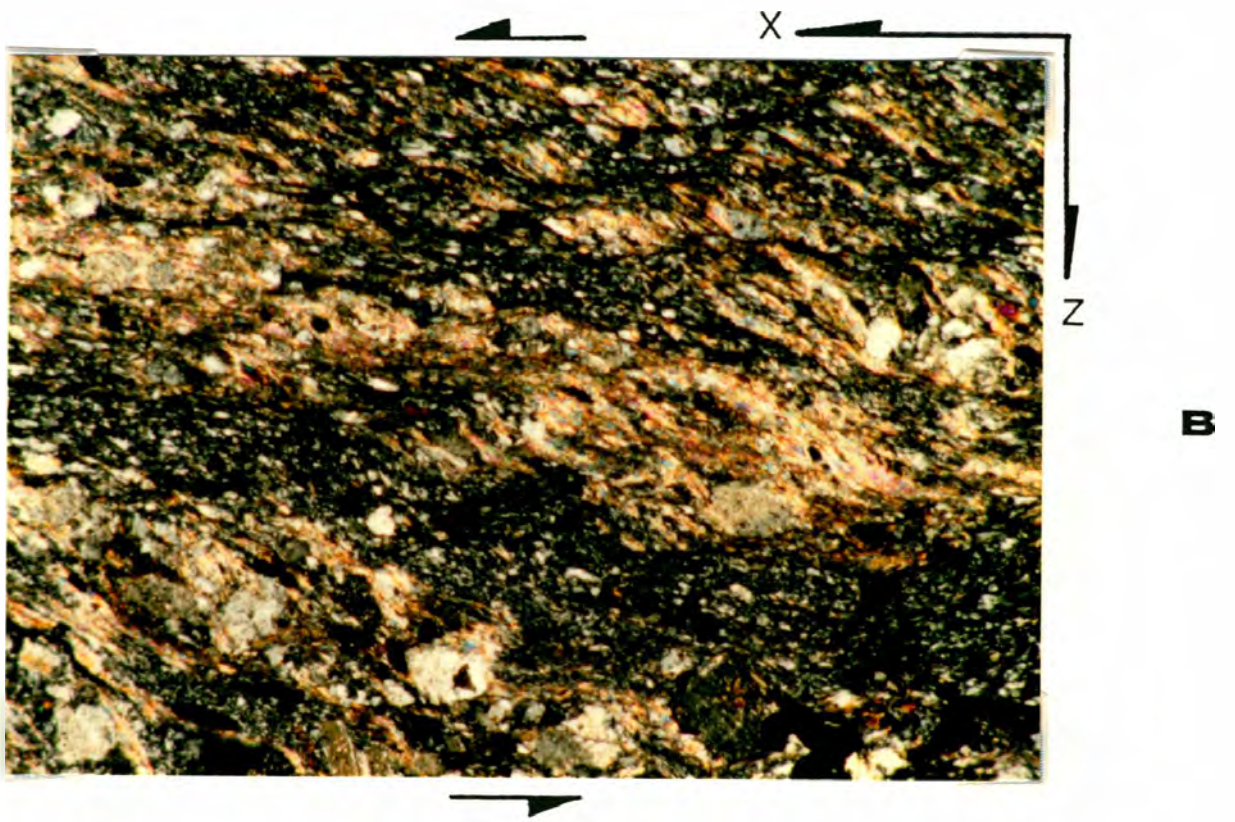
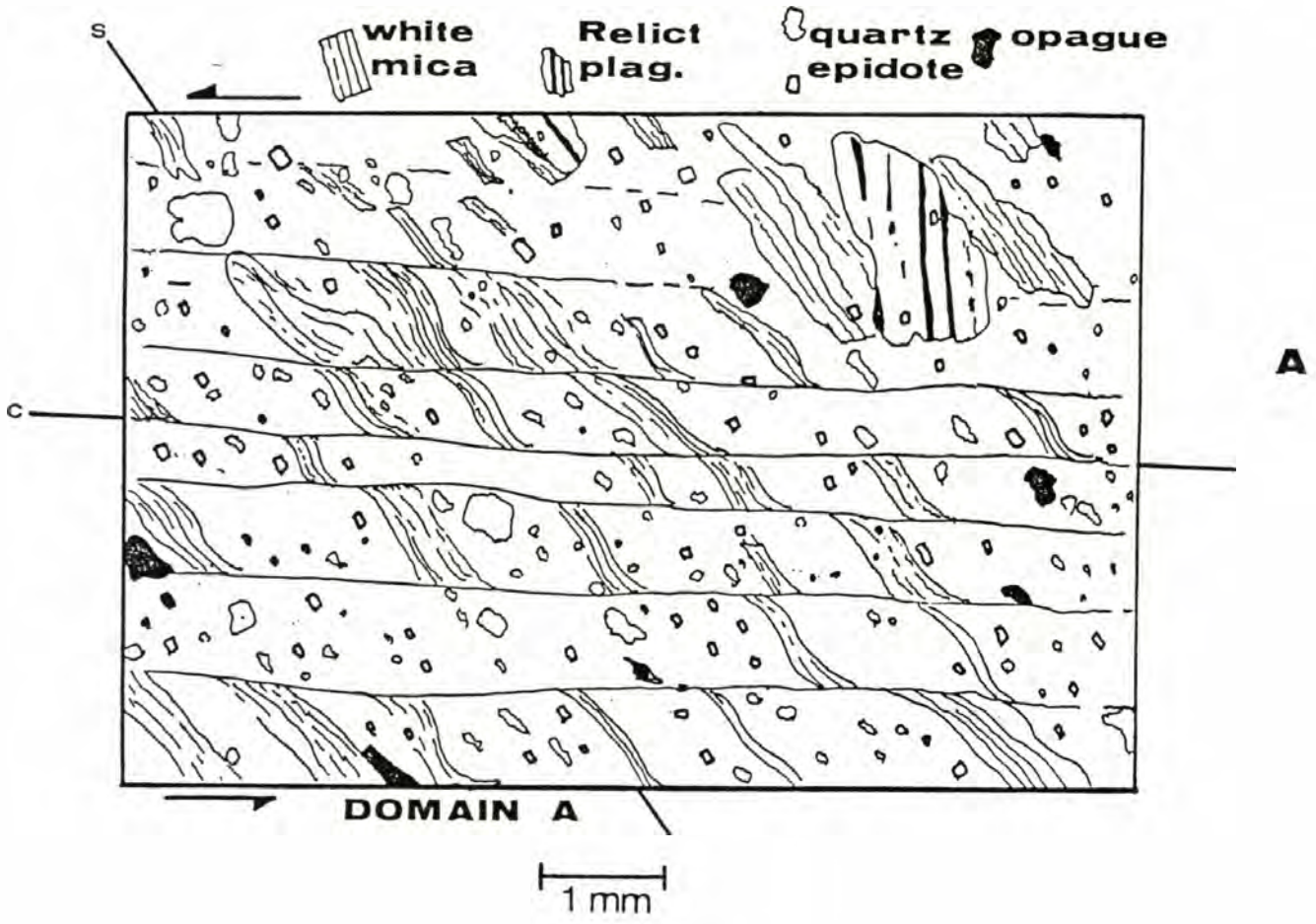
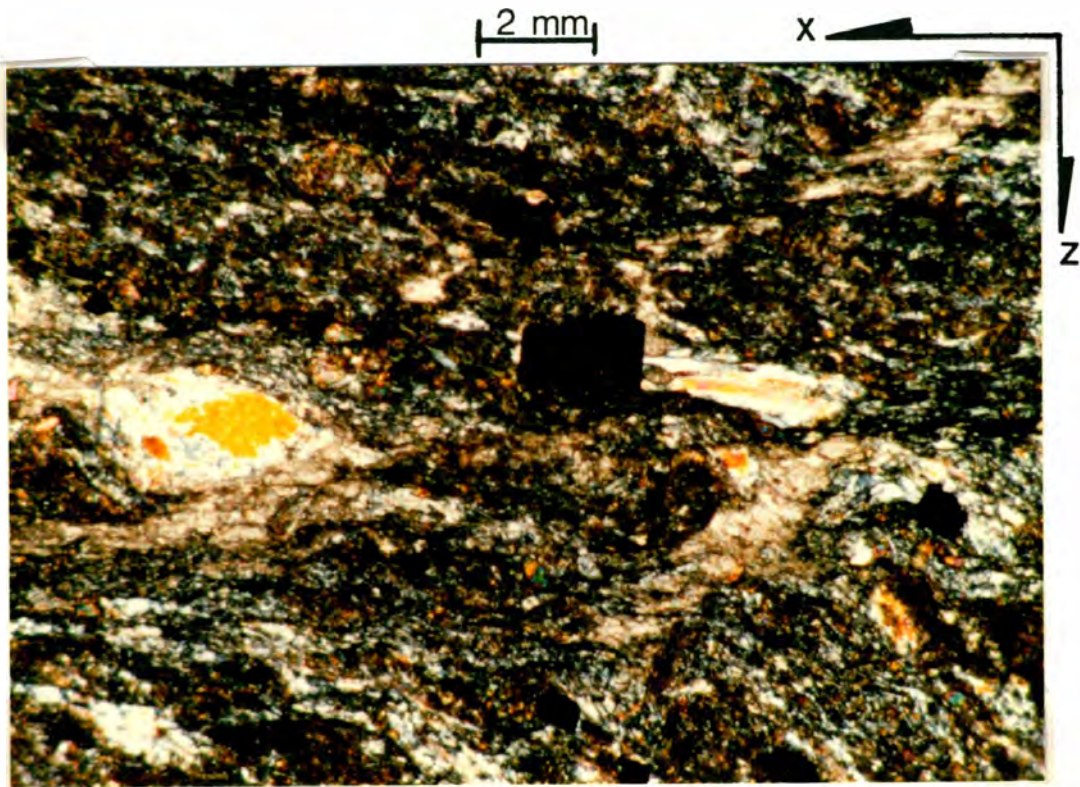
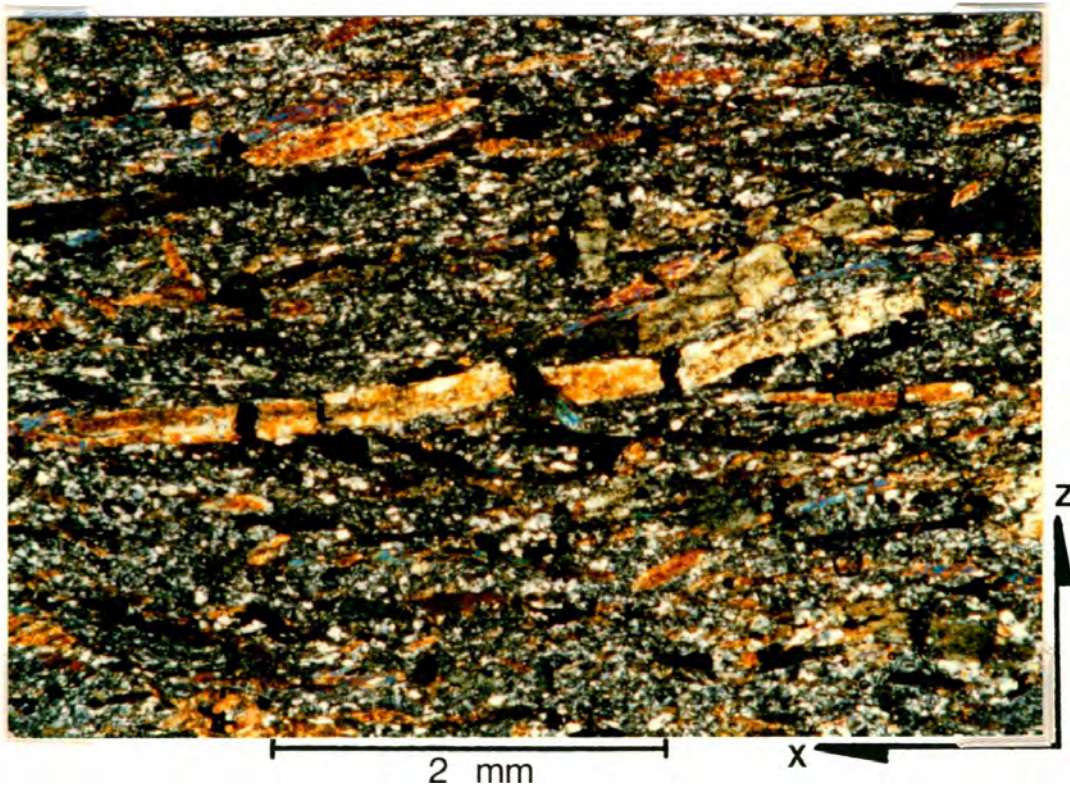


Figure 45. A) Magnetite grain showing straight quartz fibers in a pressure shadow from domain A (103). Sample also contains epidote + quartz + albite + calcite. B) Amphibolite from domain B (240.5) showing boudinaged hornblende prisms and a sheared quartzo-feldspatic matrix. Note the porphyroblasts are extended less than the porphyroblasts in domains A (Figure 43) and domain C1 (Figure 48A).



A



B

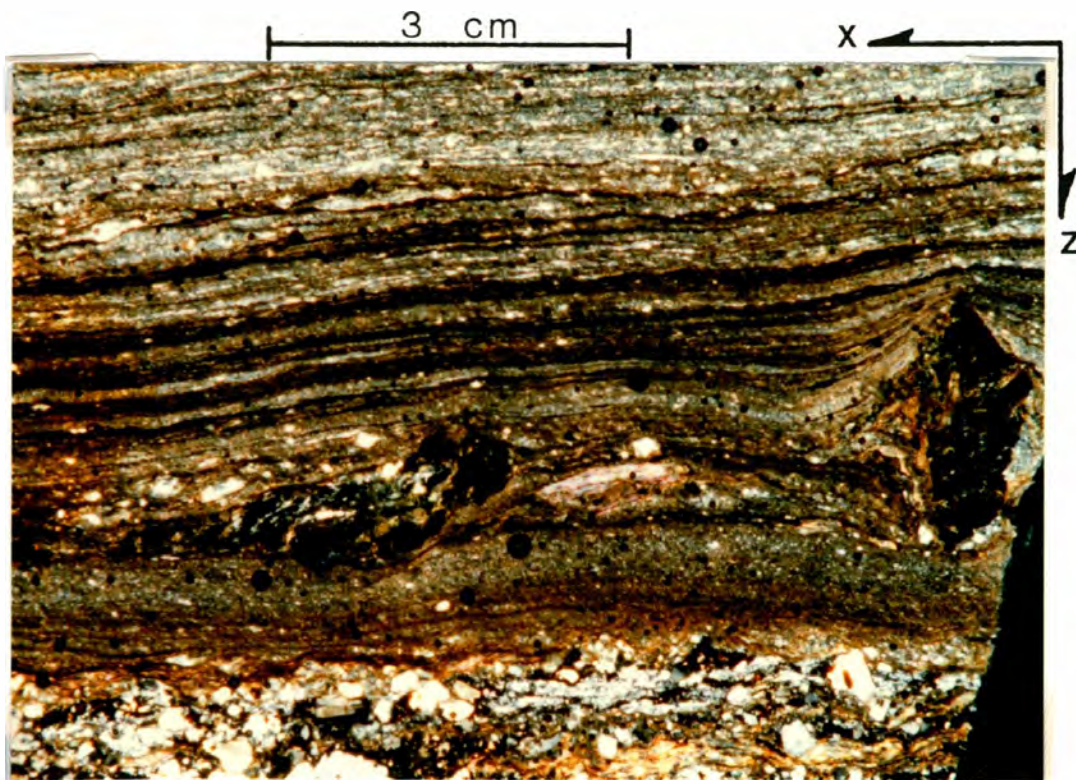


Figure 46. Photomicrograph of a garnet bearing quartzo-feldspathic biotite schist from domain B (30). Garnets in this sample are boundinaged and chloritized indicating that the D2 shearing occurred, in part, while sub-garnet zone metamorphic conditions prevailed, or later in the metamorphic cycle.

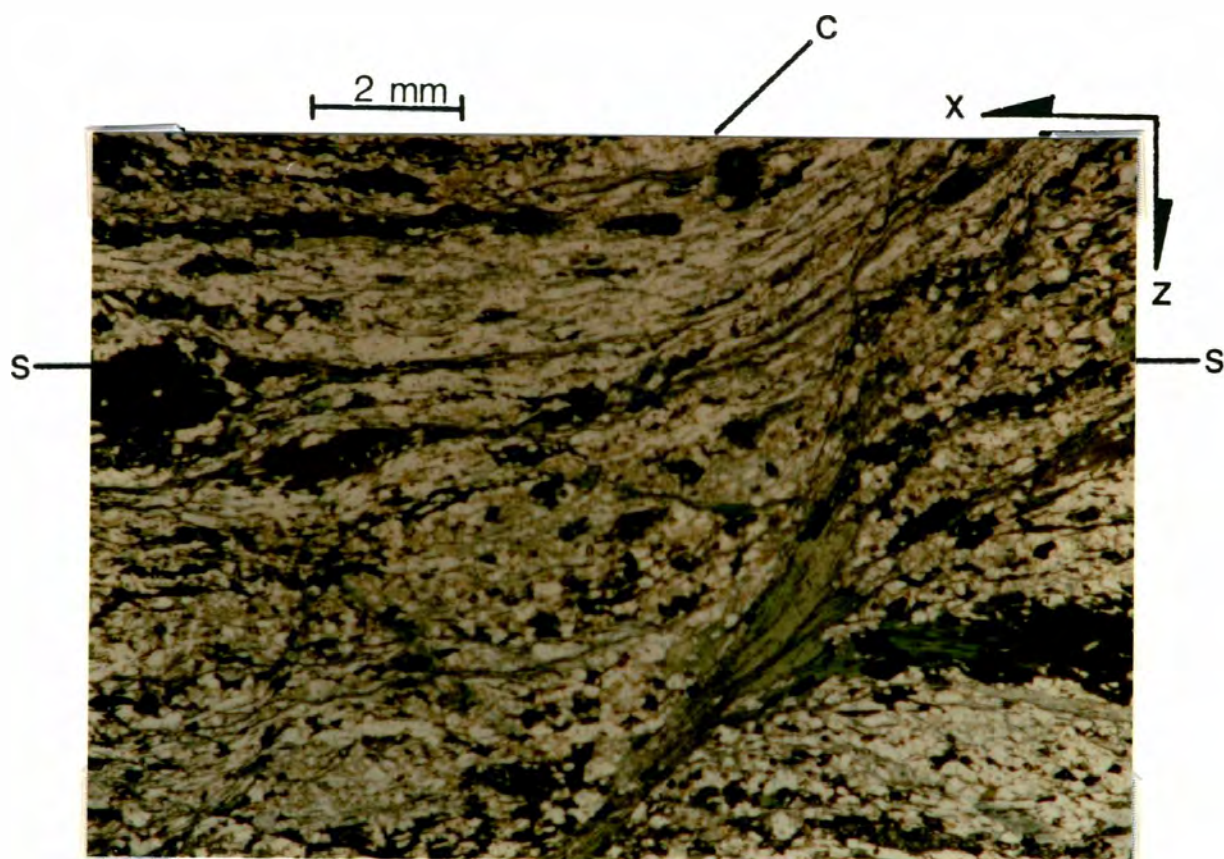
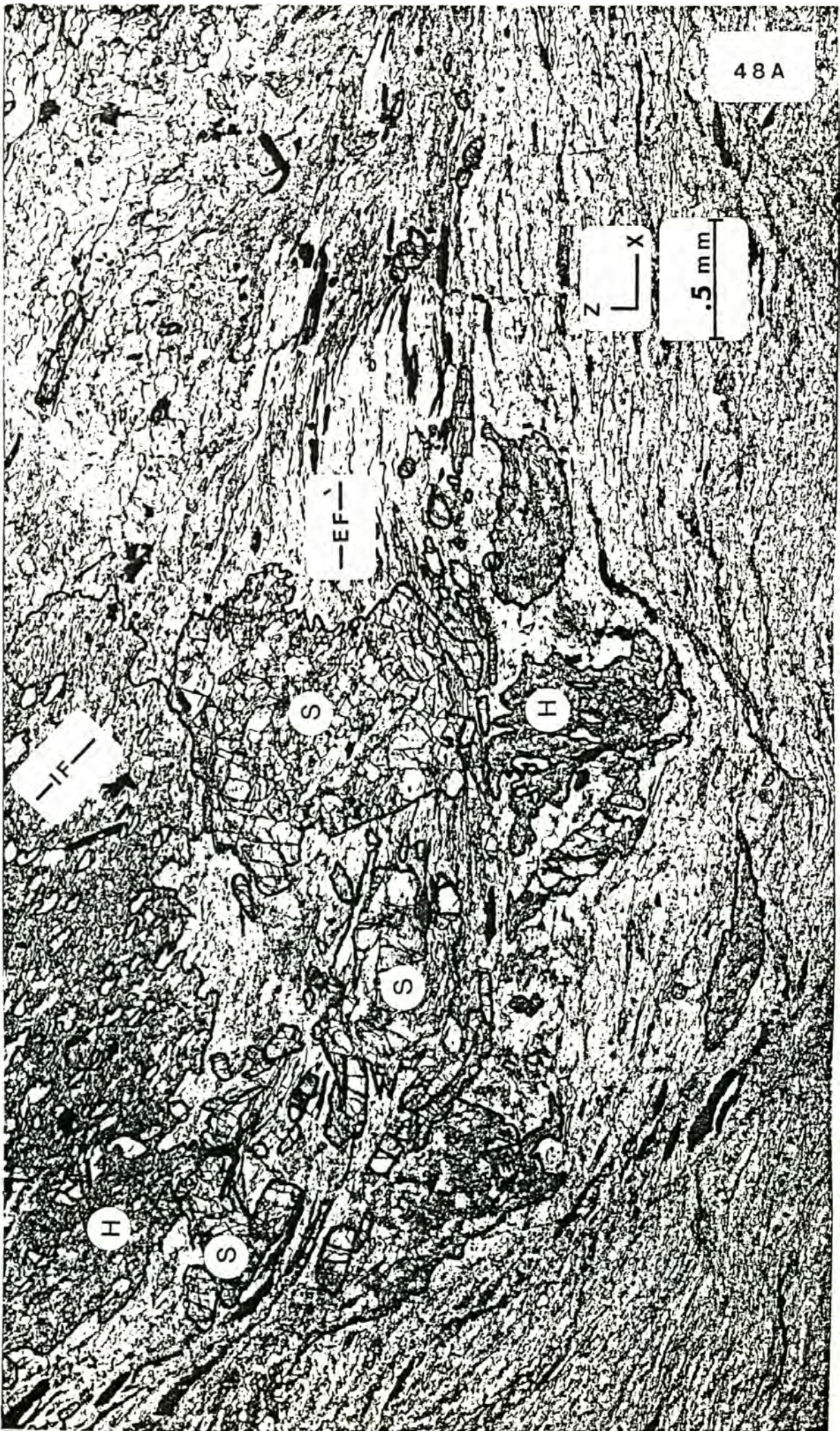


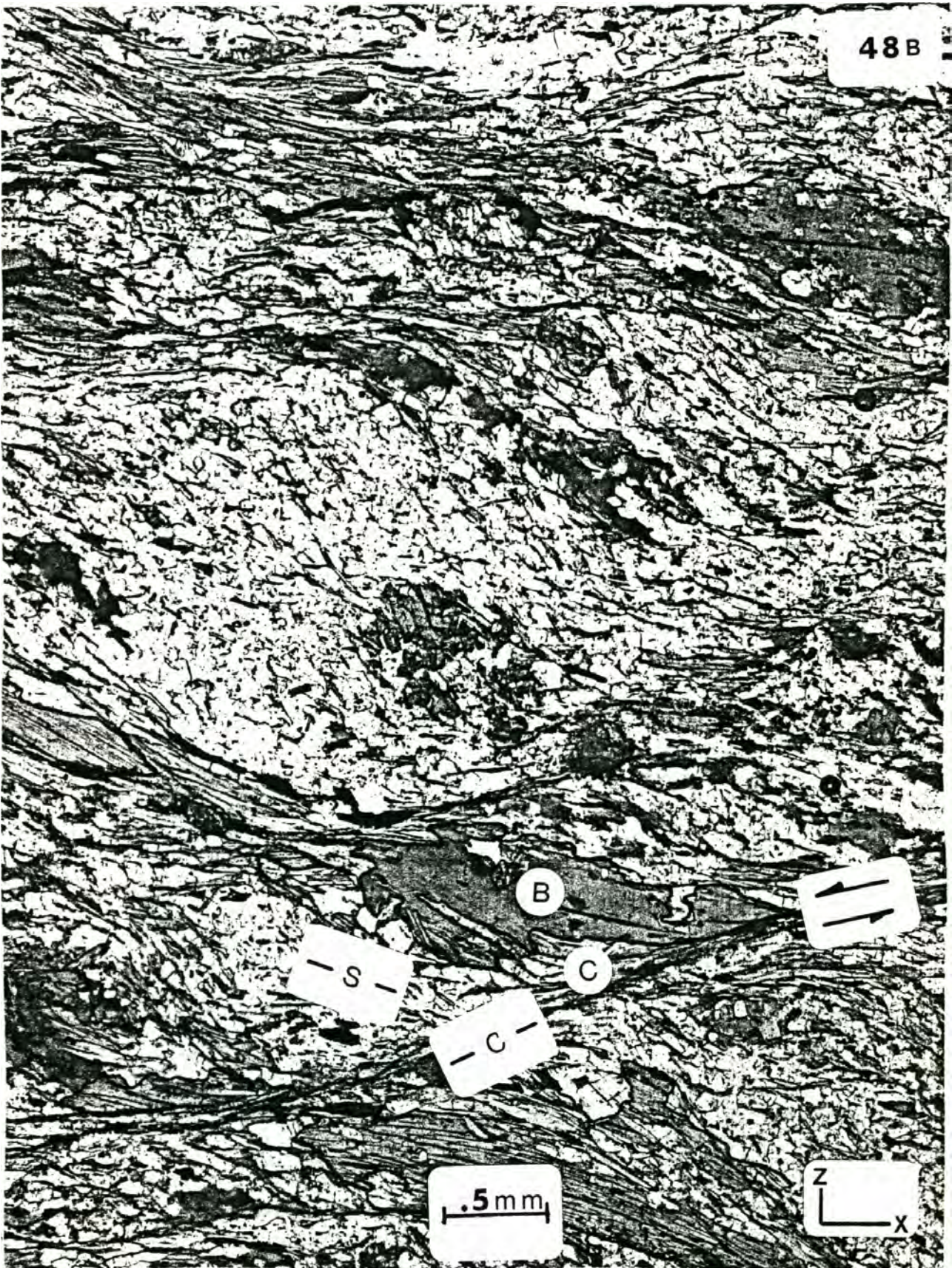
Figure 47. Photomicrograph of a quartzo-feldspathic schist from domain C1 (2) showing the retrogression of biotite to chlorite adjacent to a C surface. Biotites are commonly chloritized in D2 tectonites indicating that the D2 shearing occurred, in part, while sub-biotite zone metamorphic conditions prevailed.

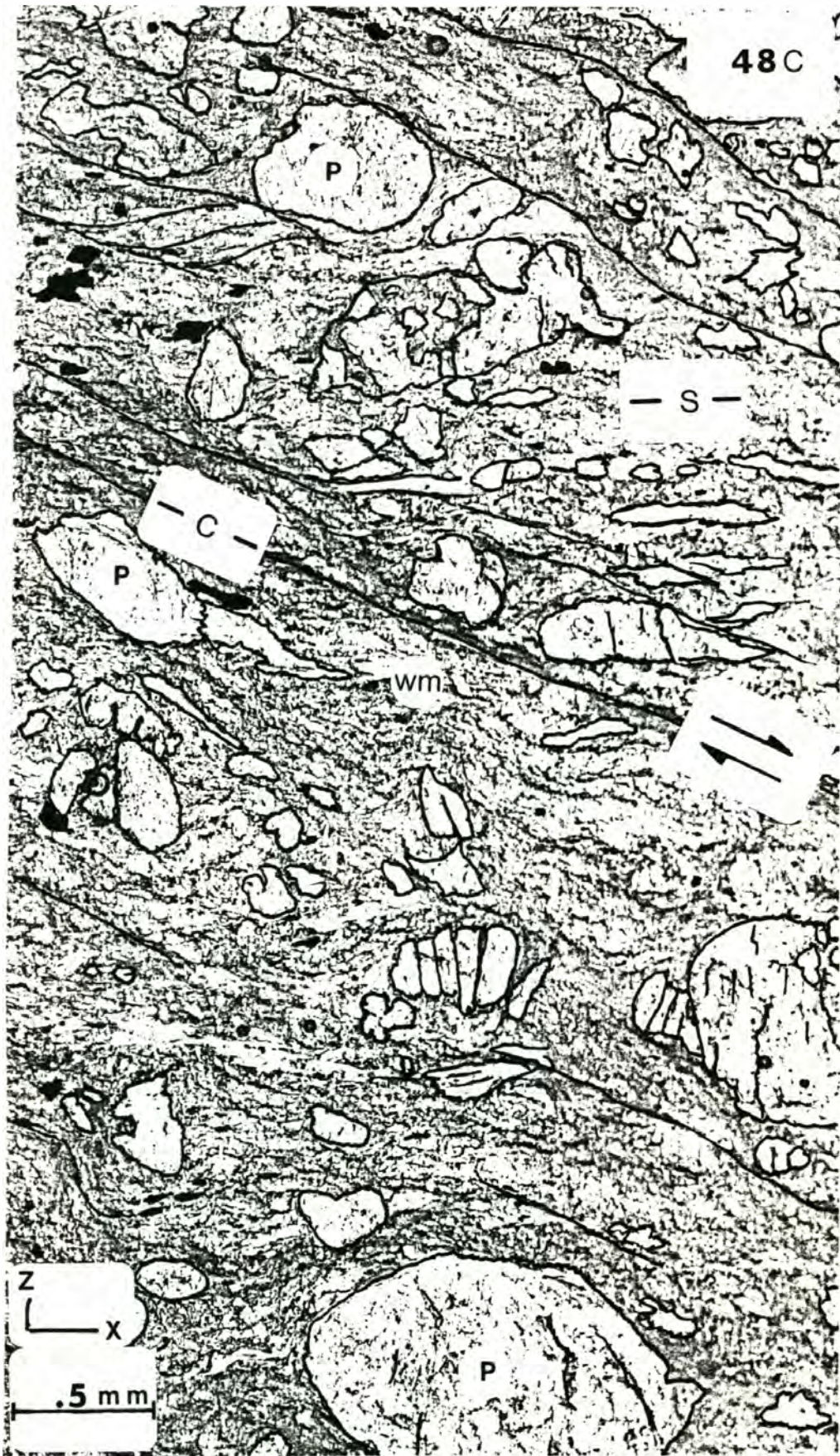
Figure 48. Microfiche enlargements of various structural features.

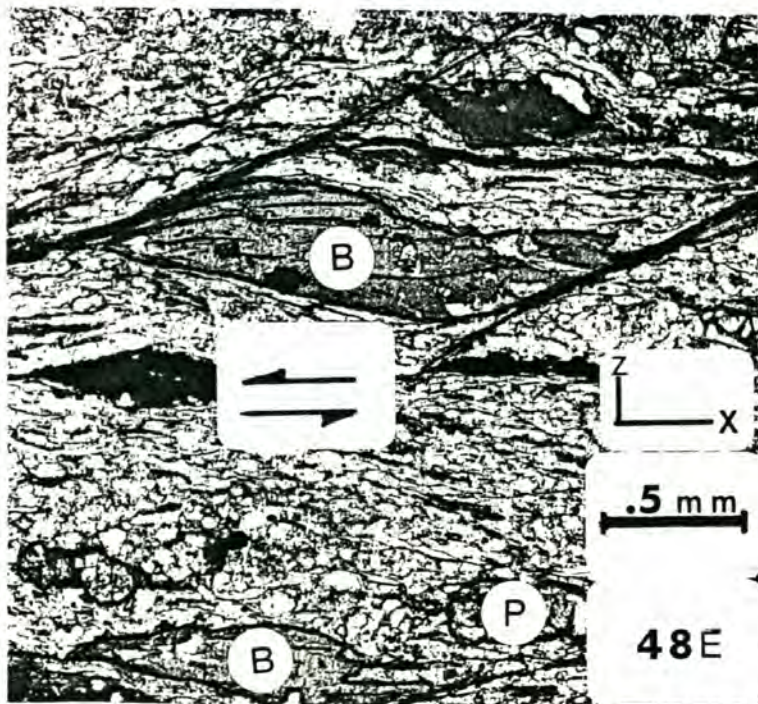
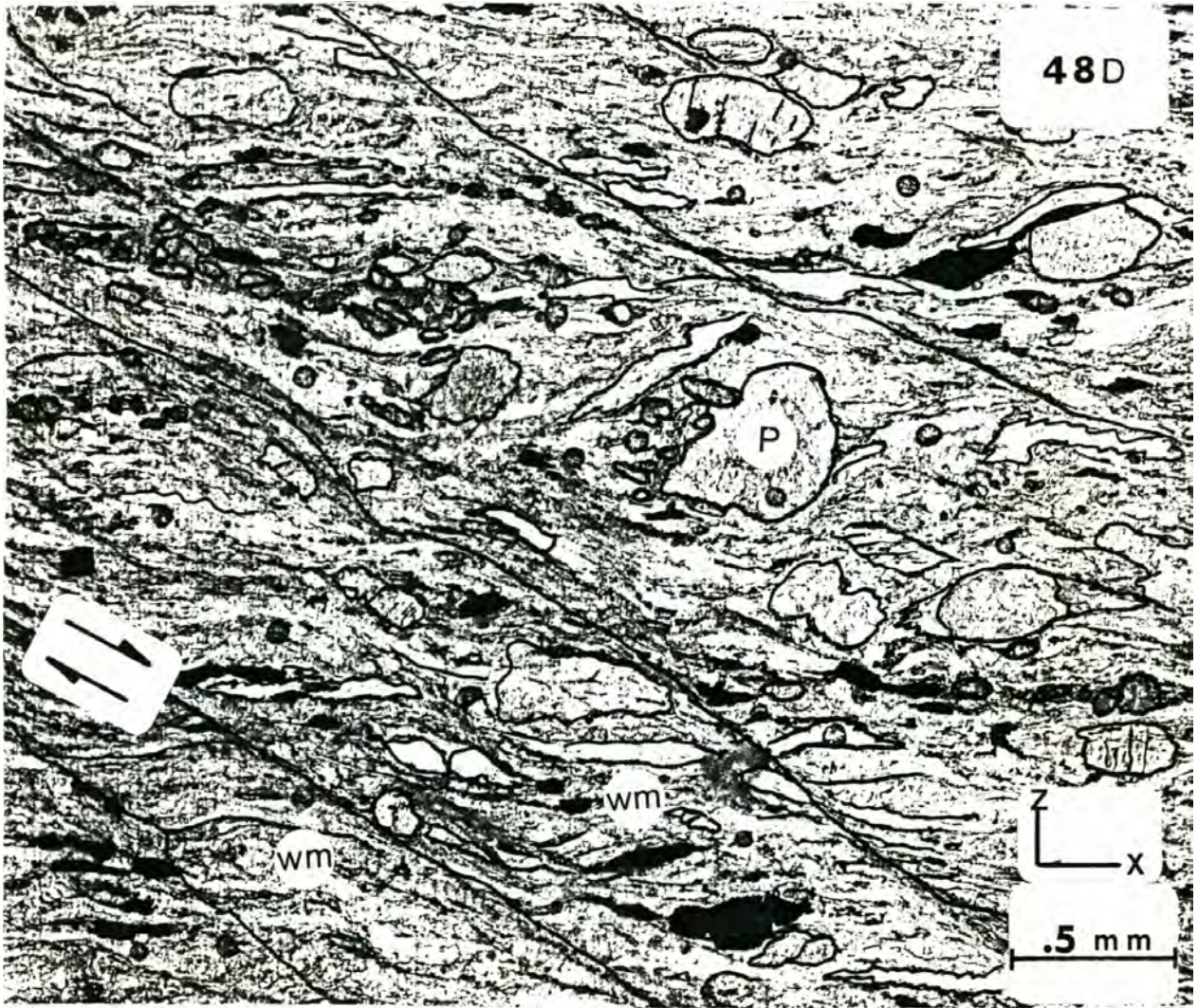
Abbreviations- staurolite (S), hornblende (H), biotite (B), chlorite (C), plagioclase clasts (P), white mica (WM), quartz (Q), mylonitic zone (MZ), idiomorphic epidote (E), Internal and External Fabrics (IF,EF).

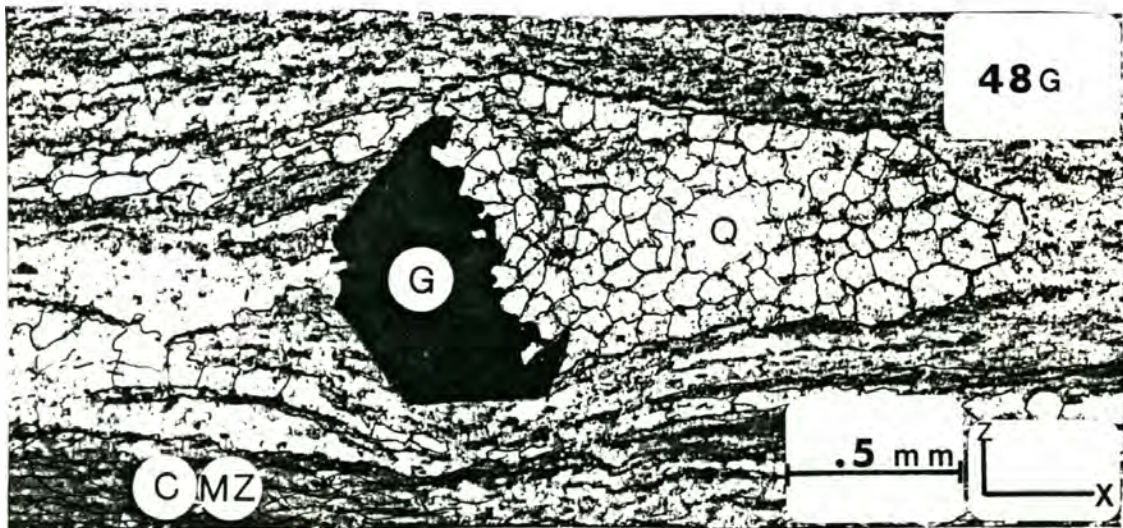
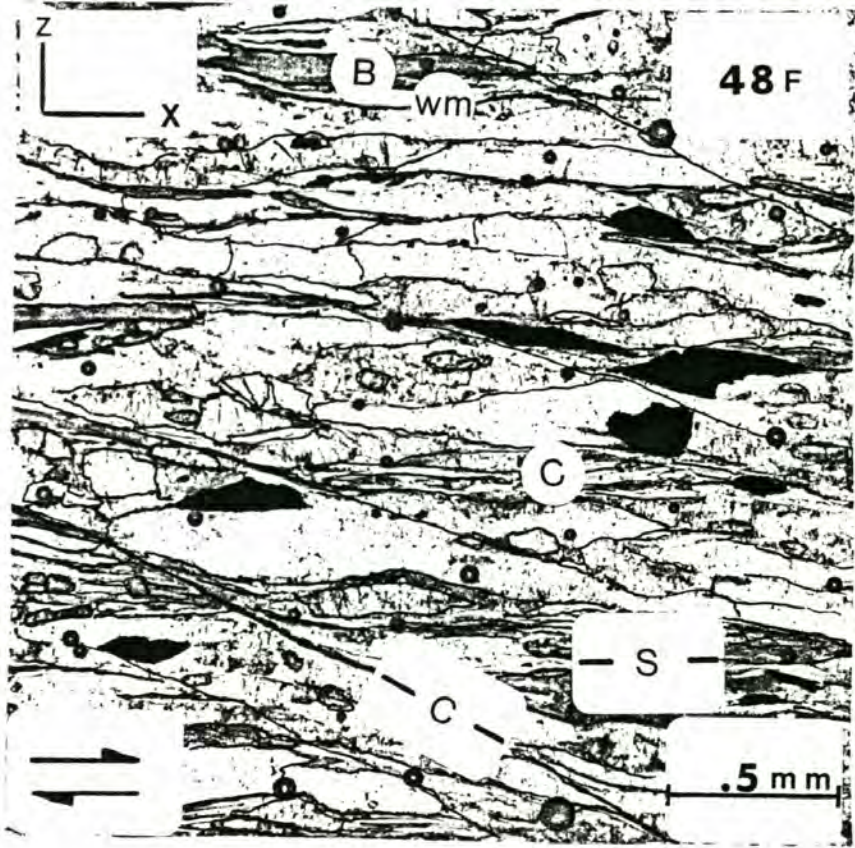
- A) Pelitic mica schist from domain C1 (3) showing the boudinage (approximately 100%) of staurolite, the planar internal fabric in hornblende which is discordant to the external foliation, and the staurolite + hornblende assemblage indicative of high pressure metamorphism (Selverstone, et al., 1984).
- B) S-C mylonite from a mica schist in domain C1 (2) showing a left-lateral shear sense and chloritization (lighter) of biotite (darker) adjacent to the C-surfaces.
- C) S-C mylonite from the brown phyllite unit (97) in domain A showing dextral shear and boudinage of the plagioclase clasts.
- D) S-C mylonite from the metaconglomerate unit (54b) in domain A showing dextral shear.
- E) Type 2 S-C mylonite (biotite fish) of Lister and Snoke (1984) from the quartzo-feldspathic schist unit in domain C1 (3b) showing sinistral shear.
- F) S-C mylonite from a mica schist (7) in domain C2 showing dextral shear.
- G) Strain shadow behind garnet in a graphitic quartz biotite schist (72) from domain B.
- H) S-C mylonite from a semipelite (113) in domain A showing a dextral shear sense and a boudinaged plagioclase clasts (+/- 100% extension).
- I) Micaceous quartzo-feldspathic schist (167) from domain C1 showing biotite fish which give a sinistral shear sense.
- J) Micaceous quartzo-feldspathic schist (167) from domain C1 showing boudinaged epidote (over 100% extension) and biotite fish which give a sinistral shear sense of shear.

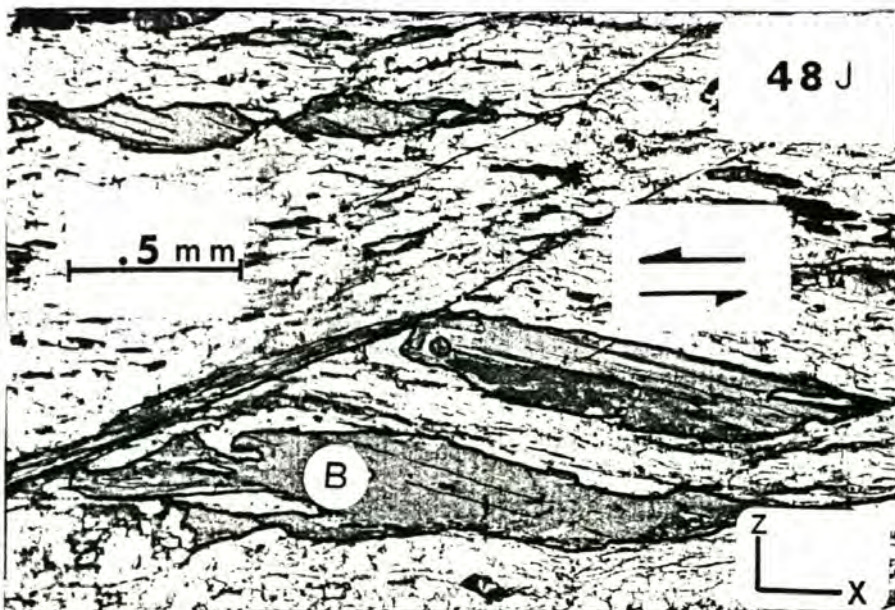
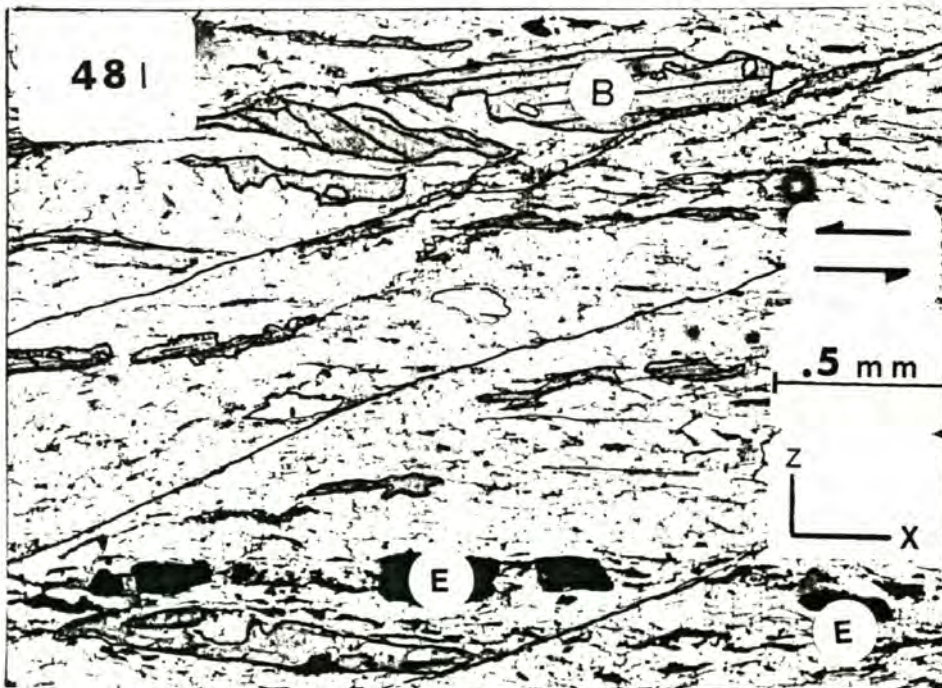
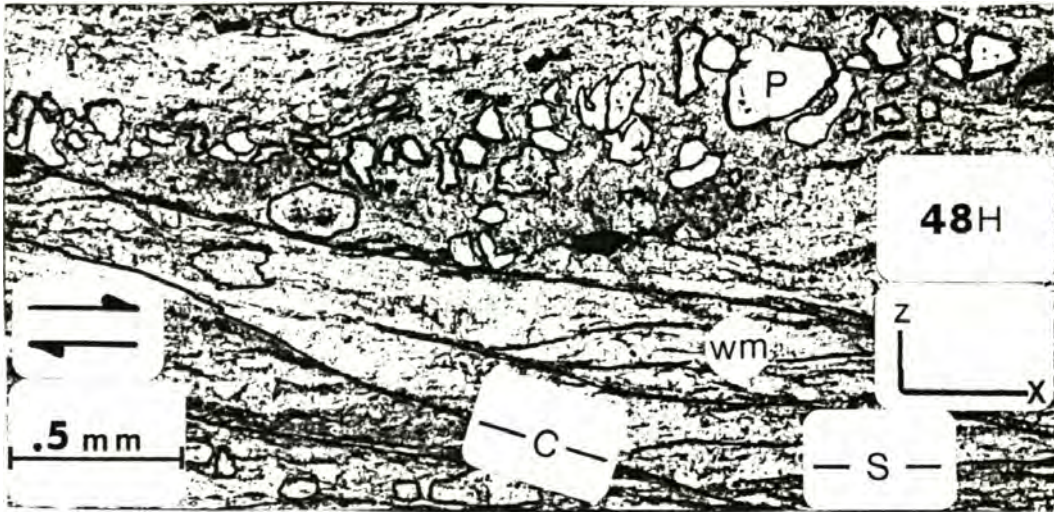












surfaces in the S-C mylonites developed simultaneously, at separate times (Berthe, et al., 1979) during the second deformation, or the S and C surfaces are a composite fabric (Lister and Snoke, 1984) from both the first and second deformations. The second and third scenarios are supported by retrogression of the commonly observed biotite to Fe-chlorite adjacent to the C surfaces (Fig. 47, 48b), suggesting that the shear along these planes is later than the formation of the S surfaces.

Later Isolated Structures

Structural Features Related to the Hidden Lake Pluton

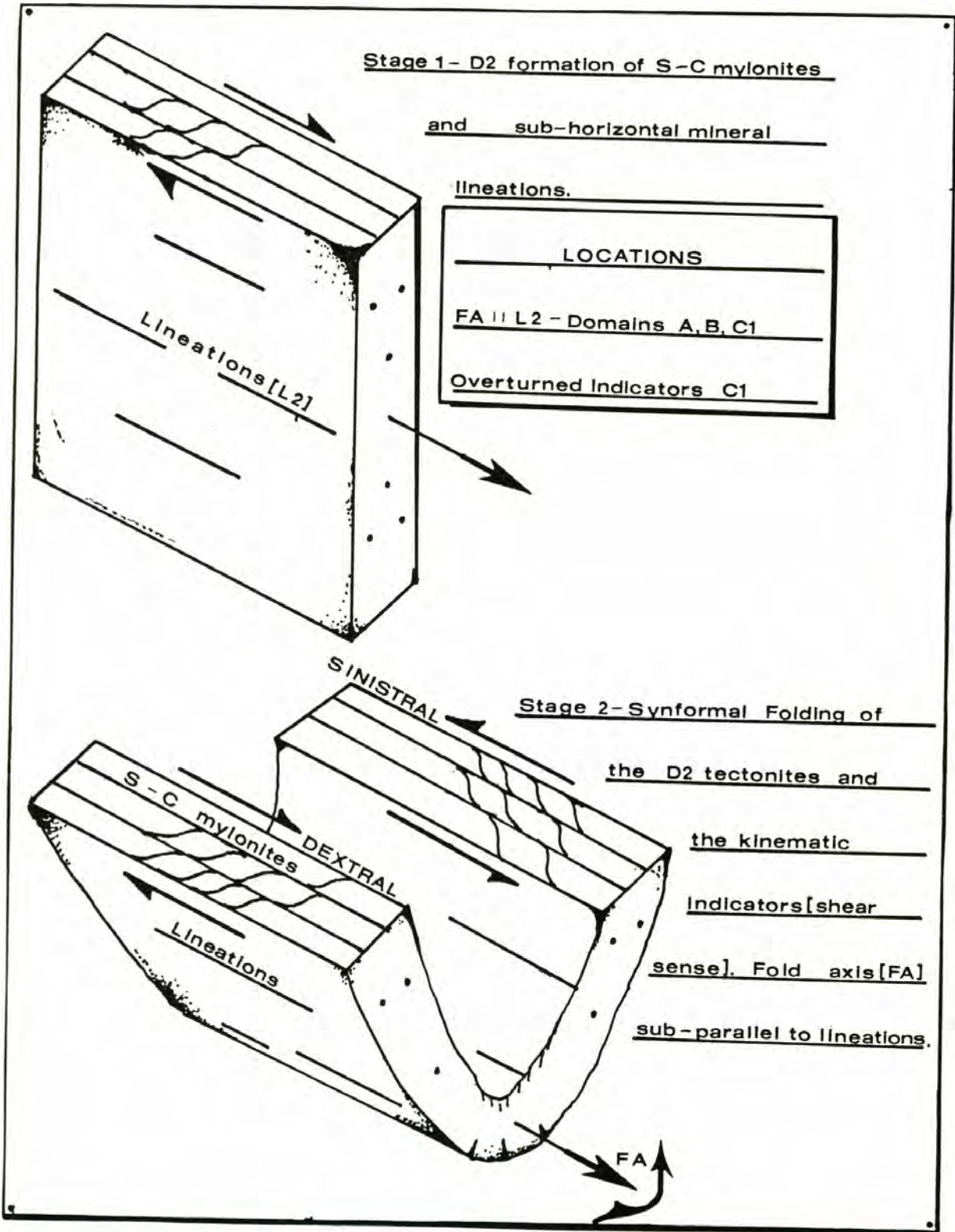
The S2 foliations in domain C1 strike to the west-northwest and dip steeply to moderately to the northeast (Fig. 35), parallel to the contact with the Hidden Lake pluton, except immediately to the south of the two southernmost mapped faults (Fig. 38 D-D') where the dip reverses to the south-southwest. This geometry may represent natural variability in the S2 orientations (fanning). However, the proximal nature of the dip reversals to the two southernmost faults suggests folding. If such folds exist, they are asymmetric and tight and may be related to offset along the faults (drag folds). No penetrative fabric (lineation or axial planar cleavage) appears to be associated with these tight folds, which may be due to the talc-lined faults taking up much of the shouldering deformation in this domain. The faults follow drainages, separate domain C1 into 3 structural blocks (Fig. 38 D-D'), and are talc-lined due to the smearing out of dissected ultramafite bodies. The downward projection of these faults to depth suggests that they may root in the Hidden Lake pluton and may be reverse faults related to intrusional compression or shouldering during emplacement. If these faults are related to the emplacement of the Hidden Lake pluton then the shouldering of the blocks was essentially

vertical due to the preservation of sub-horizontal L2 lineations in domain C1 (Fig. 36). A thin (less than 1 meter) contact aureole containing diopsidic pyroxene is observed in the quartz mica schists immediately adjacent to the northwestern margin of the Hidden Lake pluton.

The S2 foliations in the Cascade River Schist along the northeastern margin of the Hidden Lake pluton are concordant to the pluton-schist contact, strike to the north-northeast and dip steeply to the west-northwest (Fig. 50). The S2 foliations away from the contact have their normal northwesterly strike. The Hidden Lake pluton is foliated along this contact. The foliations strike to the north-northeast and parallel the S2 foliations in the adjacent schist. The Hidden Lake pluton along this contact is intensely sheared, and contains a lineation defined by feldspar augen in a thoroughly sheared, well-foliated matrix. The fabric diminishes over a distance of 150 meters towards the center of the pluton. The intensely sheared, augen bearing pluton grades into well-foliated, weakly foliated, and finally massive pluton towards the center of the pluton. These fabrics may represent an earlier chilled (?) border zone, which was later sheared during emplacement of a later phase of the pluton. This is evidenced by the steep mineral lineations, and the horizontal asymmetric tension gashes, which give a southeast up sense of shear in this mylonitic zone.

Pre-tectonic Versus Post-tectonic Emplacement of the Hidden Lake Pluton with Respect to D2- Haugerud et al. (1987) state that penetrative deformation had ceased by 73 Ma, the age of the Hidden Lake pluton, since the pluton generally lacks a foliation. However, the pluton may be pre-tectonic since deformation may be partitioned around the pluton (Patterson et al., 1988). The concordancy of the S2 foliations with the borders of the pluton, and the fact that the pluton is not observed to cross-cut the

Figure 49. Possible cause of the anomalous consistent sinistral sense of shear in domain C1 (Fig. 38 D-D' shows the location of the possible synform and the location of the sinistral sense of shear indicators with a bar symbol).



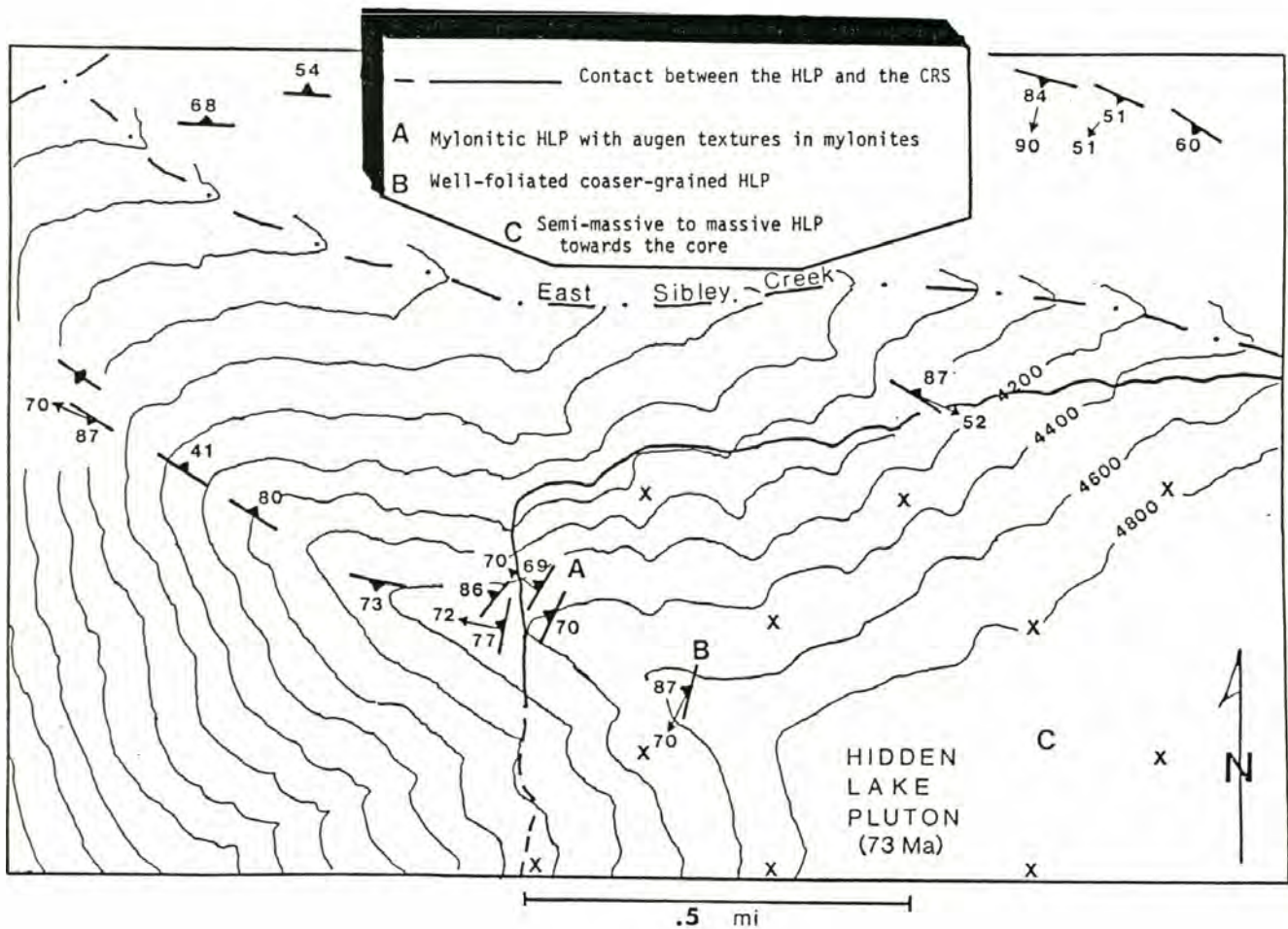


Figure 50. Map showing the structural features along the northwestern margin of the Hidden Lake pluton. The foliations along the pluton margin are concordant to the S2 foliations in the adjacent schists, as well as contain a steep mineral lineations and horizontal tension gashes indicating vertical shear direction. The strong fabric in the Hidden Lake pluton along this margin grades into massive pluton over a distance of approximately 150 meters (See A, B and C). The fabric in the pluton is interpreted to be the result of emplacement and unrelated to the D2 deformation.

D2 tectonites, precludes a definite statement concerning the timing of intrusion and D2 deformation. However, the following observations suggests that the Hidden Lake pluton is post-tectonic with respect to the second deformation: 1) the thin contact aureole along the northeastern margin; 2) the lack of deformation of the pluton along the northeastern margin; 3) the vertical shear direction for the mylonitized pluton along the northwestern margin; and 4) the possible shouldering zone, involving faulting and folding of the D2 tectonites, along the northeastern margin of the Hidden Lake pluton. If the pluton is post-tectonic with respect to D2, then the S2 foliations and L2 lineations in domain C1 (Fig. 35, 36) are rotated in a counterclockwise sense from the S2 foliation and L2 lineations in domains A and B (Fig. 37f). This deflection is due to the warping of the D2 fabric during intrusion of the pluton.

The weight of the evidence favors post-tectonic emplacement of the Hidden Lake pluton with respect to the second deformation, which suggests that D2 had ceased by 73 Ma in domains B and C1. However, this deformation appears to have been active at 75 Ma since the intrusive Marble Creek pluton contains a steep foliation and sub-horizontal mineral lineation (Cary, pers. comm.). Ductile deformation continued into the Eocene in the Skagit Gneiss since 45 M.y. old blastomylonitic granitic dikes cut the foliation in the gneiss but contain a sub-horizontal mineral lineation parallel to the regional trend (Babcock and Misch, 1988).

Late Folds

Macroscopic (Fig. 38a), mesoscopic and microscopic folding of the S2 foliations is common in domains A, B, and western domain C2 (Fig. 37c). The mesoscopic folds are generally open (Fig. 51), parallel or concentric type folds which plunge shallowly to the northwest (Fig. 37E). The

macroscopic folds are inferred from the large-scale foliation geometry, and in many cases are also suggested by S, Z, and M parasitic folds which give systematic sense of closure of these larger structures. The S₂ foliations in domain A strike to the northwest and dip steeply to the southwest, with some foliations dipping moderately to steeply to the northeast as a result of later folding concentrated in the eastern part of domain A (Fig. 35, 38 A-A'). Also a large-scale northwest shallowly plunging antiform in domain A is further evidenced by the repetition of the conglomerate unit (Fig. 26). The poles to the foliations in domain B are dispersed along a great circle, reflecting the NW plunging large-scale folds (Fig. 35, 38). Similarly, mesoscopic fold axes plunge shallowly to the northwest in domains A and B, commonly parallel to the stretching lineations.

A locally penetrative crenulation, observed in domains A, B, and northeastern domain C₂, is correlated with the later folds due to the spatial association of the crenulations with the folds. The resultant crenulation lineation plunges shallowly to the northwest and is sub-parallel to L₂ stretching lineations and later fold axes. This crenulation is accomplished through the folding and bending of the S₂ foliation, but, in general, is not associated with the development of a new axial planar cleavage (Fig. 53). The one exception is a well-developed axial planar cleavage in the graphitic mica schists in northwestern domain C₂ (Fig. 52), which appears to be related to a large-scale synform along the western margin of domain C₂ (Fig. 38 B-B'). In this case it appears that the incompetent nature of these rare mica-rich pelitic schists allowed for the development of a penetrative axial planar cleavage. This contrasts with the competent quartz and quartzofeldspathic protoliths in the domains A and B, which apparently resisted

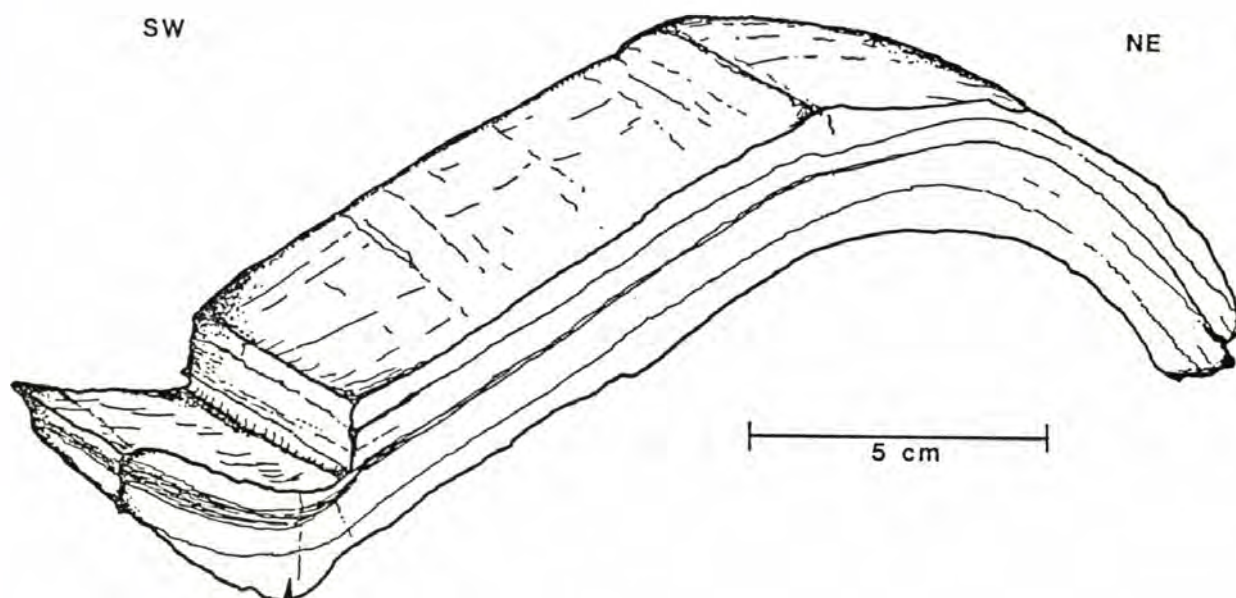


Figure 51. Handsample sketch of a mesoscopic open fold in a quartz biotite schist from domain B (131c). Such folds fold the S2 fabric (and S1 fabric in western domain C2) and plunge shallowly to the northwest. These commonly asymmetric S and Z parasitic folds give the sense of vergence, or the direction of closure, of the probable macroscopic folds.

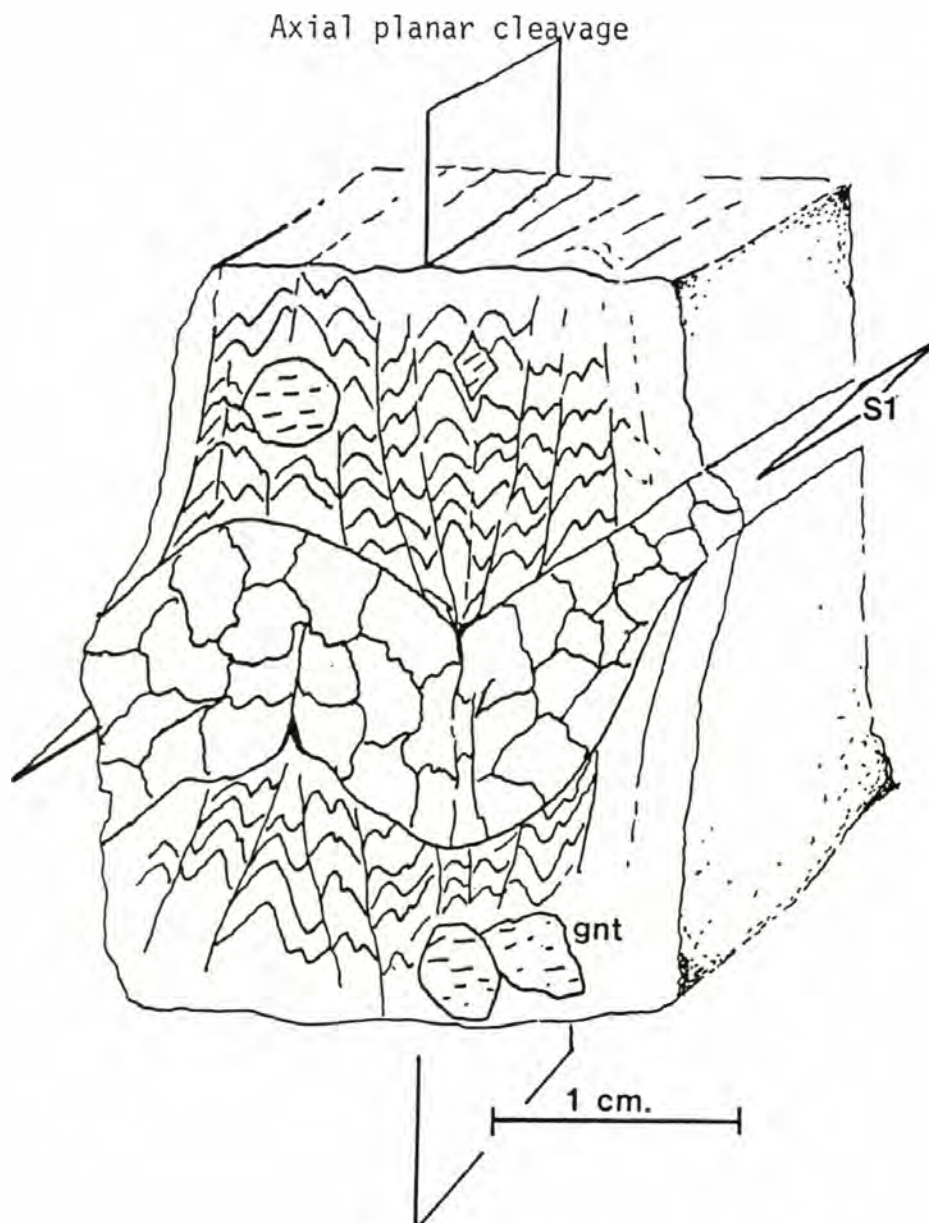
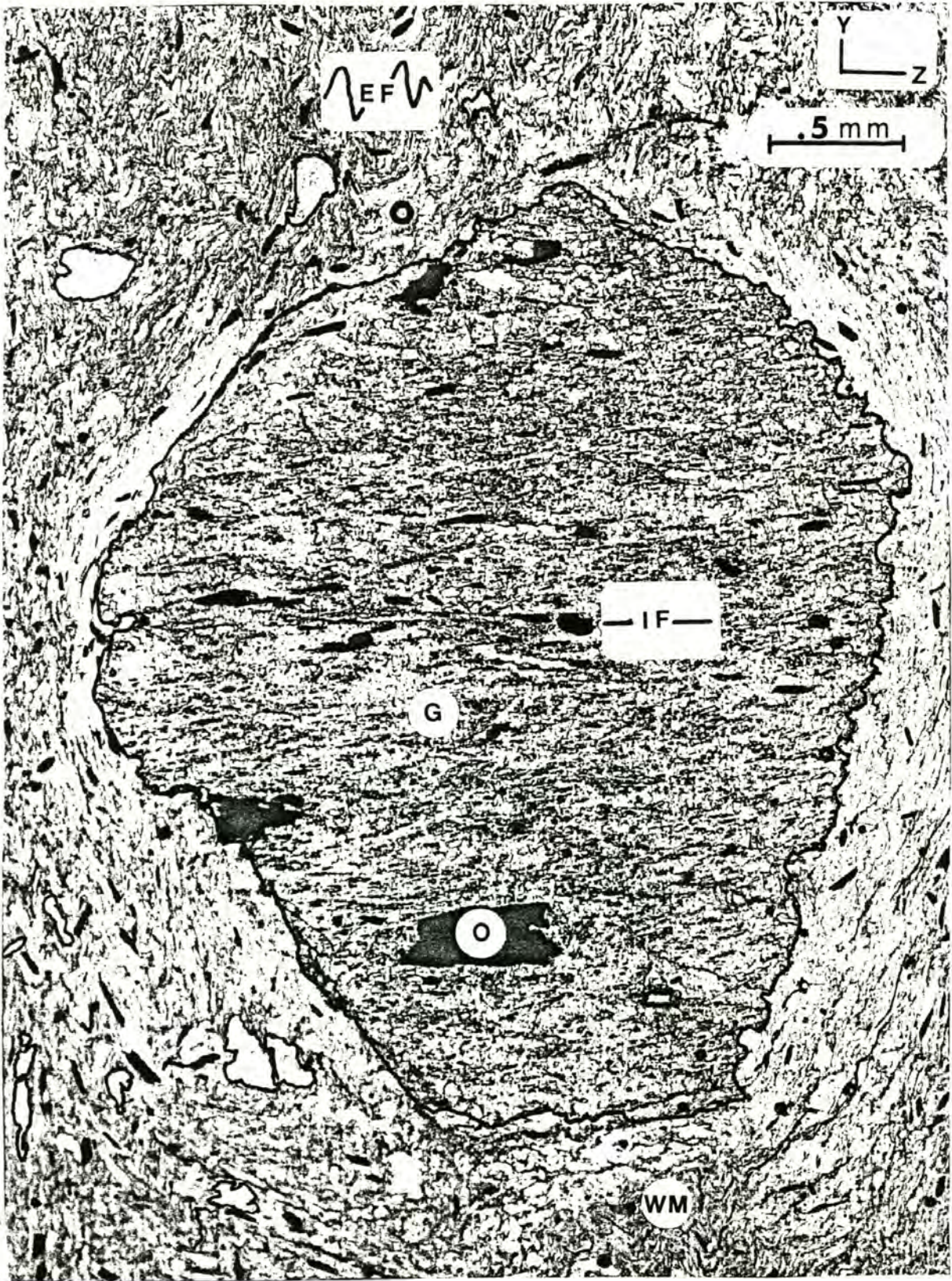


Figure 52. Sketch of a graphitic garnet mica schist handsample from western domain C2 (124, see Figure 23 for photo) showing a rare, well-developed axial planar cleavage. Most crenulated rocks lack a new thoroughly penetrative cleavage. The fabrics associated with the crenulation lineation and axial planar cleavage are L3 and S3 since they fold S2 fabrics. The axial planar cleavage in this sample is approximately vertical and may be related to a macroscopic late fold (synform) along the western part of domain C2 (Fig. 38 B-B').

Figure 53. Microfiche enlargement of a semipelite in domain A showing a planar internal foliation (IF) in a garnet porphyroblast which is discordant with, and predates, the crenulated external fabric (EF). The crenulations are observed in the YZ plane plane of the D2 L-S tectonites. Abbreviations- Garnet (G), Opaque (O), and White Mica (WM).



the development of a throughly penetrative axial planar cleavage to the later folds.

Extension veins filled with calcite and quartz are observed in domains A (Fig. 37F) and B. These veins are planar, or lack asymmetric tips, and are approximately perpendicular to the fold axes (Fig. 37E,F). The lack of asymmetry in these veins suggests that they post-date the penetrative, noncoaxial D2 shearing event, and are possibly correlatable with the brittle Le Conte fault shear regime.

The later folds, associated crenulations, and extension veins may be related to the strike-slip offset along the Le Conte fault. This is suggested by: 1) the proximity of the possibly synthetic folds to the fault; 2) the sigmoidal geometry and the thinning of the rock units proximal to the fault (Fig. 26, 27); and 3) the occurrence of steeply dipping northeast striking symmetric extension veins, which appear to be unrelated to the D2 shear regime and conform to the expected tension direction in a dextral, strike-slip, wrench regime.

The later folds and crenulations are late- to probably post-metamorphic features since the folds are of a lower strain state (open interlimb angles) and fold than the high strain, late-metamorphic, D2 fabric (Ridley, 1986). The associated crenulations are semi- to non-penetrative and post-date porphyroblast growth (Fig. 53). The Le Conte fault is post-metamorphic since this structure truncates the isograds and juxtaposes contrasting P-T regimes (see Metamorphic Section).

Lamprophyre Dikes

A Tertiary west-northwest/east-southeast directed extensional event is recorded by north-northeast trending (Fig. 37) undeformed lamprophyre and leuco-gabbro dikes. The dikes cross-cut the D2 fabrics and the Hidden

Lake pluton and are thus post-73 Ma. Dike wall irregularities match, which indicates that the dikes formed during a brittle failure in a tensional regime. This regime may be related to a regional west-northwest and east-southeast extensional event that began about 50 Ma in the Pacific Northwest (Heller, et al., 1987).

Discussion

Hypothetical Macroscopic Fold to the Southeast of the Field Area

The western Cascade River unit (See Rock Units) appears to preserve a stratigraphic sequence from sub-arc plutonics (MMQD), to arc volcanics of the greenschist unit, to supra-arc sediments of the metaconglomerate and metamarl-semipelite-pelite units (Figs. 6, 27). This sequence appears to young towards the northeast. The Cascade River unit in the northeastern part of the field area, although more strongly metamorphosed, has a protolith stratigraphy that is comparable to the western Cascade River unit (Fig. 28). The conglomerate-bearing quartzo-feldspathic unit on the northeast passes into metasemipelites, pelitic graphitic mica schists, and then quartz mica schists to the southwest. Here stratigraphic younging is apparently to the southwest (Fig. 27). This observation is supported by the direction of fining in graded beds in the quartzo-feldspathic schist unit. To the southeast of the study area, in the vicinity of Mount Johannesburg, there appears to be a closure of this structure marked by the convergence of the western and eastern Cascade River units. A macroscopic syncline is the most reasonable structure (Fig. 27) that relates the western and northeastern Cascade River units. This syncline is cut longitudinally by the Le Conte fault, along which there is a significant dip and strike-slip components.

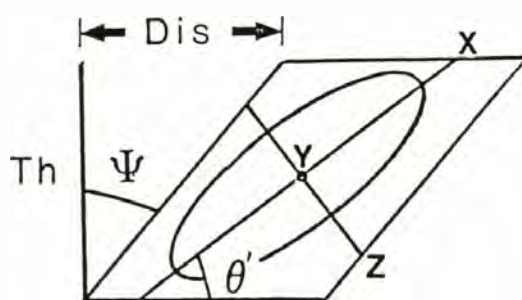
When considered on a regional scale, the stratigraphy and structure of the Cascade River unit are consistent with the interpretation of a

regional, northwest trending syncline (Fig. 27). A major question remains concerning the metamorphic gradient, which cross-cuts the macroscopic syncline (E.H. Brown, pers. comm.), and contains rocks metamorphosed to 3-4 kb on western limb and 8-10 kb on the northeastern limb. This gradient is rather abrupt for a continuous stratigraphic sequence (see Metamorphic Section). Unrecognized faults may have juxtaposed the contrasting P-T regimes. The contrasting pressure regimes on the limbs of this structure indicates that these areas were at different crustal levels during metamorphism.

The Napeequa unit lies in the center of the hypothesized major syncline (Fig. 27). It was presumably thrust over the underlying Cascade River unit since the Napeequa lithologies, including ultramafite and gabbro, were not likely deposited on top of the arc-related Cascade River unit metasediments and metavolcanics (see Fig. 38 B-B' for thrust symbol).

Estimates of the Amount of Right-Lateral Ductile Shear Offset

Right-lateral ductile shear is recorded in the D2 tectonites. An approximation of the amount of shear can be arrived at by estimating the angle between the shear zone trend and the long axis of the strain ellipsoid (θ'), assuming a homogeneous simple shear regime. A minimum and maximum amount of offset can be deduced using probable end-member values for θ' and assuming a shear zone width of 2.5 km (width of domains A and B)(Fig. 54). High shear strain is recorded in the prolate spheroidal conglomerates and highly boudinaged porphyroblasts in domain A, and less boudinaged porphyroblasts in domain B, suggesting that θ' is less than 10 degrees. The estimated offset is 8, 17, and 86 km, using angles of 10, 5, and 1 degrees, respectively (Fig. 54). These estimates do not take into account many factors, such as: 1) the



$$\text{Dis}/\text{Th} = \tan \Psi = \gamma \quad \tan 2 \theta' = -2/\gamma$$

<u>Thickness(Th)</u>	<u>θ'</u>	<u>Distance(Dis)</u>
2.5 kilometers	10 degrees	8 kilometers
2.5 kilometers	5 degrees	17 kilometers
2.5 kilometers	1 degree	86 kilometers

Figure 54. Possible amounts of D2 ductile offset assuming a homogeneous simple shear zone, with a width of 2.5 km (width of domains A and B), and theta between 1 to 10 degrees. Probable theta is 5 to 10 degrees on the basis of the angle between C surface and stretching lineation trends. This estimation is based on the fact that in ductile shear zones simple shearing leads to a progressive approach towards to shear plane of the XY plane of the ellipsoid and progressive approach of X, the extension direction, to this shear line (Ramsey and Graham, 1970).

inhomogeneous nature of the shear; or 2) the alteration of the width of the shear zone by later folding and faulting. However, the exercise does demonstrate that significant offset produced the D2 tectonites.

Tectonics and Orogeny

Northward Translation and Ductile Shear- Discordant paleomagnetic remanent magnetizations observed in the Cordillera have been interpreted by some (Irving et al., 1985; Beck, in press) to indicate that the Crystalline Core (Beck and Noson, 1972) and other terranes have been translated northward from the vicinity of Baja California. Much of the criticism of this extreme northwards translation centers on the lack of recognition of the structures that could accommodate such a translation. Some of the structures have been identified (Fraser-Straight Creek fault, Ross Lake fault, Denali fault, etc.), but the sum of the displacements on these strike-slip faults does not equal the extreme displacements inferred from the paleomagnetic studies. A significant amount of this displacement may be hidden in unidentified, distributed, right-lateral, ductile shear zones in mobile orogenic belts such as in the Cascade River area and as demonstrated by Brown (1987, 1988) for the Late Cretaceous (91-87 Ma) shear zones in the Northwest Cascades System.

Relationship Between Plate Velocity Vectors and Structures- The Crystalline Core has been suggested to be a broad, right-lateral, orogenic ductile shear zone (Brown and Talbot, manuscript). Indeed, the velocity vectors for both the Kula and Farallon oceanic plates constructed from data of Engebretson et al. (1985) during the 84-74 Ma stage are north trending and highly oblique to the North American coast trend (Fig. 55). The obliquity and magnitude of these vectors applies not only to the present latitude and longitude of the Crystalline Core, but to positions significantly to the south (Table 10), and the vectors thus apply also to

a far-traveled terrane originating in present-day California. This is due to the substantial distance of the Euler pole from the coastal trend, as well as the approximate great circle distribution of these positions about the Euler pole.

Table 10. Orientation of the Velocity Vectors along Western North America at 85 Ma

<u>Location</u>	<u>Latitude</u>	<u>Longitude</u>	<u>east of north</u>	<u>cm/yr</u>
1. Field Area	48.50	238.75	30.24	10.70
2. Chiwaukum Graben	47.00	239.00	29.85	10.62
3. Cape Mendicino	37.5	236.00	22.99	10.41

Furthermore, the end of ductile, right-lateral, strike-slip shear in the study area by 73 Ma, based on interpretation that the Hidden Lake pluton is post-tectonic, agrees with the transition of the velocity vectors to a more easterly, or convergent, trend for both the Kula and Farallon oceanic plates from 74-36 Ma (Engebretson et al., 1985). The more northerly, or oblique, trend (340-360 degrees) of the Eocene faults (i.e. Straight Creek, Entiat, Le Conte, and other mapped faults), which commonly cut the more northwesterly penetrative fabrics in the Crystalline Core, agrees with the more northeasterly orientation of the velocity vectors from 74-37 Ma. Noteworthy is the normal, or convergent, orientation of the velocity vectors during the Eocene for the Farallon plate (Fig. 55). The Kula plate is significantly oblique from 85-74 Ma, more normal from 74-56 Ma, and then oblique from 56-37 Ma. This may coincide with the production of a broad, right-lateral, strike-slip, ductile shear during the height of the Late Cretaceous orogeny in the Crystalline Core; followed by the period of more northerly trending, right-lateral, strike-slip faulting (Entiat fault, etc..) and ductile shear in the Skagit Gneiss which is

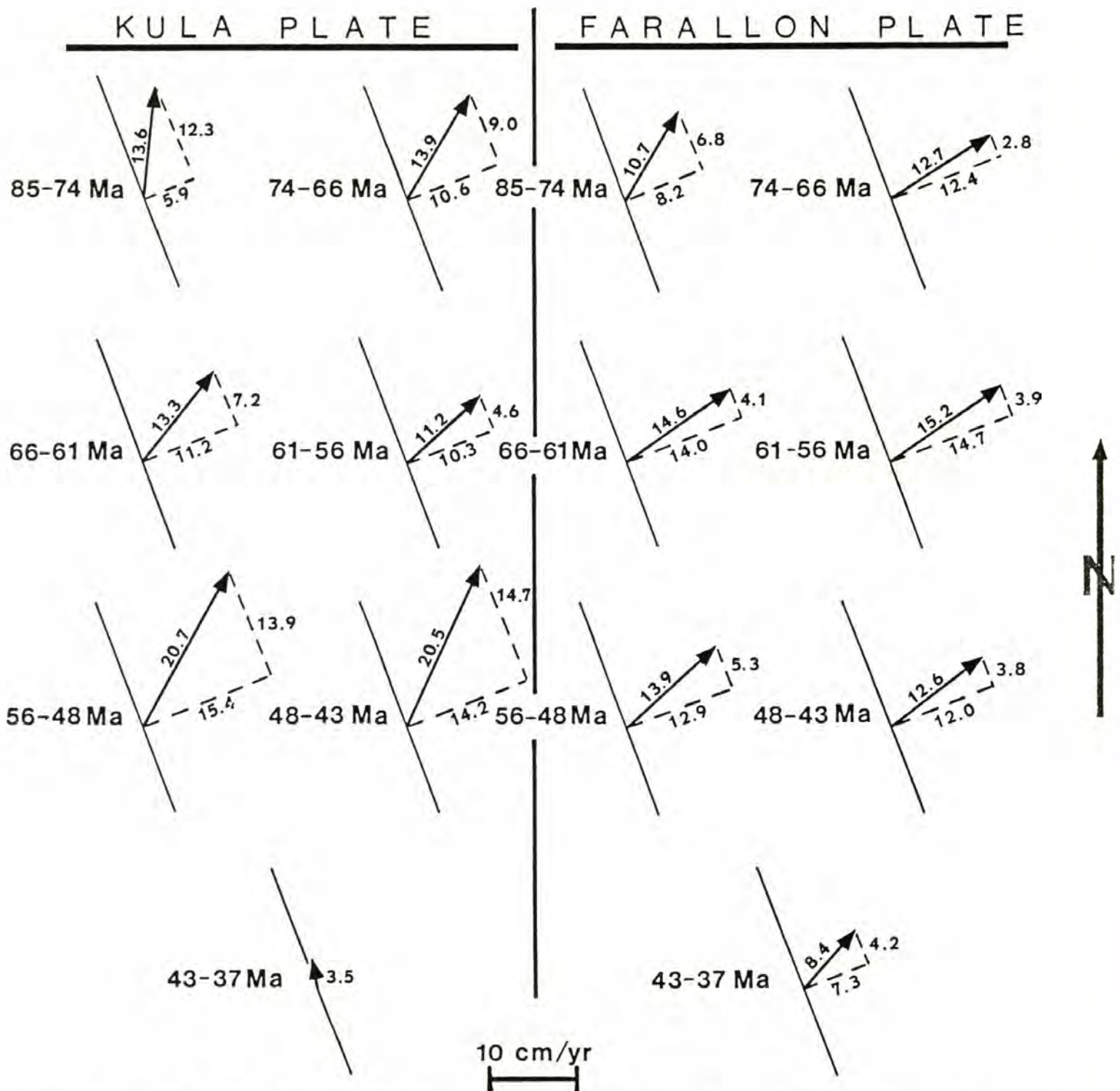


Figure 55. Farallon and Kula oceanic plate velocity vectors. The diagram was constructed using North America is fixed plate motion data of Engebretson (et al., 1985) for the field area coordinates.

still at depth (Babcock and Misch, 1988), during the Eocene. The later dip-slip component documented for several of these faults may be correlated with the reduction in normal convergence rate from 56-37 Ma for the probably outboard Farallon plate.

Summary

The three questions that were posed in the introduction, under statement of the problems, are used to summarize the general findings of this study.

1) What is the composition, distribution, and previous tectonic setting of the Cascade River Schist protoliths?

The rock units in the study area are divisible into the Cascade River and Napeequa units of Tabor et al. (in press), which are divided into a western Cascade River unit, central Napeequa unit, and northeastern Cascade River unit in the study area. The Cascade River unit contains arc-affinity metaclastites, metavolcanics, metasemipelites, metamarls and minor metapelites and marble. The Napeequa unit contains quartz biotite schists, ultramafites, metagabbros and amphibolites. The Cascade River unit contains a mappable stratigraphy. The stratigraphy observed in the study area correlates with the stratigraphy observed along strike outside the study area by Tabor (1961), Cary (pers. comm.), and the author with E.H. Brown. This arc-related stratigraphy fines, and probably youngs, towards the centrally located oceanic-related Napeequa unit. The fining and inferred younging of the rocks suggest that the Napeequa unit was structurally emplaced over the Cascade River unit, possibly along a thrust, since it is unlikely that oceanic-related Napeequa unit, containing metaperidotite, would depositionally overlay arc-related Cascade River unit.

2) What were the temperature-pressure conditions of metamorphism?

Metamorphic zones and facies in the field area increase from the biotite zone of the greenschist facies, west of the Le Conte fault, to the garnet and staurolite-kyanite zones of the epidote amphibolite facies east of the fault. Using a petrogenetic grid, mineral assemblages and geothermobarometry, the greenschist facies is estimated to have been metamorphosed to pressures of 3-5 kb and temperatures of 450-500 C, whereas the amphibolite facies is estimated to have been metamorphosed to 8-10 kb and 600-700 C. Pressure estimates of 9 kb for the amphibolite facies in the Cascade River Schist, estimated using geobarometry and the presence of staurolite + hornblende, are comparable to that suggested by Whitney (1987) for the higher temperature (650-720 C) Skagit Gneiss suggesting an isobaric thermal increase to the northeast. Structural control of the greenschist-amphibolite boundary by the Le Conte fault is indicated by the first appearance of garnet, oligoclase, and hornblende approximately along the fault, as well as by barometric estimates adjacent to this structure. The 3-5 kb pressure differential across this structure suggests that 9-15 km of dip-slip movement has occurred along this structure since metamorphism. This is in addition to 10 km of strike-slip motion recorded by offset of the metaconglomerate unit in the Cascade River Schist.

3) What were the number, sequence, and kinematics of the deformational events affecting the Cascade River Schist, as well as their relationship to metamorphism?

Two penetrative and three localized deformations are observed in the study area. The first deformation was syn-metamorphic and is characterized by steeply dipping S tectonites containing a weak down-dip mineral lineation, and flattened conglomerate clasts. The second

deformation was late-metamorphic, commonly retrogressive, and is characterized by steeply dipping L-S tectonites containing a sub-horizontal stretching lineation, dextral kinematic indicators, and distinctly prolate ellipsoidal conglomerate clasts. Overprinting D1 and D2 tectonites are: 1) localized faults and folds attributed to shouldering by the 73 m.y. old Hidden Lake pluton, which affects D2 tectonites and thus gives a probable minimum age of D2 shear; 2) microscopic (crenulations), mesoscopic, and macroscopic open to tight folds observed in the vicinity of the Le Conte fault and attributed to the wrenching strain along this structure; and 3) lamprophyre dikes which were intruded in a tensional regime after emplacement of the Hidden Lake pluton.

REFERENCES

- Babcock, R.S., and Misch, P., manuscript, Origin of the Skagit Migmatites, North Cascades Range, Washington State.
- Babcock, R.S., and Misch, P., 1988, Evolution of the Crystalline Core of the North Cascades Range: in Ernst, W.G. ed., Metamorphism and Crustal Evolution of the Western United States, Prentice Hall, New Jersey, Rubey v. 7, p. 214-232.
- Beck, M.E., in press, Paleomagnetism of Continental North America: Implications for Displacement of Crustal Blocks within the Western Cordillera, Baja California to British Columbia: in Pakister, L.C., and Mooney, W.D., eds., Geophysical Framework of the Continental United States, Geological Society of America.
- Beck, M.E., and Noson, L., 1972, Anomalous Paleolatitudes in Cretaceous Granitic Rocks: Nature, v. 235, p. 11-13.
- Berman, R., Brown, T., and Greenwood, H., 1985, An Internally Consistent Thermodynamic Database for Minerals in the System $\text{Na}_2\text{O}-\text{K}_2\text{O}-\text{CaO}-\text{MgO}-\text{FeO}-\text{Fe}_2\text{O}_3-\text{Al}_2\text{O}_3-\text{SiO}_2-\text{TiO}_2-\text{H}_2\text{O}-\text{CO}_2$: Atomic Energy of Canada Ltd. Technical Report, 377, p. 1-62.
- Berman, R., unpublished, PTXss88 Program: Geological Society of Canada.
- Berthe', D., Choukroune, P., and Jegouzo, P., 1979, Orthogneiss, Mylonite and Noncoaxial Deformation of Granites: the Example of the South American Shear Zone: Journal of Structural Geology, v. 1, p. 31-42.
- Bohlen, S.R., and Liotta, J.J., 1986, A Barometer for Garnet Amphibolites and Garnet Granulites: Journal of Petrology, v. 27, part 5, p. 1025-1034.
- Brown, E.H., and Talbot, J.L., manuscript, Orogen-Parallel Extension in the North Cascades Crystalline Core, Washington.
- Brown, E.H., 1988, Metamorphic and Structural History of the Northwest

- Cascades, Washington and British Columbia: in Ernst, W.G., ed., *Metamorphism and Crustal Evolution of the Western United States*, Prentice Hall, New Jersey, Rubey v. 7, p. 197-213.
- Brown, E.H., 1987, *Structural Geology and Accretionary History of the Northwest Cascades System, Washington and British Columbia: Geological Society of America Bulletin*, v. 99, p. 201-214.
- Brown, E.H., and Forbes, R.B., 1986, *Phase Petrology of Eclogitic Rocks in Fairbanks District, Alaska: Geological Society America, Memoir 164*, p. 155-167.
- Brown, E.H., 1978, *A P-T Grid for Metamorphic Index Minerals in High Pressure Terranes: Geological Society of America, Abstracts with Programs*, v. 10, no. 7, p. 373.
- Brown, E.H., 1977, *The Crossite Content of Ca-Amphibole as a Guide to Pressure of Metamorphism: Journal of Petrology*, v. 18, part 1, p. 53-72.
- Cater, F.W., Jr., 1982, *The Intrusive Rocks of the Holden and Lucerne Quadrangles, Washington: The Relation of Depth Zones, Composition, Textures, and Emplacement of Plutons: United States Geological Survey Professional Paper 1221*, p. 1-108.
- Engebretson, D.C., Cox, A., and Gordan, R.G., 1985, *Relative Motions Between Oceanic and Continental Plates in the Pacific Basin: Special Paper 206, Geological Society of America*, p. 1-58.
- Evans, B.W., and Berti, J.W., 1986, *Revised Metamorphic History for the Chiwaukum Schist, North Cascades, Washington: Geology*, v. 14, p. 695-698.
- Ferry, J.M., and Spear, F.S., 1978, *Experimental Calibration of the Partitioning of Fe and Mg between Biotite and Garnet:*

- Contributions to Mineralogy and Petrology, v. 66, p. 113-117.
- Flinn, D., 1962, On Folding During Three-dimensional Progressive Deformation: Geological Society of London, Quarterly Journal, v. 118, p. 385-433.
- Fugro Northwest, Inc., 1979, Interim Report on the Geologic Feasibility Studies for Copper Creek Dam.
- Ganguly, J., and Saxena, S., 1984, Mixing Properties of Aluminosilicate Garnet: Constraints from Natural and Experimental Data, and Application to Geobarometry: American Mineralogist, v. 69, p. 88-97.
- Hammarstrom, J.M., and Zen, E., 1986, Aluminum in Hornblende: An empirical Igneous Geobarometer: American Mineralogist, v. 71, p. 1297-1313.
- Haugerud, R.A., Tabor, R.W., and Stacey, J., 1987, What is the Core of the Northern Cascades, Washington?: A New Look at the Structure and Metamorphic History of the Skagit Gneiss of Misch (1966): Geological Society of America, Abstracts with Programs, v. 10, no. 7, p. 74.
- Heller, P.L., Tabor, R.W., and Suczek, C.A., 1987, Paleogeographic Evolution of the United States Pacific Northwest during Paleogene Time: Canadian Journal of Earth Science, v. 24, p. 1652-1667.
- Hodges, K.V., and Spear, F.S., 1982, Geothermometry, Geobarometry and the Al_2SiO_5 Triple Point at Mt. Moosilauke, New Hampshire: American Mineralogist, v. 67, p. 1118-1134.
- Holdaway, M.J., 1971, Stability of Andalusite and Aluminum Silicate Phase Diagram: American Journal of Science, v. 271, p. 97-131.
- Hollister, L.S., Grissom, G.C., Peters, E.K., Stowell, H.H., and Sisson, V.B., 1987, Confirmation of the Empirical Correlation of Al in Hornblende with Pressure of Solidification of Calc-alkaline Plutons: American Mineralogist, v. 72, p. 231-239.

- Huang, W.L., and Wyllie, P.J., 1975, Melting Reactions in the System NaAlSi₃O₈-KAlSiO₈-SiO₂ to 35 Kilobars, Dry and with Excess Water: *Journal of Geology*, v. 83, p. 737-748.
- Hunziker, J.C., and Martinotti, G., 1984, The Austroalpine System in the Western Alps: A Review: *Memoir Society Geol It.*, v. 29, p. 233-250.
- Irvine, T.N., and Barager, W.R.A., 1971, A Guide to the Chemical Classification of Common Volcanic Rocks: *Canadian Journal of Earth Science*, v.8, p. 523-548.
- Irving, E., Woodsworth, G.J., Wynne, D., and Morrison, A., 1985, Paleomagnetic Evidence for Displacement from the South of the Coast Plutonic Complex, British Columbia: *Canadian Journal of Earth Science*, v. 32, p. 584-598.
- Leake, B.E., 1979, Amphibole Nomenclature: *American Mineralogist*, v. 78, p. 1023-1043.
- Le Maitre, R.W., 1984, A Proposal by the IUGS Subcommittee on the Systematics of Igneous Rocks for a Chemical Classification of Volcanic Rocks Based on the Total Alkali Silica (TAS) Diagram: *Australian Journal of Earth Sciences*, v.31, p. 243-255.
- Lister, G.S., and Snoke, A.W., 1984, S-C Mylonites: *Journal of Structural Geology*, v. 6, p. 617-638.
- Maruyama, S., Suzuki, K., and Liou, J.G., 1983, Greenschist-Amphibolite Transition Equilibria at Low Pressures: *Journal of Petrology*, v. 24, p. 583-604.
- Mattinson, J.M., 1972, Ages of Zircons from the Northern Cascade Mountains, Washington: *Geological Society of America Bulletin*, v. 83, p. 3679-3784.
- Misch, P., 1966, Tectonic Evolution of the Northern Cascades of Washington State: in Gunning, H.C. ed., *A Symposium on the Tectonic History and*

- Mineral Deposits of the Western Cordillera: Canadian Institute of Mining and Metallurgy, Special vol. 8, p. 101-148.
- Misch, P., 1968, Plagioclase Compositions and Non-anatectic Origin of the Migmatitic Gneisses in the Northern Cascade Mountains of Washington State: Contributions to Mineralogy and Petrology, v. 17, p. 1-70
- Misch, P., 1971, Metamorphic Facies Types in the Northern Cascades: Geological Association of Canada, Cordilleran Section Symposium, Programs and Abstracts, p. 22-23.
- Misch, P., and Rice, J.M., 1975, Miscibility of Tremolite and Hornblende in Progressive Skagit Metamorphic Suite, North Cascades, Washington: Journal of Petrology, v. 16, part 1, p. 1-21.
- Misch, P., and Onyeagocha, A.C., 1976, Symplectite Breakdown of Ca-Rich Almandines in Upper Amphibolite-Facies Skagit Gneiss, North Cascades, Washington: Contributions to Mineralogy and Petrology, v. 54, p. 189-224.
- Misch, P., 1977, Bedrock Geology of the North Cascades: in Brown, E.H., and Ellis, R.C., eds., Geological Excursions in the Pacific Northwest: Geological Society of America Annual Guidebook, Seattle, Washington, p. 1-62.
- Misch, P., 1979, Geologic Map of the Marblemount Quadrangle, Washington: Washington Department of Natural Resources, Division of Geology and Earth Resources, Map GM-23.
- Misch, P., 1987, Type Section of the Skagit Gneiss, North Cascades, Washington: Geological Society of America Centennial Field Guidebook, Cordilleran Section, p. 1-67.
- Miyashiro, A., 1974, Volcanic Rock Series in Island Arc and Active Continental Margins: American Journal of Science, v. 274, p. 321-

355.

- Mullen, E.D., 1983, MnO-TiO₂-P₂O₅: A Minor Element Discriminant for Basaltic Rocks of Oceanic Environments and its Implications for Petrogenesis: *Earth and Planetary Science Letters*, v. 62, p. 53-62.
- Newton, R., and Haselton, M., 1981, Thermodynamics of the Garnet-Plagioclase-Al₂SiO₅-Quartz Geobarometer: in Newton, R.C., Navrotsky, A., Wood, B.J., eds., *Thermodynamics of Minerals and Melts I: Advances in Geochemistry*, Springer and Verlag, New York, p. 131-147.
- Passchier, C.W., and Simpson, C., 1986, Porphyroclast Systems as Kinematic Indicators: *Journal of Structural Geology*, v. 8, p. 831-843.
- Patterson, S.R., and Tobisch, O.T., 1988, Using Pluton Ages to Date Regional Deformations: Problems with Commonly Used Criteria: *Geology*, v.16, p. 1108-1111.
- Pearce, J.A., and Cann, J.R., 1973, Tectonic Setting of Basic Volcanic Rocks Determined Using Trace Element Analysis: *Earth and Planetary Science Letters*, v. 19, p. 290-300.
- Pigage, L.C., and Greenwood, H.J., 1982, Internally Consistent Estimates of Pressure and Temperature: The Staruolite Problem: *American Journal of Science*, v. 282, p. 943-969.
- Piwinski, A.J., and Wyllie, P.J., 1970, Experimental Studies of Igneous Rock Series: Felsic Body Suite from Needle Point Pluton, Wallowa Batholith, Oregon: *Journal of Geology*, v. 78, p. 52-76.
- Ramsey, J.G., and Gramham, R.H., 1970, Strain Variation in Shear Belts: *Canadian Journal of Science*, v. 7, p. 786-813.
- Ridley, J., 1986, Parallel Stretching Lineations and Fold Axes Oblique to a Shear Displacement Direction--a Model and Observations: *Journal of Structural Geology*, v. 8, p. 647-653.
- Silverstone, J., Spear, F.S., Franz, G., and Morteani, G., 1984, High-

- Pressure Metamorphism in the SW Tauern Window, Austria: P-T Paths from Hornblende-Kyanite-Staurolite Schists: *Journal of Petrology*, v. 25, part 2, p. 501-531.
- Shervais, J.W., 1982, Ti-V Plots and the Petrogenesis of Modern and Ophiolitic Lavas: *Earth and Planetary Science Letters*, v. 59, p. 101-118.
- Simpson, C., and Schmid, S.M., 1983, An Evaluation of Criteria to Deduce the Sense of Movement in Sheared Rocks: *Geological Society of America Bulletin*, v. 94, p. 1281-1288.
- Sun, S.S., and Nesbitt, R.W., 1978, Geochemical Regularities and Genetic Significance of Ophiolitic Basalts: *Geology*, v. 6, p. 689-693.
- Tabor, R.W., Haugerud, R.A., Miller, R.B., Brown, E.H., and Babcock, R.S., in press: Accreted Terranes of the North Cascades Range, Washington, *International Geological Congress Field Trip Guide*, Trip 307.
- Tabor, R.W., Zartman, R.E., and Frizzel, V.A., 1987, Possible Tectonostratigraphic Terranes in the Northern Cascades Crystalline Core, Washington: in Schuster, J.E. ed., *Selected Papers on the Geology of Washington*, Washington Division of Mines and Earth Resources Bulletin, v. 77, p. 107-126.
- Tabor, R.W., 1961, *The Crystalline Geology of the Area South of Cascade Pass, Northern Cascade Mountains, Washington*: University of Washington, Seattle Washington, Ph.D. thesis, p. 1-205.
- Thompson, J.B., Jr., and Norton, S.A., 1968, Paleozoic Regional Metamorphism in New England and Adjacent Areas: in Zen, E., ed., *Studies of Appalachian Geology, Northern and Maritime*, New York, p. 319-327.
- Williams, H., and McBirney, A.R., 1979, *Volcanology*: Freeman, Cooper and

Company, San Francisco, p. 310-313.

Whitney, D.L., 1987, Garnet Zoning and P-T Paths for the Metamorphism of the Skagit Gneiss, North Cascades, Washington: M.S. thesis, University of Washington, Seattle, Washington, p. 1-71

Yardley, B.W., 1978, Genesis of the Skagit Gneiss Migmatites, Washington, and the Distinction between Possible Mechanisms of Migmatization: Geological Society of America Bulletin, v. 89, p. 941-951.

APPENDIX 1
Mineral Assemblages

The location of each sample is given in Plate 2 (Sample Site Map).

Abbreviations- quartz (qtz), plagioclase (plg), white mica (whm), chlorite (chl), biotite (bt), epidote (epd), actinolite (act), calcite (cal), tourmaline (trm), opaque (opq), ilmenite (ilm), rutile (rut), sphene (sph), pyrite (pyr), graphite (grh), relict plagioclase clasts (RPC), possible quartz clasts (PQC).

X, x = greater and less than approximately 10%, respectively. R, r = retrogressive product that is greater and less than approximately 10%, respectively (not all retrogressed most retrogressed samples noted).

** = Geothermobarometric sample (see Metamorphic Section). An = microprobe determined anorthite component of plagioclase.

Rock Units West of the Le Conte Fault
Cascade River Unit

Greenschist Unit- Plagioclase clasts contain abundant sausserite.

#	qtz	plg	RPC	chl	bio	epd	act	opq	pyr	cal	NOTES
98	X	X	X	X	x	X	x	x			chloritized bio., S-C mylonite
114	X	X	X	x		X		x			
300	X	X	X	x	x	X	x	x	x	x	S-C mylonite
203	X	X	x	X	x	X	x	x			
204	XX	X		x	x	X	x	x			
205	X	X	X	x	x	x		x			
206	X	X	X	x	x	x		x			

Brown Phyllite Unit-

#	qtz	plg	RPC	whm	chl	epd	opq	pyr	trm	sph	cal	NOTES
97	X	X	X	X	x		x	x				sub-rounded RPC, S-C mylonite
97b	X	X	X		x	x	x				x	sub-rounded RPC (An 02)
162	X	X	X	X	x	x					x	" " "
207	X	X	X	X	X		x	x	x	x		" " "

Metaconglomerate Unit- Dominantly dacitic and granitic clasts.

#	qtz	plg	RPC	whm	chl	bio	epd	opq	cal	sph	trm	NOTES
14	X	X	X	X	x	x		x		x	x	
16	X	X	X	X	X		x					
47a	X	X	X	x	x	x	x					
47b	X	X	X	x	x	x	X	x				
47b	X	X		x		x	X	x				dacite clast (in 47b)
54a	X	X	X	x	X		x	x				
54b	X	X	X	X	x	x	x	x				S-C mylonite
55	X	X		x	x	x						granitic clast
95	X	X	X	X	x	x	x	x	x			opq = magnetite
95	X	X	x	x	x		x					dacite clast (in 95)
96	X	X	X	X	x		x	x	x	x		epd = zoisite

#	qtz	plg	RPC	whm	chl	bio	epd	opq	cal	sph	trm	NOTES
105	X	X	x	x	x		x	x	x	x		S-C mylonite
112	X	x	X	X	r	x	x	x	x		x	Fe-chlorite(retro)
113	X	X	X	X	x		x	x	x	x		S-C mylonite
144	X	X	X	x	x	x			x	x		RP Clasts 50%
144c	X	X	X	X	x	x	x	x	x		x	An 04
159b	X	X	X	X	x		x	x	x			
161	X	X	x	X	x		x		x	x		An 02
208	X	X	X	X	x	x	X		x	x	x	S-C mylonite

Metatuff Unit- Thin (10 meters) traceable unit directly east of the conglomerate unit.

#	qtz	plg	RPC	whm	chl	NOTES
110	X	X	X	x	x	lappilli bearing

Metamarl-semipelitic-peliteUnit-

#	qtz	plg	RPC	whm	chl	bio	epd	opq	cal	sph	trm	rut	grh	NOTES
10a	X	X	x	X			x	x	x					10a,b,c interlayered
10b	X	X		X	r	x		x	(magnetite)					x +chloritoid, garnet
10c	X	X		X			x	x	x	x				x
12	X	X	X	x	r		x		X	x	x			An = 00
15	X	X	X	X				x		x	x		x	opq = ilmenite
45	X	X		X	x		x		x	x				+pyrite, PQC
46a	X	X		X	x		x		x	x				+PQC
48	X	X		X	x		x	x	x					
52	X	X	X	x	x		x		x	x				
100	X	X	X	X	x	x	x		x	x				+PQC
103	X	x	x	X	r	x	x	x		x	x	x		+chloritoid
106	X	X	X	X	x		x	x	x	x	x			+PQC
107	X	X		X	x			x		x		x	x	+PQC
108	X	x		X	x	x	x	x		x	x			S-C mylonite
140	X	x		X			x	x	x	x	x			+chloritoid
141	X	x	X	X		x	x			x				+PQC
209	X	x		X	r	x		x			x			+chloritoid

Rock Units East of the Le Conte Fault
Napeequa Unit

Quartz Biotite Schists and related rock types- Includes subordinate calcareous, micaceous quartzite and quartzite interbeds.

Abbreviations- Above plus garnet (gnt) and clinozoisite (cln). White mica is probably muscovite east of the Le Conte Fault.

** = Geothermobarometric sample (see Metamorphic Section). An = microprobe determined anorthite component of plagioclase.

#	qtz	plg	whm	chl	gnt	bio	grh	opq	epd	cal	sph	rut	cln	NOTES
17	X	x				X	x	x					x	
21	X	x	X	X		X	x	x						
24	X	x						x						+diopsidic pyroxene

#	qtz	plg	whm	chl	gnt	bio	grh	opq	epd	cal	sph	rut	cln	NOTES
26b	X	x			x	X	x							
29a	X	X	x		x	X	x							
29b	X	X		X		x		x	X					29, 30 RPC
30	X	X	x	r	x	x	x	x	(ilmenite)			x		An 00 **
32	X	x				X		x	x	x	x			+apatite
34b	X	X	x	X		x		x		x	x	x		
43	X	x		X		x		x	x		x			
60	X		X	x		x	x	x						An 16
64	X	x	x		x	X	x				x			
72	X	x		R	x	x	x			x				+Fe chlorite
73	X	x		x	x	X	x	x				x		
129b	x						x			X				carbonate pod
137	X	x	X	x	x	x	x	x	x			x	x	An 20
137b	X	x	X	x	x	X	x	x					x	
149	X	x	x			X	x							
150c	X	x		x		X	x	x				x		+tourmaline
151	X		x	x	x	X	x	x						
153	X	X		x		X	x	x		x	x			
156	X	X		X		X		x		x				+apatite
176	X						x							quartzite
177	X	x		x		X	x				x			S-C mylonite
240a	X	x		x	x	x	x	x						
240b	X	X		x		X		x	x	X				

Amphibolite Unit- Interlayered with the more abundant quartz biotite schists and related rock types.

Abbreviations- above plus hornblende (hbl).

#	qtz	plg	hbl	chl	bio	opq	epd	cal	rut	sph	NOTES
131b		X	X		X		x			x	An 00
179		X	X			x					An 15
240c	X	X	X	x	X	x	x				
240d		X	X		X	x	x				

Metagabbro Unit- Two bodies: (1) North of the Hidden Lake Pluton (#157 and 25c). (2) East of the Cascade River (Cascade River Road)(#44).

#	qtz	plg	hbl	chl	bio	opq	epd	cal	NOTES
25c1	x	X	X						+zoisite
44	x	X	X	x			x		+plg = oligoclase
157		X	X						
157b		X	X						sheared equivalent of 157

Ultramafic Unit- Pods, lenses and layers within the Napeequa Unit.

Abbreviations- Antigorite (antg), tremolite (trem), magnesite (magn), forsterite (fors), opaque (probable chromite or magnetite).

#	antg	trem	magn	fors	talc	opaque	NOTES
25	X			X	X		antigorite replaces forsterite
25c2		X			X		foliated (ghost grains)

#	qtz	plg	RPC	bio	whm	chl	gnt	hbl	epd	opq	sph	rut	cal	NOTES
229	X	X	X	X	x			x	x	x				+hbl layer

Mica Schists- Mica schist interlayers in the quartzose feldspathic conglomerate unit (above) are similar in composition to these schists, although separately mappable. Abbreviations- Above plus ilmenite (ilm).

#	qtz	plg	bio	whm	gnt	chl	epd	hbl	cal	opq	ilm	rut	sph	NOTES
77	X	X	X		x	X	x	X		x				
78	X	X	X	X										An 32
82	X	X	X		x	x		X		x				
118a	X	X	X	X	X			X			x			

#	qtz	plg	bio	whm	gnt	chl	epd	hbl	cal	opq	ilm	rut	sph	NOTES
118b	X	X	X	X	X	r	x	X	x		x	x		An 49 **
170	X	X	X			x	x		x					
192	X	X	X	X	x	x				x				

Calcic amphibolites and Mica Schists- Associated with the marble marker bed.

#	qtz	plg	RPC	hbl	epd	cln	cal	gnt	bio	whm	chl	rut	opq	sph	NOTES
120	X	X	X	X			X	x			x	x	x	x	
120b	X	X	X		X		x		X				x	x	+probable RPC
121	X	X	x	X			X	x	r	X	x	x	x	x	(ilmenite) An 32 **
122	X	X	X						X		X	x	x	x	
188	X	X		X	x		x	x	X		X	x		x	
189	X	X			X		x		X	X		x	x	x	
190	X	X		X	x		x		X	X		x	x		
191b	X	X	x	X			x	X					x	x	
83b	X	X			X		x		X		x			x	

Amphibolites- Mappable layers in the northeastern part of the field area.

Quartz poor subdivision-

#	qtz	plg	hbl	bio	chl	epd	cal	sph	rut	opq	NOTES
6a	x	X	X	X		x	x	x			lucco-amphibolite
6b	x	X	X	X		x		x			dark amphibolite
80	x	X	X	X		X		x	x	x	
81	x	X	X	x	x	x		x	x	x	
117	x	X	X	x				x		x	+hematite
169	x	X	X	X	x	X	x	x		x	
170b	x	X	X	X	x	X		x		x	
173	x	X	X	X	x	X	x				
238	X	X	X	X						x	

Quartz rich sub-division Quartz and plagioclase sub-equal in abundance. #165, 148 and 158 in the Napeequa unit and are from a thick layer north of the Hidden Lake Pluton. Abbreviations- Above plus hematite (hem).

#	qtz	plg	hbl	chl	epd	sph	opq	hem
90a	X	X	X		X	x	x	x
90b	X	X	X		X		x	
91	X	X	X		X	x		x
165	X	X	X		X			
148	X	X	X		X			
158	X	X	X	x	X			

Graphitic Mica Schists- Minor pelitic unit. Other rare pelites are observed as interlayers in the conglomeratic quartzo-feldspathic unit. Abbreviations- Above plus staurolite (str) and tourmaline (trm).

#	qtz	plg	gnt	str	bio	chl	whm	hbl	grh	opq	ilm	rut	trm	NOTES
93	x	X	X		X	x		X	x					bio replacing hbl
93(2)	X	X	X		X	r	X		x		x	x		+ minor epidote
93b	X	X	X		X	x		x	x		x	x		An 28 **
94	X	X	X		x	x	X		x					
124	x	X	X	x	x	x	X				x		x	

Quartz Mica Schists- Mappable layer in the northern part of the field area.

#	qtz	plg	whm	bio	chl	gnt	opq	ilm	rut	grh	NOTES
84	X	x	x	X	x	x			x	x	
87	X		x	X			x			x	+ tourmaline
89	X	x	x						x	x	+ hematite
92	X	x	x	X		x				x	
220a	X	X	X	X		x	x				+ apatite
220b	X	X	x	X		x	x	x	x		+ apatite An 21 **

Plutonic Rocks

Hidden Lake Pluton-

Abbreviations- qtz (quartz), plg (plagioclase), bio (biotite), epd (epidote), cln (clinozoisite), ser (sericite), sph (sphene). r = trace replacement product.

#	qtz	plg	kspar	bio	epd	cln	ser	sph	cal	opq	NOTES
18	X	X	x	X	r	r	r	x		x	plagioclase- normal zonation
20	X	X	x	X	r		r	x		x	
36	X	X	x	X		r	r				
42	X	X	x	X			r		r		biotite is chloritized

APPENDIX II

GEOCHEMICAL ANALYSIS RESULTS FOR THE CRS

File name A:JD.ROC

Sample	6	117	173	188	158	240
Group #	1.00	1.00	1.00	1.00	2.00	2.00
Qual	0	0	0	0	0	0
Key	0	0	0	0	3	3
Ref	0	0	0	0	0	0
SiO ₂	66.85	56.16	50.12	60.92	60.93	49.18
TiO ₂	0.49	1.22	2.80	1.12	0.67	3.84
Al ₂ O ₃	14.90	14.61	18.45	14.25	14.26	16.35
FeO	3.22	8.15	9.47	7.39	8.70	11.91
MnO	0.12	0.12	0.15	0.10	0.17	0.14
MgO	2.51	7.80	4.47	5.81	4.61	4.50
CaO	6.32	7.85	7.92	4.56	9.28	6.25
Na ₂ O	4.77	3.75	5.14	3.73	0.79	3.28
K ₂ O	0.34	0.16	1.14	2.20	0.08	3.27
P ₂ O ₅	0.17	0.30	0.47	0.00	0.06	0.00
Total	99.68	100.12	100.13	100.08	99.54	98.72
NI	35.0	178.0	16.0	0.0	11.0	0.0
CR	51.0	534.0	22.0	0.0	13.0	0.0
SC	12.0	27.0	32.0	0.0	35.0	0.0
V	81.0	205.0	256.0	0.0	311.0	0.0
BA	191.0	163.0	241.0	0.0	0.0	0.0
RB	9.0	3.0	24.0	0.0	2.0	0.0
SR	494.0	721.0	531.0	0.0	159.0	0.0
ZR	136.0	153.0	199.0	0.0	49.0	0.0
Y	11.0	16.0	27.0	0.0	18.0	0.0
NB	9.3	13.7	52.9	0.0	2.2	0.0
GA	0.0	0.0	0.0	0.0	0.0	0.0
CU	45.0	45.0	39.0	0.0	13.0	0.0
ZN	35.0	94.0	73.0	0.0	47.0	0.0
FeO*	3.22	8.15	9.47	7.39	8.70	11.91
F/F+M	0.571	0.515	0.683	0.563	0.658	0.728
Rb/Sr	0.018	0.004	0.045	0.000	0.013	0.000
K/Rb	314	443	394	0	332	0
K/Ba	14.8	8.1	39.3	0.0	0.0	0.0
den	2.44	2.60	2.63	2.52	2.59	2.66

4 4	2 6 A	7 B	3 3 G	3 3 H
2.000	3.000	3.000	4.000	4.000
0	0	0	0	0
3	7	7	8	8
0	0	0	0	0
54.60	60.49	52.38	78.82	78.79
0.33	0.69	0.81	0.21	0.07
14.62	18.33	19.82	12.17	13.54
7.02	7.01	9.40	2.30	0.78
0.12	0.11	0.18	0.02	0.01
5.83	3.79	4.62	0.31	0.00
9.45	5.05	9.55	0.66	0.82
3.59	3.02	2.78	4.93	5.93
0.37	1.22	0.17	0.27	0.04
0.00	0.11	0.15	0.03	0.00
95.93	99.82	99.87	99.91	99.98
0.0	21.0	10.0	17.0	16.0
0.0	31.0	29.0	6.0	1.0
0.0	9.0	30.0	4.0	0.0
0.0	178.0	212.0	39.0	14.0
0.0	778.0	347.0	253.0	32.0
0.0	41.0	6.0	12.0	4.0
0.0	513.0	488.0	279.0	78.0
0.0	77.0	49.0	179.0	73.0
0.0	12.0	17.0	19.0	4.0
0.0	3.0	3.0	23.0	9.0
0.0	19.0	22.0	10.0	21.0
0.0	27.0	41.0	15.0	4.0
0.0	85.0	82.0	24.0	11.0
7.02	7.01	9.40	2.30	0.78
0.551	0.653	0.675	0.820	1.000
0.000	0.080	0.012	0.043	0.051
0	247	235	187	83
0.0	13.0	4.1	8.9	10.4
2.58	2.52	2.63	2.34	2.31

33H	15G	14G	26I
4.00	5.00	5.00	5.00
0	0	0	0
8	9	9	9
0	0	0	0
62.21	79.68	60.29	49.92
0.61	0.22	1.57	0.88
18.18	12.52	13.71	18.38
6.06	1.18	12.39	12.53
0.12	0.02	0.25	0.24
2.30	0.33	2.80	4.60
4.90	0.48	4.13	10.01
3.97	5.14	3.92	2.61
1.27	0.34	0.54	0.58
0.19	0.01	0.30	0.15
99.81	99.92	99.89	99.90
88.0	14.0	0.0	8.0
68.0	3.0	0.0	23.0
14.0	8.0	31.0	41.0
119.0	10.0	267.0	342.0
672.0	216.0	299.0	140.0
47.0	9.0	13.0	134.0
537.0	171.0	134.0	326.0
86.0	144.0	116.0	57.0
16.0	40.0	40.0	18.0
5.0	5.0	2.0	0.0
22.0	10.0	19.0	20.0
19.0	21.0	26.0	0.0
93.0	23.0	78.0	62.0
6.06	1.18	12.39	12.53
0.729	0.784	0.819	0.735
0.088	0.053	0.097	0.411
224	314	345	36
15.7	13.1	15.0	34.4
2.48	2.32	2.58	2.69

File name A:JD.ROC

Sample	26H	33HC	31HC	33GC
Group #	5.00	1.00	2.00	2.00
Qual	0	10	10	10
Key	9	1	1	1
Ref	0	0	0	0

SiO2	55.48	62.21	78.79	78.82
TiO2	0.88	0.61	0.07	0.21
Al2O3	16.72	18.18	13.54	12.17
FeO	11.14	6.06	0.78	2.30
MnO	0.24	0.12	0.01	0.02
MgO	5.13	2.30	0.00	0.51
CaO	7.44	4.90	0.82	0.66
Na2O	2.45	3.97	5.93	4.93
K2O	0.31	1.27	0.04	0.27
P2O5	0.10	0.19	0.00	0.03
Total	99.89	99.81	99.98	99.91

CR	1.0
SC	37.0
V	367.0
BA	103.0
RB	9.0
SR	318.0
ZR	60.0
Y	20.0
GA	17.0
CU	162.0
ZN	35.0

FeO*	11.14
F/F+M	0.689
Rb/Sr	0.028
K/Rb	286
K/Ba	25.0
den	2.63

File name A:MMOD.ROC

Sample	15G	14G	26I	26H	7B	26A
Group #	2.00	2.00	2.00	2.00	1.00	1.00
Qual	10	10	10	10	10	10
Key	1	1	1	1	1	1
Ref	0	0	0	0	0	0

SiO2	79.68	60.29	49.92	55.48	52.38	60.49
TiO2	0.22	1.57	0.88	0.88	0.81	0.69
Al2O3	12.52	13.71	18.38	16.72	19.82	18.33
Fe2O3	1.18	12.39	12.53	11.14	9.40	7.01
MnO	0.02	0.25	0.24	0.24	0.18	0.11
MgO	0.33	2.80	4.60	5.13	4.62	3.79
CaO	0.48	4.13	10.01	7.44	9.55	5.05
Na2O	5.14	3.92	2.61	2.45	2.78	3.02
K2O	0.34	0.54	0.58	0.31	0.17	1.22
P2O5	0.01	0.30	0.15	0.10	0.15	0.11
Total	99.92	99.89	99.90	99.89	99.87	99.82

APPENDIX 3

Mineral Compositions

	#220				#194			
	Plg	Ilm	Gnt	Bio	Plg	Ilm	Gnt	Bio
SiO ₂	61.6	.33	37.1	35.1	62.4	.08	37.3	34.6
TiO ₂	.02	58.3	.07	2.38	n.a.	49.7	.07	2.12
Al ₂ O ₃	24.0	b.d.	21.2	18.8	23.6	.06	20.7	18.1
FeO	b.d.	46.8	31.0	20.3	.16	49.0	32.6	20.2
MnO	b.d.	1.39	4.13	.11	n.a.	1.33	2.45	.11
MgO	b.d.	b.d.	1.63	8.36	n.a.	.11	2.59	8.98
CaO	4.32	b.d.	5.74	.11	4.93	n.a.	4.01	n.a.
Na ₂ O	9.20	b.d.	.01	.13	9.06	n.a.	n.a.	n.a.
K ₂ O	.11	.11	b.d.	9.29	.10	n.a.	n.a.	7.75
NiO	n.a.	n.a.	n.a.	n.a.	n.a.	.03	n.a.	n.a.
Cr ₂ O ₃	n.a.	n.a.	n.a.	n.a.	n.a.	.09	n.a.	n.a.
Total	99.2	106.9	99.4	94.6	100.3	100.4	99.7	92.0
N =	3	2	6	3	3	5	4	5
Si	2.75	.02	2.97	4.95	2.76	b.d.	3.01	5.45
Ti	b.d.	2.04	b.d.	.25	n.a.	1.91	b.d.	.25
Al	1.26	n.d.	2.00	3.12	1.23	b.d.	1.97	3.36
Fe	b.d.	1.82	2.08	2.39	.01	2.09	2.20	2.66
Mn	b.d.	.03	.28	.01	n.a.	.06	.17	.02
Mg	b.d.	b.d.	.20	1.76	n.a.	.01	.31	2.25
Ca	n.d.	b.d.	.49	b.d.	.23	n.a.	.35	n.a.
Na	1.02	b.d.	b.d.	.02	.78	n.a.	n.a.	n.a.
K	.05	b.d.	b.d.	1.67	.01	n.a.	n.a.	1.55
Ni	n.a.	n.a.	n.a.	n.a.	n.a.	b.d.	n.a.	n.a.
Cr	n.a.	n.a.	n.a.	n.a.	n.a.	b.d.	n.a.	n.a.

n.a. = not analyzed, b.d. = below detection (rounding to two decimals).
 Plg = plagioclase, Ilm = ilmenite, Gnt = garnet, Bio = biotite. N =
 number of microprobe spots sampled. All garnets are rim compositions.

	#134				#118			
	Plg	Ilm	Gnt	Bio	Plg	Ilm	Gnt	Bio
SiO ₂	61.4	.11	37.6	34.5	55.7	.20	37.4	35.0
TiO ₂	n.a.	48.4	.11	2.44	n.a.	51.3	.09	2.74
Al ₂ O ₃	23.6	.07	1.96	19.8	28.2	.12	20.8	18.2
FeO	.16	50.2	31.7	19.3	.20	47.7	31.0	20.8
MnO	n.a.	1.65	2.94	.11	n.a.	.70	1.4	.06
MgO	n.a.	.18	2.95	8.91	n.a.	.14	2.63	8.41
CaO	5.66	n.a.	4.17	n.a.	10.4	n.a.	6.04	n.a.
Na ₂ O	8.48	n.a.	n.a.	n.a.	5.95	n.a.	n.a.	n.a.
K ₂ O	.10	n.a.	n.a.	9.19	.09	n.a.	n.a.	8.87
NiO	n.a.	.03	n.a.	n.a.	n.a.	.03	n.a.	n.a.
Cr ₂ O ₃	n.a.	.16	n.a.	n.a.	n.a.	.04	n.a.	n.a.
Total	100.3	100.3	100.3	94.3	100.5	100.6	99.4	94.1
N =	4	3	4	2	4	5	2	5
Si	2.72	.01	3.00	5.30	2.50	.01	3.01	5.43
Ti	n.a.	1.86	.01	.28	n.a.	1.95	.01	.32
Al	1.27	b.d.	1.96	3.59	1.49	.01	1.97	3.32
Fe	.01	2.17	2.12	2.48	.01	2.02	2.09	2.69
Mn	n.a.	.07	.13	.02	n.a.	.03	.10	.01
Mg	n.a.	.01	.35	2.04	n.a.	.01	.31	1.94
Ca	.27	n.a.	.36	n.a.	.50	n.a.	.52	n.a.
Na	.73	n.a.	n.a.	n.a.	.52	n.a.	n.a.	n.a.
K	.01	n.a.	n.a.	1.80	.01	n.a.	n.a.	1.69
Ni	n.a.	.03	n.a.	n.a.	n.a.	b.d.	n.a.	n.a.
Cr	n.a.	.09	n.a.	n.a.	n.a.	b.d.	n.a.	n.a.

n.a. = not analyzed, b.d. = below detection (rounding to two decimals).
 Plg = plagioclase, Ilm = ilmenite, Gnt = garnet, Bio = biotite. N =
 number of microprobe spots sampled. All garnets are rim compositions.

	#93				#184 (* see below)		
	Plg	Ilm	Gnt	Bio	Plg	Gnt	Bio
SiO ₂	61.0	.14	37.3	35.6	60.8	38.0	37.3
TiO ₂	n.a.	52.1	.08	1.80	n.a.	.07	1.66
Al ₂ O ₃	24.6	.08	21.1	18.4	24.6	21.0	17.4
FeO	.09	45.7	31.8	18.4	.15	24.5	12.8*
MnO	n.a.	.27	.26	.02	n.a.	8.10*	.12
MgO	n.a.	.05	2.92	10.6	n.a.	4.40	15.3
CaO	6.14	n.a.	6.21	n.a.	6.17	4.10	n.a.
Na ₂ O	8.56	n.a.	n.a.	n.a.	8.47	n.a.	n.a.
K ₂ O	.10	n.a.	n.a.	8.79	.11	n.a.	9.38
NiO	n.a.	.02	n.a.	n.a.	n.a.	n.a.	n.a.
Cr ₂ O ₃	n.a.	.03	n.a.	n.a.	n.a.	n.a.	n.a.
Total	100.5	98.4	100.1	93.6	100.3	100.1	93.9
N =	3	4	4	2	4	5	3
Si	2.70	.01	3.01	5.47	2.70	2.99	5.47
Ti	n.a.	2.00	.08	.21	n.a.	b.d.	.21
Al	1.28	.01	1.98	3.32	1.29	1.96	3.32
Fe	b.d.	1.95	2.12	2.37	.01	1.62	2.37
Mn	n.a.	.01	.02	b.d.	n.a.	.54	b.d.
Mg	n.a.	b.d.	.35	2.42	n.a.	.52	3.41
Ca	.29	n.a.	.53	n.a.	.29	.35	n.a.
Na	.74	n.a.	n.a.	n.a.	.73	n.a.	n.a.
K	.01	n.a.	n.a.	1.72	.01	n.a.	1.78
Ni	n.a.	.02	n.a.	n.a.	n.a.	n.a.	n.a.
Cr	n.a.	.03	n.a.	n.a.	n.a.	n.a.	n.a.

n.a. = not analyzed, b.d. = below detection (rounding to two decimals).
 Plg = plagioclase, Ilm = ilmenite, Gnt = garnet, Bio = biotite. N =
 number of microprobe spots sampled. All garnets are rim compositions.
 * (184) = Evidence for retrogression of the garnet and biotite observed
 petrographically (see Geothermobarometry).

	#30			#121			#10b (* see below)	#139b	
	Plg	Ilm	Gnt	Plg	Ilm	Gnt	Gnt	Hbl Core	Hbl Rim
SiO ₂	67.4	.15	37.6	60.2	.17	37.8	37.5	43.9	41.6
TiO ₂	.02	58.0	.08	n.a.	52.1	.09	.10	1.02	.63
Al ₂ O ₃	24.0	.18	21.8	25.5	.29	20.9	20.8	11.8	15.5
FeO	b.d.	45.0	31.1	.10	47.0	30.8	33.0	18.16	18.4
MnO	b.d.	4.01	1.43	n.a.	.47	1.69	2.66	.16	.19
MgO	b.d.	b.d.	.60	n.a.	.05	2.61	1.12	8.44	6.90
CaO	4.32	b.d.	8.60	6.85	n.a.	6.39	5.34	11.1	11.3
Na ₂ O	9.20	b.d.	b.d.	7.97	n.a.	n.a.	n.a.	1.23	1.46
K ₂ O	.11	.01	b.d.	.10	n.a.	n.a.	n.a.	.73	.79
NiO	n.a.	n.a.	n.a.	n.a.	.02	n.a.	n.a.	n.a.	n.a.
Cr ₂ O ₃	n.a.	n.a.	n.a.	n.a.	.07	n.a.	n.a.	n.a.	n.a.
Total	99.54	107.3	101.3	100.7	100.0	100.3	100.5	96.6	96.9
N =	3	3	4	4	2	4	3	5	7
Si	2.96	.01	2.98	2.67	.01	3.01	3.02	6.66	6.32
Ti	b.d.	2.02	b.d.	n.a.	1.98	.01	.01	.12	.07
Al	1.03	.01	2.04	1.34	b.d.	1.97	1.97	2.11	2.77
Fe	b.d.	1.72	2.06	b.d.	1.99	2.05	2.23	2.30	2.34
Mn	b.d.	.08	.10	n.a.	.02	.11	.18	.02	.02
Mg	b.d.	b.d.	.07	n.a.	b.d.	.31	.14	1.91	1.56
Ca	b.d.	b.d.	.73	.33	n.a.	.55	.46	1.80	1.84
Na	1.02	b.d.	n.a.	.68	n.a.	n.a.	n.a.	.37	.43
K	.05	b.d.	n.a.	.01	n.a.	n.a.	n.a.	.14	.15
Ni	n.a.	n.a.	n.a.	n.a.	.02	n.a.	n.a.	n.a.	n.a.
Cr	n.a.	n.a.	n.a.	n.a.	.07	n.a.	n.a.	n.a.	n.a.

n.a. = not analyzed, b.d. = below detection (rounding to two decimals).
 Plg = plagioclase, Ilm = ilmenite, Gnt = garnet, Bio = biotite. N =
 number of microprobe spots sampled. All garnets are rim compositions.
 * #10b- Only garnet observed in the (upper) greenschist facies.

	179		98		131b			
	-----	-----	-----	-----	-----	-----	-----	-----
SiO ₂	44.1	47.0	50.9	50.5	45.9	46.6	54.1	50.0
TiO ₂	.28	.23	.46	.51	.38	.37	.14	.26
Al ₂ O ₃	13.4	10.4	4.85	5.22	7.76	7.49	1.77	6.09
FeO	16.3	15.9	13.9	14.0	17.7	17.4	15.5	17.0
MnO	.27	.27	.65	.62	.57	.55	.58	.54
MgO	9.46	11.2	14.4	14.2	10.2	10.1	15.2	12.1
CaO	11.3	11.9	11.9	12.1	11.2	11.2	12.4	11.7
Na ₂ O	1.69	1.14	.89	.95	1.40	1.56	.47	.94
K ₂ O	.33	.21	.28	.32	.45	.36	.10	.28
Total	97.1	98.3	98.2	98.3	95.5	95.7	100.1	98.8
Si	6.58	6.89	7.39	7.32	6.95	7.06	7.62	7.22
Ti	.03	.03	.05	.06	.04	.04	.02	.03
Al	2.35	1.79	.83	.89	1.39	1.34	.29	1.04
Fe	2.37	1.95	1.68	1.69	1.76	1.92	1.27	1.51
Mn	.03	.03	.08	.08	.07	.07	.07	.07
Mg	2.10	2.44	3.11	3.08	2.30	2.28	3.18	2.60
Ca	1.81	1.87	1.85	1.88	1.82	1.82	1.87	1.80
Na	.49	.32	.25	.27	.41	.46	.13	.26
K	.06	.04	.05	.06	.09	.07	.02	.05

Hornblende compositions from the greenschist (98) and lower amphibolite facies (179, 131b).